PRIMARY AND SECONDARY IONIZATION PROCESSES IN MERCURY VAPOUR

being a thesis on the electrical breakdown of mercury vapour under uniform field conditions when the cathode is a mercury pool

by

G. D. N. OVERTON, B.A.

and submitted to the University of Keele in candidature for the Degree of Doctor of Philosophy.

Department of Physics,
University of Keele.

July, 1965.

ACKNOWLEDGEMENTS

I wish to express my thanks to:

Professor D. J. Ingram, who provided laboratory facilities;

Dr. D. E. Davies, for his helpful supervision;

My friends in the Electron Physics group at Keele, for their valuable discussion;

Mr. F. Rowerth and his staff for their technical assistance.

SYNOPSIS

Because of the important industrial applications of mercury, most work in the field of mercury vapour discharges has been carried out on mercury vapour arcs. The work described in this thesis is concerned with the fundamental processes operative in mercury vapour in the Townsend region of gas discharges, when the cathode used is a mercury pool.

Apparatus has been developed with which it was possible to obtain data on breakdown potentials, primary ionization coefficients and formative time lags. Generalized secondary ionization coefficients were calculated from the breakdown potentials and primary ionization coefficients as a function of E/p_o. This curve is interpreted in the light of calculations made of the numbers of excited atoms in each of the 'P' states per ion pair, and the application of Davidson's treatment of the temporal growth of ionization.

CONTENTS

CHAPTER 1

THE SPATIAL GROWTH OF IONIZATION

Introduction

A large amount of work has been concentrated on the high pressure high current mercury discharge, because of its engineering applications. The low pressure, low current mercury discharge has by comparison been neglected. The work described in this thesis is confined to the study of mercury vapour in that part of gas discharge physics known as the Townsend or Controlled Discharge region, in which currents are in general limited to the range 10^{-12} to 10^{-6} amps in uniform applied fields. In this chapter, the basic physics of this type of discharge is presented, in order that an adequate background can exist for the interpretation of the results in mercury vapour.

1.1 The Production of Photo-electrons

Consider an evacuated tube containing two plane parallel electrodes. Ultra-violet light falls on one electrode liberating photo-electrons. The variation in photo-electric current can be studied by altering step by step the potential applied between the electrodes, from a large accelerating value to a suitable retarding value and plotting current voltage characteristics. Differentiation of this curve yields the energy distribution of the electrons. The type of distribution obtained is shewn in fig. (1). The curve, unlike a Maxwellian distribution, shews that electrons are emitted with all energies from zero to a well defined maximum, given in terms of the critical potential, V_o, by

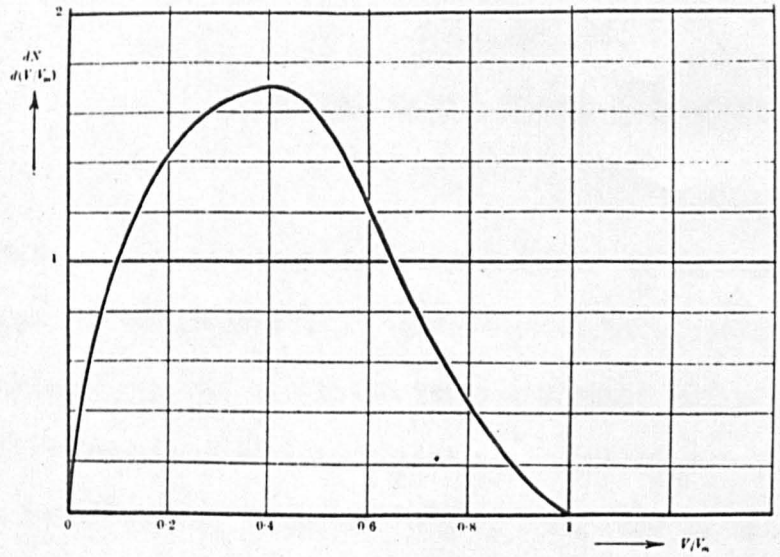

Energy distribution $dN/d(V/V_m)$ of photo-electrons released by quanta (λ 2,000 to 3,000 A) from a metal surface as a function of their relative energy V/V_m. V_m is the energy equivalent corresponding to the maximum speed

fig 1

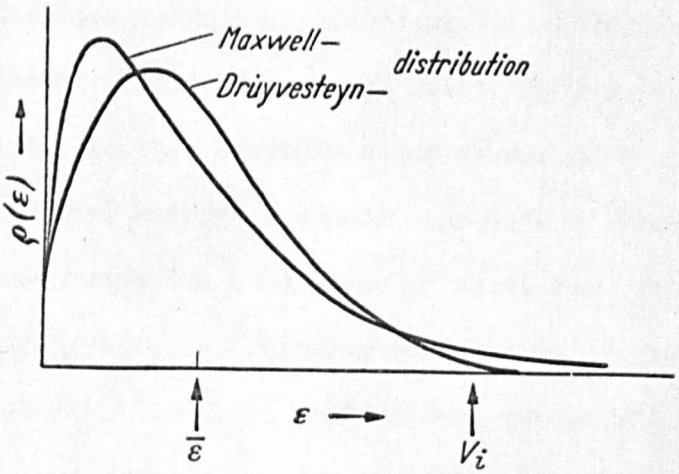

Electron energy distribution ϱ as a function of the energy ε for the same mean energy $\bar{\varepsilon}$ and the same number of electrons (the same area covered by the curve).

MAXWELL distribution: $\varrho(\varepsilon) = C' \varepsilon^{\frac{1}{2}} - \frac{\varepsilon}{\bar{\varepsilon}}$;

DRUYVESTEYN distribution: $\varrho(\varepsilon) = C \varepsilon^{\frac{1}{2}} e^{-0.55\left(\frac{\varepsilon}{\bar{\varepsilon}}\right)^2}$

fig 2

$$eV_o = \tfrac{1}{2}mv^2$$

where e is the charge on the electron and m is its mass. In the presence of an accelerating field, the form of this distribution will be maintained at any intermediate distance between the electrodes, and the current carried at any instant will be

$$I = \frac{Nev}{d}$$

where N is the number of electrons, e is their charge, v the mean velocity and d the electrode separation.

1.2 The Interaction of Electrons with Gas Atoms

1.2.1 Elastic Collisions

If gas is now introduced into the system, the form of the energy distribution may be altered by the interaction of the electrons with the gas molecules. The simplest type of interaction is an elastic collision, defined as an event in which total kinetic energy is conserved. The fractional loss of energy by an electron having such a collision is given by

$$d\varepsilon = \frac{2mM}{(M+m)^2}$$

where m is the mass of the electron and M is the mass of the atom. For most cases this fractional loss of energy is small, e.g. for the case of an electron colliding with a mercury atom of mass 200

$$d\varepsilon \simeq 5 \times 10^{-6}$$

It is to be expected, therefore, that the energy distribution of photoelectrons traversing a gap under the influence of an applied field will not be changed in form to any great extent by elastic collisions.

Assuming that the flow of electrons takes from the field E an amount of energy enough to balance losses by elastic collisions, that the electron current density is constant and the gas atoms are relatively at rest, Druyvesteyn and Penning (11) calculated the electron energy distribution function given by

$$\rho(\varepsilon) = C\varepsilon^{\frac{1}{2}}\, e^{-0.55\left(\frac{\varepsilon}{\bar{\varepsilon}}\right)^2}$$

where $\bar{\varepsilon}$ is the mean energy of the electrons calculated in this distribution. Fig. (2) shews the distribution and the Maxwellian for the same mean energy, $\bar{\varepsilon}$. Although the equation for the Druyvesteyn distribution does not predict a maximum energy, it can be seen that the curve approaches the energy axis more quickly than the Maxwellian, and the number of electrons with energies a few volts above the ionising potential is negligibly small. The distribution may be markedly changed when inelastic collisions are included.

1.2.2 Inelastic Collisions

An inelastic collision is defined as one in which the kinetic energy is not conserved; part of the energy going to raise the internal energy of the atom. The probability of an inelastic collison is defined as the number of atoms that are excited or ionised per electron per centimetre of path length at a pressure of one millimetre at $0^{\circ}C$.

1.2.3 Excitation by Electrons

Electrons with sufficient energy to excite an atom, viz;

$$\tfrac{1}{2}mv^2 \geq W_i$$

where W_i is the excitation potential, can do so providing the angular

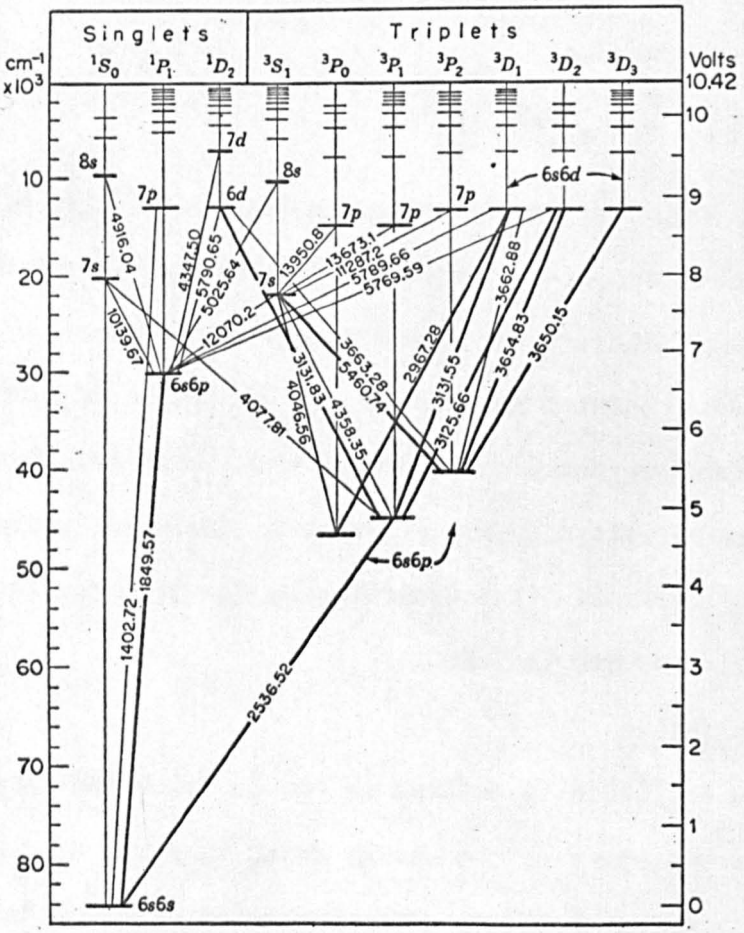

The most important energy levels and spectral lines for the neutral mercury atom.

fig 3

momentum of electron and atom with respect to the common centre of mass of the system is conserved. Therefore the change in angular momentum of the system, δp, is equal to the change in the internal angular momentum of the atom. δp is given by

$$\delta p = \delta j \left(\frac{h}{2\pi}\right)$$

where $j = (l+s)$. For example, in mercury, a transition of one of the electrons in the sixth shell (fig. (3)), from the ground state 6^1S_0 into 7^1S_0 (n=6 into n=7) is associated with $\delta j = 0$. Therefore δp is zero and only head on collisions are effective. The number of such collisions is small and negligible probability of excitation is to be expected for electrons of 7.89eV, the critical energy corresponding to that transition.

The transition 6^1S_0 to 7^1P_1 or 8^1D_1, is associated with δj equal to one or two and 6.67eV and 8.8eV respectively. In these cases excitation will result only if the atom is hit in such a direction that δp has the required value. The excitation probability is zero at the excitation potential since a negligible number of electrons fulfill this condition, and becomes positive when the electron energy is greater than the minimum energy necessary because the electron can carry away the excess energy and also balance the angular momentum.

The probability of excitation to a certain energy level is called the 'excitation function', defined as the number of electron-atom collisions leading to a transition divided by the total number of collisions. This fraction is generally of the order of 10^{-2}.

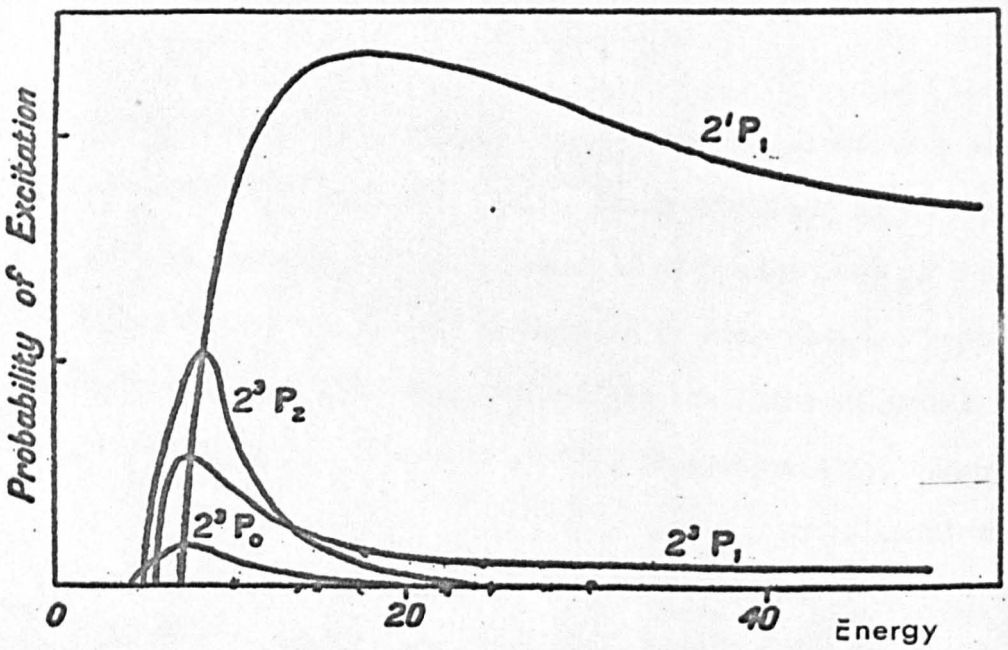

Excitation Functions P States Hg

fig 4

There are marked differences in slope and shape of the excitation functions corresponding to different transitions. For atoms with two valency electrons the function for singlet - singlet transitions rises relatively slowly reaching a broad maximum. The function for singlet - triplet transitions reaches a sharp maximum just above the critical energy and then falls quickly away. Fig. (4) shews the excitation functions for the four 'P' states of mercury as calculated by Penny (1). The shape of these curves has considerable significance when the importance of excited atoms to the breakdown process is considered. This point is amplified in chapter five of this thesis.

The difference in shape of the curves is due to the fact that in singlet - singlet transitions the total spin quantum number is unchanged. Thus before and after excitation the spin vectors of the two valency electrons must be anti-parallel. For singlet - triplet transitions S goes from zero to one, viz. the spin vectors are reorientated to be parallel. For elements such as mercury with strong spin-orbit coupling this can be brought about by electron impact. For elements with weak coupling like helium it can only occur when the impinging electron is captured by the atom and one valency electron is expelled. This electron exchange only occurs within a narrow energy range, hence the corresponding excitation function for helium has a sharper maximum than for mercury. Such stringent conditions are not attached to singlet - singlet transitions and the maximum is broad.

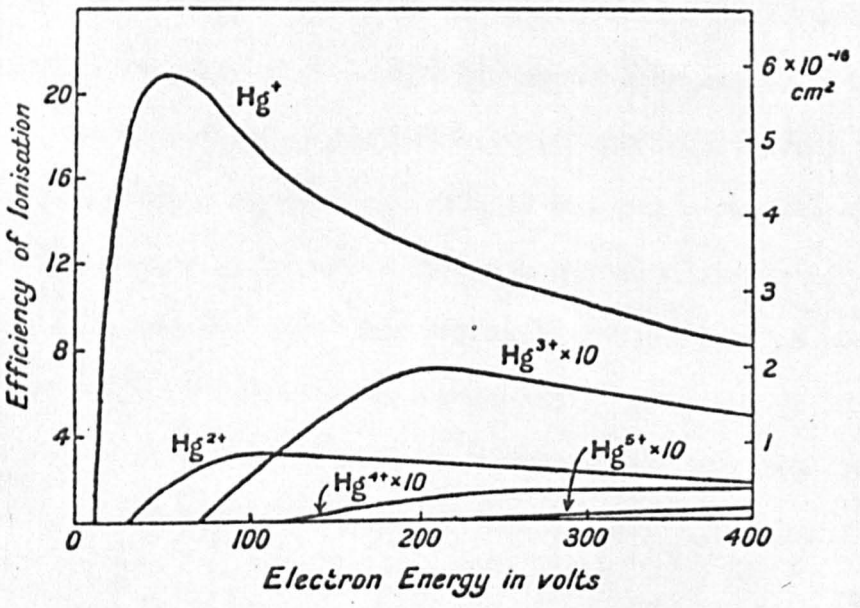

-Efficiencies of ionisation in mercury vapour.

fig 5

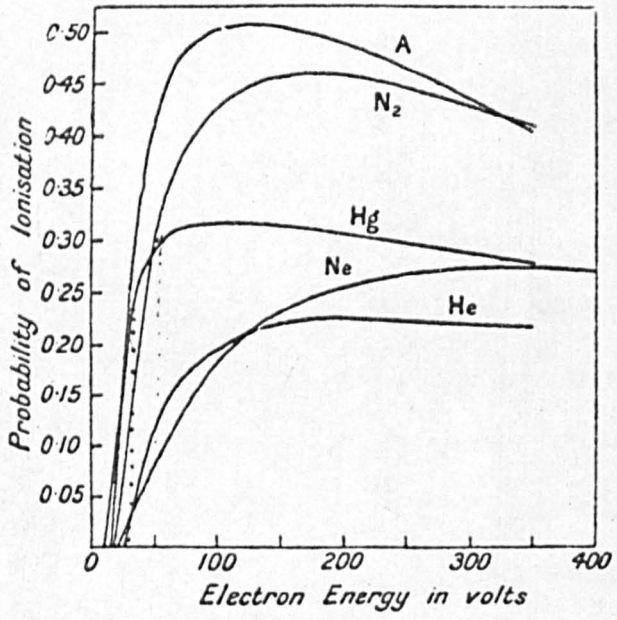

Curves showing probability of ionisation at a collision as a function of the energy of the impacting electron in volts.

fig 6

1.2.4 Ionisation by Electrons

This can be considered as an extreme form of excitation. The probability behaves in a similar manner to the probability of excitation, with the maximum further removed from the critical potential than the critical potential for excitation. Compton and van Voorhis (2) measured the number of ions formed in a gas from a known electron current beam. This number, when reduced to the number of ions formed by one electron travelling one centimetre at a pressure of one millimetre at $0^{\circ}C$, is called the 'efficiency of ionisation'. The probability of ionisation, defined in an analogous manner to the probability of excitation, is found by dividing the efficiency of ionisation by the number of collisions made or the number of mean free paths. A diagram of the ionisation efficiency for mercury vapour as obtained by Bleakney (3) is shewn in fig. (5), and the probability of ionisation for various gases including mercury vapour is shewn in fig. (6).

It can be seen that the probability of ionisation rises from zero at the ionisation potential to a maximum between 100 and 400 volts depending on the gas, after which it steadily decreases. For electrons with any particular energy the probability of ionisation generally increases with the atomic number of the gas, i.e. with the number of electrons in the atom.

1.3 The Townsend First Ionisation Coefficient

The quantities outlined above are determined from experiments in which mono-energetic beams of electrons are used. If we now

return to the case where the swarm of electrons shews an energy distribution, a few electrons in the high energy tail of the distribution only will have sufficient energy to cause ionisation. It is possible to define a coefficient analogous to the ionisation efficiency for this condition, as follows.

The mean energy of the electrons will be determined by the ratio E/p, where E is the field strength and P the gas pressure. If λ_e is the electron mean free path, $eE\lambda_e$ is the average energy gained by an electron in a mean free path in the field direction. $eE\lambda_e$ is proportional to E/p and is the controlling factor in ionisation by collision.

A photo-electron, of sufficient energy, moving through the gas in the direction of the field, will produce on average α ion pairs per centimetre of its path in the direction of the field. Thus with n_x electrons at a distance x from the cathode there will be αdx ion pairs produced in a distance dx. Thus in moving a distance dx, there is an increase in the number of ion pairs dn given by

$$dn = n_x \alpha dx$$

If the number of photo-electrons at the cathode (x=0) is n_o, and the electrode separation is d cm., we have

$$\int_{n_o}^{n_d} \frac{dn}{n} = \int_o^d \alpha dx$$

or $\frac{n_d}{n_o} = e^{\alpha d}$. In terms of current, $\frac{I}{I_o} = e^{\alpha d}$.

where I_o is the photo-electric current from the cathode. Hence the logarithm of I/I_o is proportional to the electrode separation if

$E/_P$ is kept constant. The slope of this curve is a measure of α, known as the first Townsend ionisation coefficient (4). The above derivation assumes the field is uniform and that space charge effects are negligible. The currents involved are therefore small, of the order of 10^{-13} to 10^{-8} amps.(5).

After leaving the cathode, the photo-electrons must travel a certain distance d_o before the energy distribution becomes steady and a constant mean energy is acquired corresponding to the value of $E/_P$ in the gap. This equilibrium is thought to be attained after the electron has undergone some elastic collisions (6). The above equation must therefore be altered to

$$I/_{I_o} = e^{\alpha(d-d_o)}$$

An alternative coefficient to α is the ionisation produced by an electron falling through a potential difference of one volt. In this case the current may be written as

$$I = e^{\eta(V-V_o)}$$

where V_o is a correction factor corresponding to d_o. The coefficient η is related to α by

$$\eta = \frac{\alpha}{E}$$

If the mean energy of the electron swarm is maintained constant, the fraction of the number of collisions between electrons and gas atoms leading to ionisation will remain unchanged if the gas density is altered. Thus α is proportional to p for a given $E/_p$, or

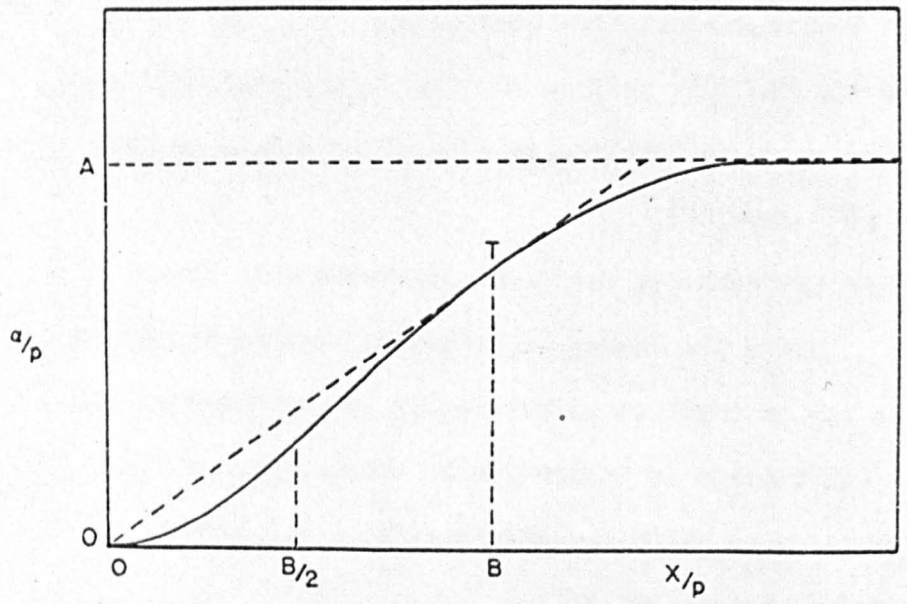

Characteristic curve for a/p, plotted against X/p

fig 7

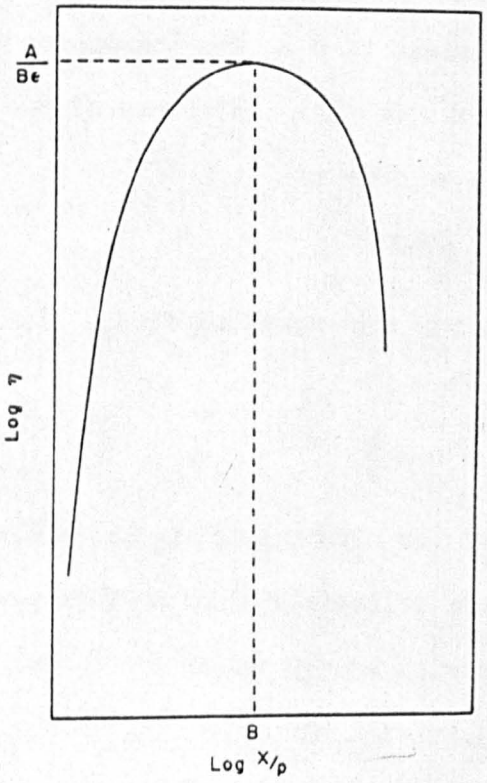

Characteristic curve for $\log \eta = \log (a/X)$ against $\log X/p$.

fig 8

$$\alpha/_P = f(E/_P)$$

1.4 The Evaluation of α/P as a function of E/P

A typical plot of α/P as a function of E/P is shown in fig. (7). The curve is characterised by an elongated letter S shape, rising from an asymptote through a point of inflexion to an apparent saturation value. At very low E/P, the mean energy of the electrons is low, so that the number of electrons in the high energy tail of the distribution is low. Thus α/P rises slowly at first. As E/P increases, the number of high energy electrons with energies greater than V_i increases, but the probability of ionisation decreases. The rate of ionisation thus becomes proportional to E/P before rising more slowly. In contrast, the quantity η has a uniform shape, rising steeply at low E/P, reaching a peak and then declining, fig. (8).

η represents the efficiency of ionisation relative to the applied field. At low E/P there is a high proportion of energy lost to excitation relative to ionisation, and η is therefore low. The ratio of excitation losses to ionisation losses decreases as E/P increases, and η rises with E/P. As E/P increases further the electrons gain energy which is not lost to ionisation, as the probability of ionisation decreases. The electrons carry away this excess energy which is ultimately delivered to the anode. η therefore decreases at higher E/P. The electrons are no longer in equilibrium with the applied field, and the average electron energy changes to higher values as the path length increases. The value of α/P will then be a function of electrode separation as well as E/P.

The peak of the η versus E/P curve represents the point of most efficient ionisation and fixes the minimum point on the Paschen curve (see section 1.5). This value also corresponds with the Stoletow point on the α/P versus E/P curve.

There has not been a single functional relation derived that will fit the whole curve of α/P as a function of E/P for any gas. This is largely because such functions must take account of the energy distribution form prevalent in the gas. This distribution is likely to change with E/P especially if the Ramsauer effect is appreciable. The way in which free paths vary with energy determines the collision frequency and hence the energy losses. These in turn will determine the shape of the high energy tail. Any change in the distribution in high energy electrons will influence α/P.

Townsend (7) on a purely classical basis, was the first to attempt an evaluation of α/P as a function of E/P. His treatment assumes an ionisation probability of unity for all electrons with energy greater than eV_i. Thus only those electrons travelling a distance x in the field direction will ionise if

$$eEx \geq eV_i$$

The number of mean free paths exceeding x is given by the kinetic theory as

$$f(x) = e^{-x/\lambda}$$

where λ is the mean free path. Therefore the number of ionising collisions per unit length, α, is given by

$$d(fx)/dx = (1/\lambda)\ e^{-x/\lambda} = \alpha$$

If λ is written as λ_i/P and x is put equal to V_i/E, then we have

$$\alpha/P = \frac{1}{\lambda_i}\ e^{-V_i/\lambda_i/E/P}$$

or

$$\alpha/P = A\ e^{-BP/E}$$

When plotted, this function starts at zero, rises to a point of inflexion at B/2; and approaches A as E/P increases indefinitely. This levelling is not always observed in practice. In terms of η the relation is

$$\eta = \frac{\alpha}{E} = \frac{A}{E}\ P\ e^{-BP/E}$$

At low E/P, η as predicted by the theory is small, then increases till E/P = B, giving the value of E/P at which the Stoletow constant occurs and at which point η = A/B. Thereafter η declines with E/P.

Although the shape of the curve is similar to the experimental curves, it is usually found that the predicted values of the constants A and B are too low. Since no account is taken of the energy distribution of the electrons, the randomisation of direction as a result of elastic collisions, and the variation of ionisation probability and free path with electron energy, the disagreement is not surprising.

The value of V_i in the equation represents the energy an electron must have before ionisation occurs. This energy in fact rises from V_i and the probability of ionisation varies accordingly. Neglect of this fact tends to make the value of α/P too high. The value of λ assumed is also greater than that which in fact occurs because of the random

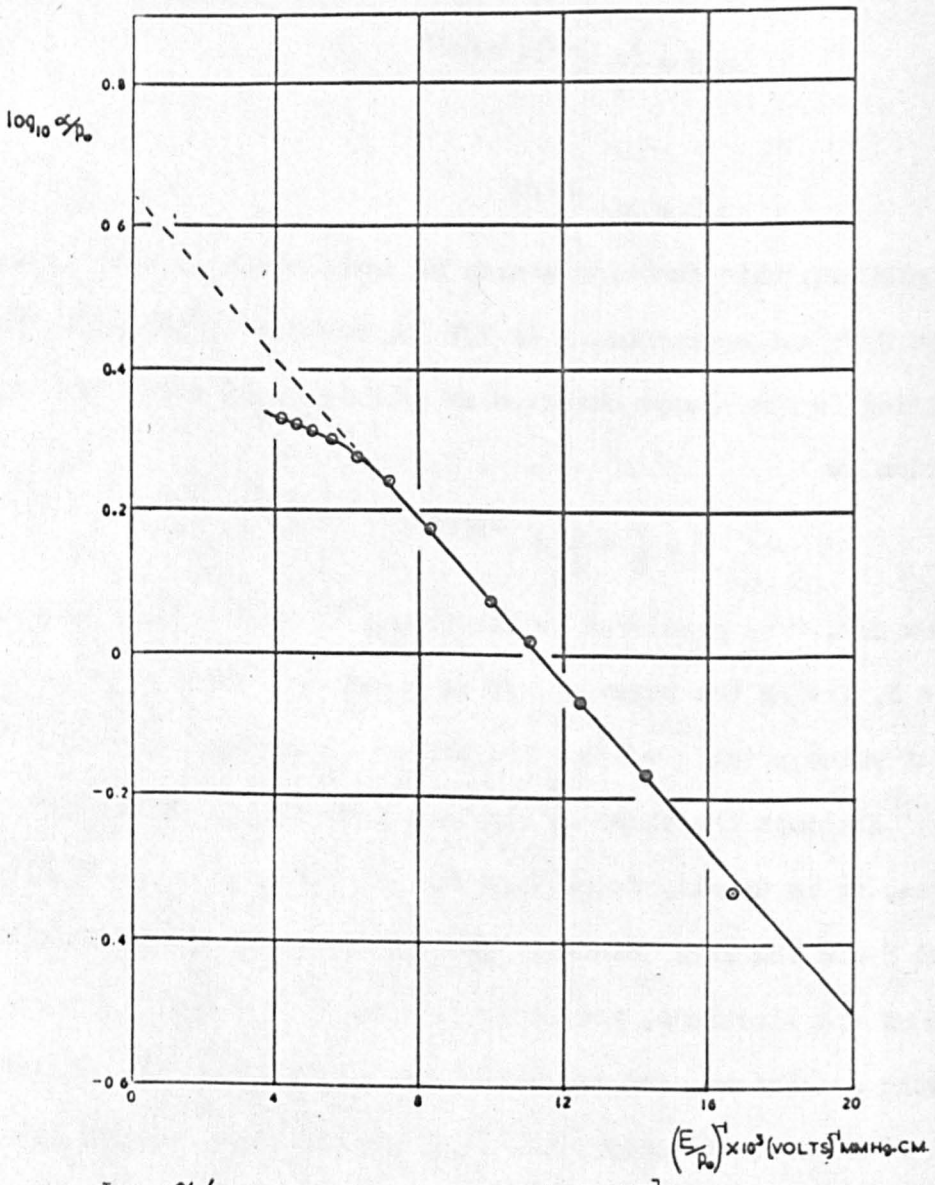

$\text{Log}_{10}\alpha/p_0$ as a function of $(E/p_0)^{-1}$. Hydrogen.

fig. 9.

electron motion. Thus more ionisation occurs per distance λ in the direction of the field than is assumed. This tends to make the value of α/P too low. The Ramsauer effect can either increase or decrease α/P depending on the variation of mean free path with electron energy. In some cases, however, these errors cancel out. Thus fair agreement is found in certain gases over a limited range of E/P. Fig. (9) shews a plot of $\log_e \alpha/P$ as a function of $(E/P)^{-1}$, from Myatt's (8) results in hydrogen. It can be seen that the curve is linear between an E/P of 50 and 160.

By adjusting the constants A and B one can adapt Tonsend's formula to fit almost any section of the experimental curves. Posin (9), for nitrogen, found four functional forms for different ranges of E/P. They are

(1) E/P 20 - 38 $\quad \alpha/P = 5.76 \times 10^{-7}\, e^{0.245\, E/P}$

(2) E/P 44 - 176 $\quad \alpha/P = 1.17 \times 10^{-4}\, (E/P - 32.2)^2$

(3) E/P 176 - 200 $\quad \alpha/P =$ proportional to E/P, linear through point of inflexion

(4) E/P 200 - 1000 $\quad (\alpha/P + 3.65)^2 = 0.21\, E/P$

An expression identical in form to that of Townsend was later derived by von Engel and Steenbeck (10), in which $A = 2aV_i/x^{\frac{1}{2}}$ and $B = 2x^{\frac{1}{2}}V_i/\lambda_1$ where a is a constant, x is the average fraction of energy lost on collision, and λ_1 is the mean free path at a pressure of one millimetre of mercury. A and B are found to be of the right magnitude, but no account was taken of the variation of x with electron energy.

Attempts at calculating α/P as a function of E/p_o for Ne where

the Ramsauer effect is small, were made by Penning and Druyvestyn (11), but the only general theory comparable in usefulness and application to the Townsend, von Engel-Steenbeck expression is that derived by Emeleus, Lunt and Meek (12). The theory evolves along kinetic theory lines. It is assumed that all electrons with energies greater than the ionising energy can ionise, and the probability of such an event is P_i. If $c \geq c_i$ where c_i is the velocity corresponding to the ionisation energy, then P(c) represents the probability of an ionising event in 1 cm. of path at 1 mm.Hg. Thus at a pressure p mm.Hg. an electron on average will create $P_i(c)p.c$ new electrons per second. The probability of an electron having a velocity c is f(c)dc, where f(c) is the velocity distribution form existing at the value of E/p_o in question. Thus the number of electrons created by electrons with velocity c is given by $P_i(c)p.c.f(c)dc$. Thus the total number of electrons created per second, given by αv, where v is the average drift velocity in the field direction, is

$$\alpha v = p \int_{c_i}^{\infty} c.P_i(c).f(c)dc$$

Thus

$$\alpha/P = P/v \int_{c_i}^{\infty} c.P_i(c).f(c)dc$$

The theory thus allows the insertion of the appropriate velocity distribution and the experimentally determined values of ionisation probabilities and electron drift velocities.

Assuming a Maxwellian distribution, good agreement between experiment and theory was found for the diatomic gases air, N_2, and H_2.

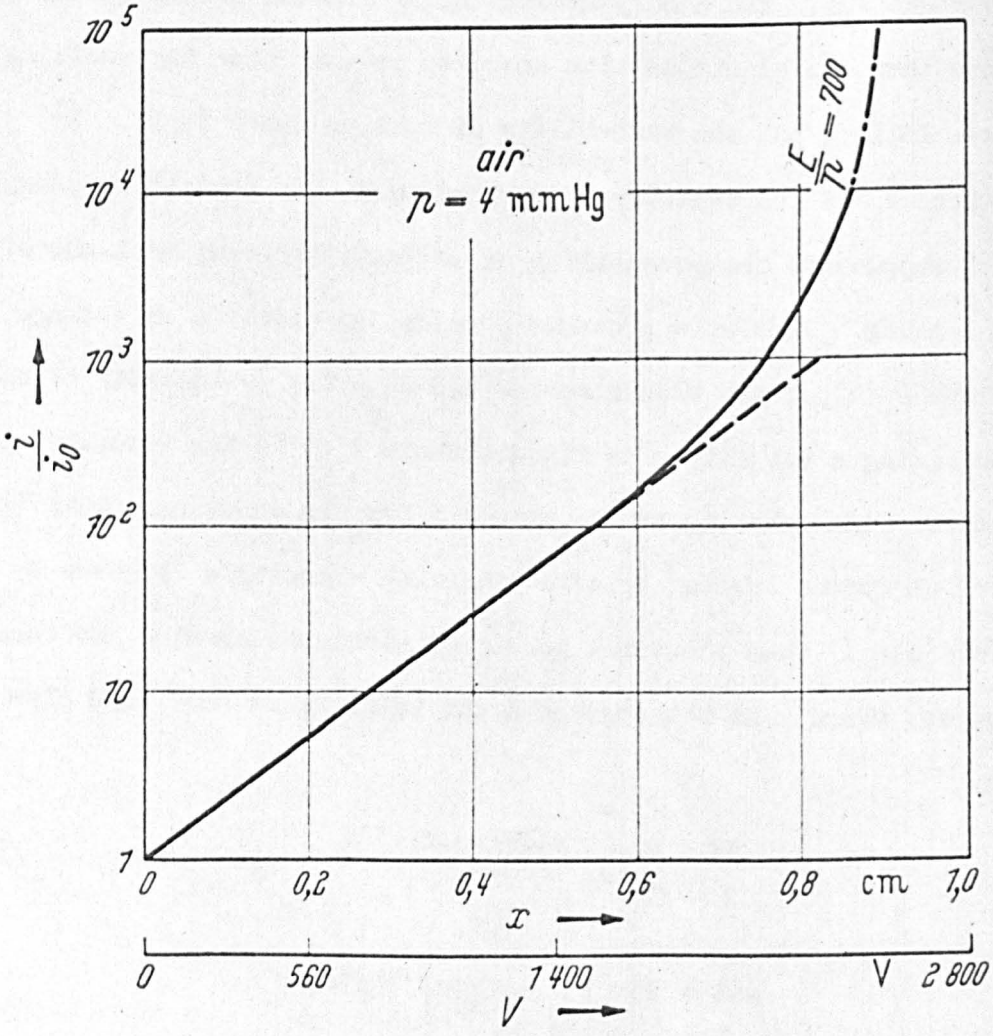

Multiplication i/i_0 as a function of the electrode spacing d or the applied voltage V at a constant and high value of E/p (700 V/cm. mm. Hg) in air at 4 mm. Hg.

fig 10

Agreement was not so good for the extreme high and low values of E/p_o. The agreement was bad for argon. The Ramsauer effect in argon fluctuates in such a manner as to give a distribution law with very few electrons in the high velocity tail, since inelastic impacts do not occur until about 10 eV is reached. The diatomic gases can undergo inelastic collisions to vibrational and rotational states at low electron energies resulting in a more even distribution of excited states which tends to reduce the Ramsauer effect and produce a distribution of energies that is approximately Maxwellian.

It can be seen that there is a great need for knowledge concerning the energy distributions in different gases before the function derived by Emeleus, Lunt and Meek can meet with any wide application. Until these data become available, useful approximations of α/P over limited ranges of E/p_o can be made by adjusting the constants A and B of the Townsend relation to form empirical expressions.

1.5 Breakdown

It was seen in section 1.4 that a plot of $\log_e I/I_o$ as a function of d was linear in the initial stages, and that the current through the gap could be expressed as

$$I = I_o \, e^{\alpha(d-d_o)}$$

where α is the primary ionisation coefficient given by the slope of the curve. As the electrode separation is increased further, however, the curve rises faster than linearly, indicating that some other processes producing ionisation are becoming important (fig. 10). As d increases to a value d_s the current is limited only by the external circuit

components and is independent of I_o. Under this condition electrical breakdown of the system is said to have occurred. The equation describing the spatial growth of ionisation is now modified to include growth at the higher values of d and is given by

$$I/I_o = \frac{e^{\alpha(d-d_o)}}{1-\omega/\alpha(e^{(d-d_o)}-1)}$$

where ω/α is known as the generalised secondary ionisation coefficient and is a function of E/p_o.

When the current tends to rise to infinity, the condition can be represented by the denominator of the above equation tending to zero. Thus the equation

$$1 - \omega/\alpha(e^{\alpha(d-d_o)}-1) = 0$$

can be taken as the criterion for breakdown. In terms of the coefficient η the breakdown criterion is

$$1 - \omega/\alpha(e^{\eta(v_b-v_o)}-1) = 0$$

where v_b is the breakdown voltage and is defined as the minimum voltage required for an infinitely small current to flow between the electrodes without the assistance of any external agency. The breakdown voltage is mainly determined by η and to a lesser extent by ω/α. The term $e^{\eta v_b}$ in the above equation is much greater than unity and hence the breakdown voltage can be represented by

$$v_b = (-\log_{\omega/\alpha})/\eta$$

Since ω/α varies little, especially at high E/p_o, as a first approximation v_b is inversely proportional to η. Thus an approximation to the curve of v_b as a function of E/p_o can be obtained by mirroring the

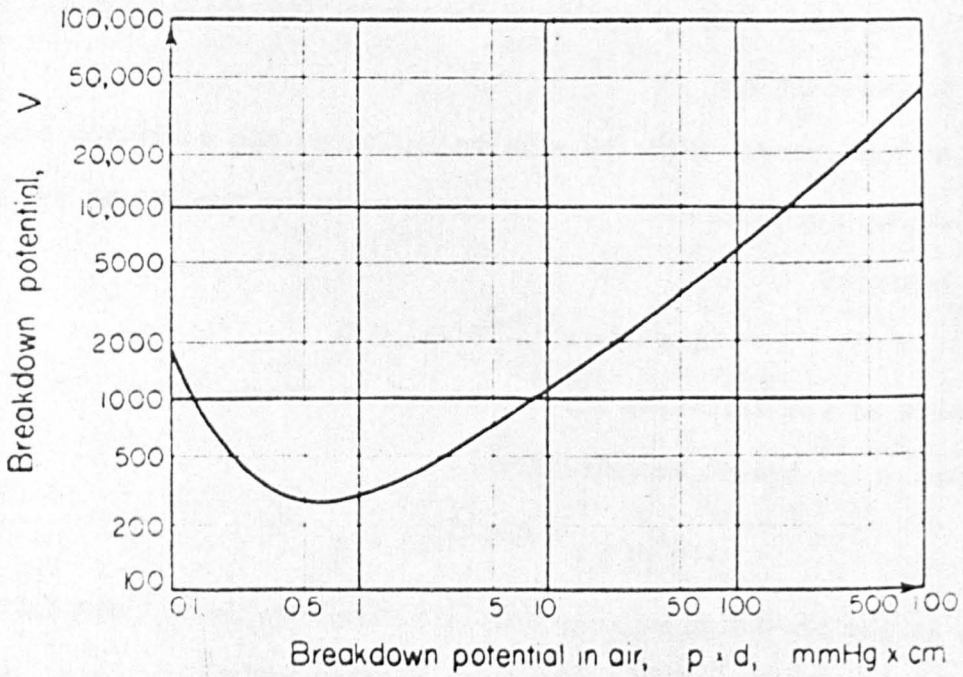
100,000
50,000
20,000
10,000
5000
2000
1000
500
200
100
Breakdown potential, V
0.1
0.5
1
5
10
50
100
500
1000
Breakdown potential in air, p x d, mmHg x cm

fig 11

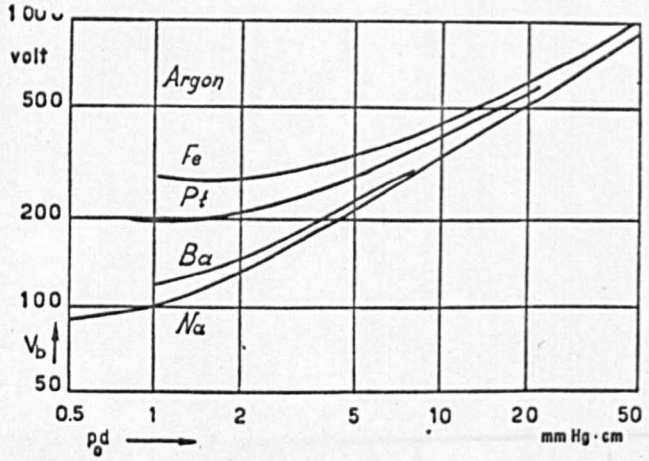

* Paschen curves for argon in conjunction with different cathode materials, on a double logarithmic scale.

fig 12

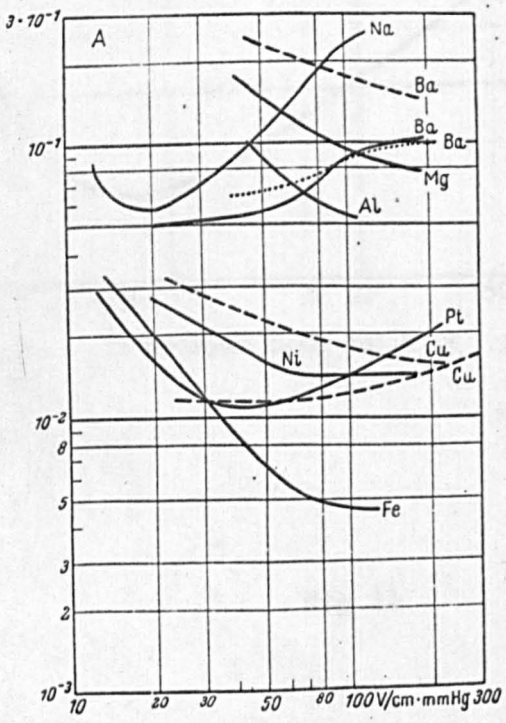

The secondary ionisation coefficient γ in argon as a function of X/p with various cathodes, according Jacobs and La Rocque (Al, Mg, Ba – – –); Ehrenkranz (Na, Pt); Schöfer (Ba ———, Ni); Engstrom (Ba ·····); Penning and Addink (Fe); Kruithof and Penning (Cu). p_0 is equivalent pressure at 0°C.

fig 13

curve of η as a function of E/p_o about a horizontal axis. However, it is often simpler to show v_b as a function of pd (gas concentration times electrode separation). Since v_b is a function of E/p_o, it is also a function of pd. Thus v_b is not dependent on p and d separately but on their product. This is known as Paschen's law. A typical Paschen curve for air is shewn in fig. (11).

Although for a given gas the shape of the Paschen curve is mainly determined by the shape of the η versus E/p_o curve, the cathode has an important influence through the magnitude of its work-function and state of cleanliness, etc. Thus the value of ω/α is of importance in comparing the breakdown voltages for different cathode materials. For instance, low breakdown voltages are associated with cathodes of alkali or alkaline earth metals, for which ω/α has high values. This is illustrated in fig. (12) in which Paschen curves for argon with different cathode materials are plotted, and in fig. (13) in which ω/α for different cathode materials in argon is plotted as a function of E/p_o.

1.6 Possible Secondary Mechanisms

As the primary electrons traverse the space between the electrodes, they interact with the gas molecules producing excited atoms and positive ions which must be the source of any secondary ionisation assuming that field emission, thermionic emission, thermal ionisation and auto-ionisation are absent. Such assumptions are justified when using a plane, parallel, cold cathode system with low current density. Possible sources of secondary ionisation are therefore excited and

metastable atoms, photons and positive ions, all or any of which may interact with the gas or cathode.

1.6.1 The action of excited atoms and resulting radiation

Because of the exponential growth of current across the gap, the vast majority of excitations and ionisations occur in the region close to the anode. The life-time of an atom excited to a resonance level is about 10^{-8} sec. Return to the ground state is therefore practically instantaneous and there is little or no chance of the atom diffusing to the cathode and causing the emission there of an electron. Collisions between excited atoms and those in the ground state cannot lead to ionisation in pure gases, since the ionisation energy is greater than the excitation energy. The process may be important in gas mixtures, where the excitation potential of one atom is higher than the ionisation potential of the other. The process may be particularly important when the atom is excited to a metastable level. The process is known as the Penning effect and Penning and Addink (13) have shown that small amounts of argon in neon can affect the breakdown voltages.

When two excited atoms collide one of them can become ionised, provided the sum of their excitation energies is greater than the ionisation energy. The process is most efficient when the excitation energies are about half the ionisation energy and when the excited atoms are in large concentration.

Metastable atoms have a relatively long life, about 10^{-1} sec. and at a pressure of 1mm.Hg. a metastable atom may have as many as

10^8 collisions. There is thus ample opportunity for the volume destruction of metastables by the raising to normal excited states with the subsequent emission of a photon by collisions with electrons or absorption of quanta or collision with other atoms. The energy relationship must be

$$h\nu \text{ or } \tfrac{1}{2}\cdot mv^2 \geq E_i - E_e$$

The long life of a metastable atom allow the possibility of diffusion to the cathode with the subsequent emission of an electron, providing $E_m > e\phi$. The coefficient for this process, γ_m, can be shown to depend on the electrode geometry of the system. The metastables formed near the anode will all diffuse to it since their concentration at the anode is zero and the concentration gradient is large. This means that the fraction of metastables moving towards the cathode is a function of the electrode separation and decreases rapidly towards the anode. Assuming infinitely plane parallel electrodes, Newton (14) has shown that

$$\gamma_m = \text{const.} \left(N + \frac{1}{\alpha d}\right)$$

where N is the mean free path of metastables moving in a gas of normal atoms. Thus γ_m falls as d increases even if the cathode is assumed to be of infinite diameter. With electrodes of finite dimensions γ_m is likely to be reduced further by diffusion of metastables from the discharge volume.

The light quanta produced in a gas discharge are of two main types: resonance radiation, resulting from the decay of normal excited atoms or metastable atoms that have been raised to some higher excited

state, and non-resonance radiation or collision induced radiation, the result of a collision which sufficiently perturbs the metastable atom to give rise to radiation by breaking the selection rules. The resultant photon can then cause emission of an electron at the cathode by the photo-electric effect, a process demonstrated to be of importance in the breakdown of helium by Llewellyn-Jones et al (15).

When photons collide with atoms they produce results analogous to those caused by electrons of equivalent energy. Thus photons are able to excite an atom when they have the required excitation energy, and an atom in the ground state can only be ionised by a photon of frequency ν if

$$h\nu \geq eV_i$$

where V_i is the ionisation potential and h is Plank's constant. The process is most efficient when $h\nu=eV_i$ when the photon gives up the whole of its energy. In a pure gas photons emitted by excited atoms will have energies less than eV_i and photoionisation can only occur by a cumulative process. Rouse and Giddings (16) have shown that mercury vapour is ionised by its resonance radiation by the transition $^3P_1 \rightarrow {}^1S_0$ (Fig. 3). The energy associated with the transition is only 4.86 eV, as compared with V_i=10.4 eV. The ionsiation process is probably

$$Hg + h\nu \rightarrow Hg(6^3P_1)$$

$$Hg(6^3P_1) + Hg(6^3P_0)_{metastable} \rightarrow Hg_2^+ + e$$

The second step is a collision between an excited atom and a metastable atom resulting in a molecule with potential energy of about 9.6 eV.

Together with the heat of dissociation, 15 eV, this is sufficient to ionise the molecule.

In gaseous mixtures, photo-ionisation can be important when the resonance radiation of one type of atom has energy greater than or equal to the ionsiation energy of the second type. The process has been used by Loeb and Meek (17) and Reather (18) to explain the streamer mechanism.

The importance of photo-ionisation is a gas can only be appreciable where high densities of excited and metastable atoms occur. Photo-electric emission at the cathode is likely to be of greater importance where the energy $h\nu$ must be such that $h\nu \geq e\phi$ where $e\phi$ is the work function of the cathode surface. Resonance photons produced near the anode can reach the cathode unscattered (δ process) or alternately may be hindered in their motion through the gas by repeated emission and absorption by ground state atoms. This inprisonment of radiation may result in a considerable delay in the arrival of the photons at the cathode. The delay will depend on the cross-section for absorption and the life-time of the particular resonance state.

1.6.2 Secondary ionisation due to positive ions

For an elastic collision between a positive ion and a neutral gas atom, the energy loss can be written as

$$\delta E_i = \frac{2nM}{(n+M)^2} E_i$$

where n is the mass of the positive ion and M is the mass of the gas atom. Since $n \simeq M$

$$E_i \simeq \frac{2m^2}{4m^2} E_i = \tfrac{1}{2} E_i$$

Thus a positive ion loses half its energy in elastic collisions with gas atoms and at all but very low gas densities, where E/p_o is very high, will not gain much energy from the applied field. The energy of the ions will, therefore, not be very much greater than the thermal energies of the neutral atoms. Thus the probability of an inelastic collision resulting in excitation or ionisation will be extremely small. The probability of charge transfer, though great at low kinetic energies, will result in neutral atoms with velocities little different from the normal thermal distribution. The efficiencies of positive ions and the neutral atoms resulting from charge transfer, as ionising agents, will be very low and they may, therefore, be neglected.

Positive ions can, however, liberate electrons from metal surfaces. The phenomenon has been examined by Oliphant (19) and by Oliphant and Moon (20) and by Massey (21). It has been shown that the efficiency of the process depended on the ionisation potential of the atom and the work function of the surface; the efficiency increasing as the former increased and the latter decreased. The mechanism involved may be two-fold, depending on the energy of the ions. The incidence of high energy positive ions on a cathode has been considered by Kapitza (22) to cause a transfer of kinetic energy of the ion to thermal energy of electrons resulting in thermionic emission from the cathode. The energy distribution of electrons produced by positive

ions as determined by Oliphant and Moon is such as would be expected if the process were thermionic.

When the energies of the ions are of the order of thermal energies, as in Townsend discharges, another mechanism becomes important. An ion approaching the cathode may become an excited atom by the transport of an electron from the cathode to the ion, moving between states of equal energy. The transition is most probable when

$$e\phi = E_i - E_a$$

where $e\phi$ is the work function of the cathode, and E_i and E_a are the energies of ion and atom respectively. If the excited atom collides with the cathode before radiation occurs, the atom may give up its potential energy to a metallic electron, which may be ejected in a collision of the second kind. For this to occur $E_i \geq 2\ e\phi$.

An ion of sufficient velocity may penetrate the potential barrier before capturing an electron by resonance transition. The excited atom can then give up its energy to a second electron, giving a normal unexcited atom and an electron. For this to occur, the energy relation must be

$$E_f = E_i - e\phi$$

where E_f is the energy at the top Fermi-level.

1.7 Conclusion

From the above discussion of the possible secondary processes in Townsend discharge, it can be seen that secondary ionisation phenomena occurring in the gas depend on high concentrations of excited atoms.

Since the probability of excitation for most gases is small, about 10^{-2} (23), then such processes only become important at high pressures, about 760 mm.Hg. The more important processes are likely to involve emission from the cathode. A decision as to the relative importance of these processes cannot be obtained from the current growth curves, since each process leads to an equation of the same analytic form as the general Townsend formula (24), ω/α being a composite coefficient depending on which combination of secondary processes is prevalent. Studies of the temporal growth of current to breakdown can solve this problem. For instance, if electron emission from the cathode due to positive ions is operative, the delay time $\frac{d}{W+} \simeq 10^{-5}$ sec, where d is the gap separation and W+ the ion drift velocity. Similarly if the incidence of unscattered photons is dominant then the delay time is of the order $d/W_- \simeq 10^{-6}$ sec. where W_- is the electron drift velocity. Likewise metastable atoms involve a delay time $d^2/D \simeq 10^{-3}$ sec. where D is the diffusion coefficient for metastables. The temporal growth of ionsiation will be studied in the next chapter.

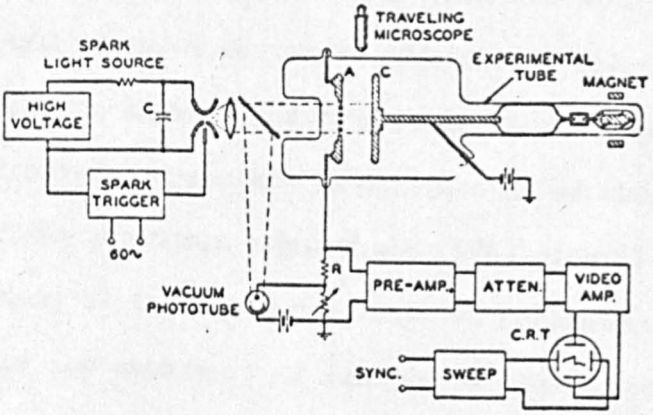

Experimental arrangement for studying the microsecond transient current.

fig 14

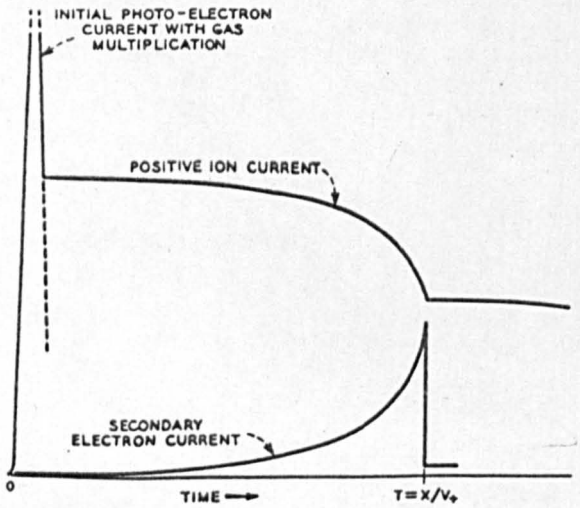

Varney's schematic curves for current components to his exact solution of the fast-current equation in plane parallel geometry.

fig 15

CHAPTER 2

THE TEMPORAL GROWTH OF IONISATION

2.1 Introduction

There are two approaches to the temporal growth of ionisation in a Townsend discharge. The approach of Hornbeck(25) and Varney (26), and of Molnar (27) is aimed at the direct measurement of the secondary coefficient as a result of the action of positive ions and metastables at the cathode. The second approach, which is presented in its most complete form by Davidson (28) aims at the interpretation of formative time lags in terms of ratios of the different coefficients.

2.2 The Approach of Varney

Hornbeck's initial purpose was to evaluate γ_i, the number of electrons liberated at the cathode per incident positive ion. His analysis, however, would not allow γ_i to be evaluated with any precision. Varney used similar apparatus to determine γ_i to that employed by Hornbeck. A diagram of the apparatus is shewn in fig. (14).

A flash of light of duration about 10^{-7} seconds, produced from an air spark-gap is focussed on the cathode of a discharge tube. The resulting photo-electrons are accelerated by the applied field, which is less than that required for breakdown. The positive ions produced by the interaction of primary electrons with gas molecules drift to the cathode and there liberate secondary electrons. An oscilloscope is used to display the current which consists of an electron and a positive ion component, as a function of time. A typical trace is shewn in fig. (15).

Varney shewed that the electron component i_- and the positive ion component i_+ were given by the following relations,

$$i_- = \frac{n_o \varepsilon V_+}{d} \left(\gamma_i (e^{\alpha d} - 1) e^{\alpha V_+ (1+\gamma_i) t}\right) \qquad (2.1)$$

$$i_+ = \frac{n_o \varepsilon V_+}{d} \left(\left(\frac{\gamma_i e^{\alpha d}}{1+\gamma_i} - 1 \right) e^{\alpha V_+ (1+\gamma_i) t} + \frac{e^{\alpha d}}{1+\gamma_i} \right) \qquad (2.2)$$

if $0 \leq t \leq d/V_+$, where d is the electrode separation, V_+ the positive ion drift velocity, ε is the electronic charge, n_o the number of electrons liberated by the flash, and α is the first Townsend ionisation coefficient. The total current i, given by

$$i = i_+ + i_-$$

is therefore equal to

$$i = \frac{n_o \varepsilon V_+}{d} \left\{ \left[\gamma_i (e^{\alpha d} - 1) + \frac{\gamma_i}{1+\gamma_i} (e^{\alpha d} - 1) \right] e^{\alpha V_+ (1+\gamma_i) t} + \frac{e^{\alpha d}}{1+\gamma_i} \right\} \qquad (2.3)$$

The appearance of a horizontal oscilloscope trace means that the current is constant with time, since d and V_+ are constant. Thus the time dependent term in equation (2.3) vanishes if the coefficient of the term is zero, viz;

$$\gamma_i (e^{\alpha d} - 1) + (\gamma_i / 1+\gamma_i)(e^{\alpha d} - 1) = 0$$

or

$$\gamma_i = \left[e^{\alpha d} / (e^{\alpha d} - 1) \right]^{\frac{1}{2}} \qquad (2.4)$$

Thus if α and d are known, γ_i can be found.

2.3 The Approach of Molnar

A Townsend discharge was stimulated by photo-electrons generated

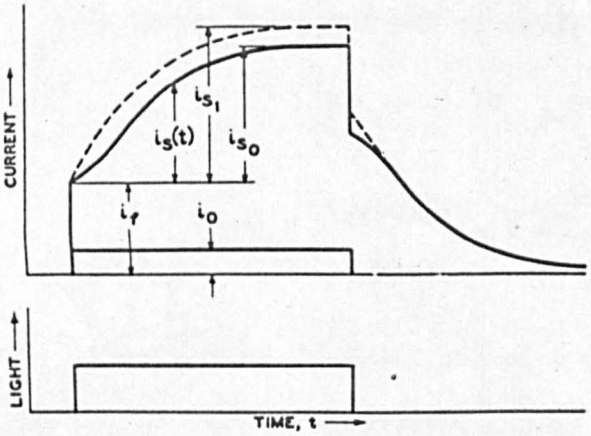

. Diagram illustrating the theoretical curve forms of current versus time to be expected from metastable action in the Townsend gap of figure 9.33, as observed oscilloscopically by Molnar.

fig 16

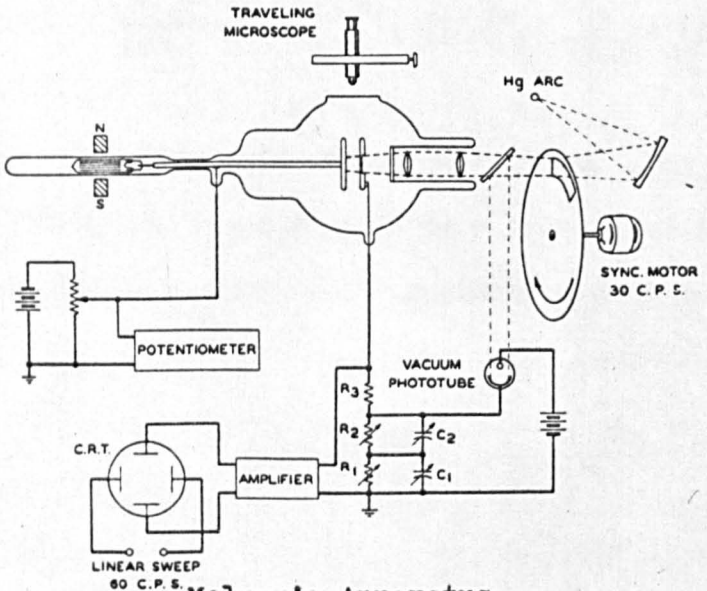

Molnar's Apparatus.

fig 17

by a shuttered light beam focussed on the cathode of a gas filled tube. The transient character of the resulting current between the electrodes was observed with an oscilloscope. The current, fig. (16), was composed of a component closely in step with the stimulating light pulse, and a component which lagged by the order of a millisecond. This component was attributed to the action of metastable atoms. The fast component includes the primary electron current amplified by ionisation and emission due to ion and photon effects, which reaches a steady state after about 10 micro-seconds. From the analysis of such traces the fraction of emission due to metastables, ions and photons could be obtained. The experiment was thus more comprehensive than that designed by Hornbeck and Varney, in which only γ_i, the contribution due to positive ions, could be established.

A diagram of the apparatus is shown in Fig. (17). The actual current measurement was made by employing a null method. By means of a partially reflecting mirror, some of the light was directed into a vacuum photo-tube, which then generated a current pulse exactly in step with the primary current in the Townsend tube. This current flowed through two resistor-capacitor combinations, R_1C_1 and R_2C_2, by means of which a voltage pulse could be formed similar in shape and size to the Townsend current but opposite in sign. The fast component of the Townsend current could usually be matched closely with an RC combination having a time constant of 0.1 to 30 milliseconds. When these components were adjusted to a best fit to the Townsend current there remained a component negative in amplitude and intermediate in

time constant. The amplitude of this component was measured by the decrease necessary in the fast component to bring the current trace up to the base line.

Molnar showed that ω/α (designated γ) was given by

$$\gamma = f_{esc} \{\gamma_i + \frac{\alpha_r}{\alpha_i} f_{rk} \gamma_r + \frac{\alpha_m}{\alpha_i} f_{mk} \gamma_m + f_{mr} f_{rk}, \gamma_r\} \qquad (2.5)$$

where γ_i, γ_r, γ_m represent the number of electrons liberated at the cathode per ion, per photon and per metastable respectively, and α_i, α_r, α_m represent the number of ions, photons and metastables produced per cm. per electron; f_{esc} is the fraction of electrons liberated at the cathode which enter the discharge stream; f_{rk}, f_{mk} are the fractions of photons and metastables generated in the gas which reach the cathode; f_{mr} is the fraction of metastables generated in the gas which are converted to radiating atoms; f_{rk}, is the fraction of photons from these atoms which reach the cathode.

The fast component of the current is given by the Townsend equation with the γ coefficient given by γ_{fast}, where

$$\gamma_{fast} = f_{esc} \left(\gamma_i + \frac{\alpha_r}{\alpha_i} f_{rk} \gamma_r\right) \qquad (2.6)$$

and the total current is described by the Townsend equation with

$$\gamma = \gamma_{fast} + \gamma_{slow}$$

where

$$\gamma_{slow} = f_{esc} \left(\frac{\alpha_m}{\alpha_i} f_{mk} \gamma_m + \frac{\alpha_m}{\alpha_i} f_{mr} f_{rk}, \gamma_r\right) \qquad (2.7)$$

Molnar made detailed time constant studies of the slow component of the current. He measured the time constant of the slow component T_1, the amplitude of the fast component i_f, the slow component, i_{s_1}, and the intermediate, i_{s_2}, component for various applied voltages. T_1 was shown to be related to the time constant of decay of metastables, τ_1, by

$$\tau_1 = T_1 \frac{i_f + 1.3\, i_{s_2}}{i_f + 1.3 i_{s_2} + i_{s_1}} \qquad (2.8)$$

τ_1 is related to the diffusion constant of the metastable D_m, and the probability of volume destruction per second in the gas, G, by the relation

$$\frac{1}{\tau_1} = \frac{\pi^2 D_m}{d^2} + G \qquad (2.9)$$

Plots of $1/\tau_1$ against π^2/d_2 therefore yield straight lines with slope D_m and intercept G. The technique thus allows the evaluation of D_m. This was determined for argon, neon and xenon.

A radiation conversion process was used to measure the relative amount of electron emission produced by a metastable drifting to the cathode compared with a photon of the same energy. Two experimental arrangements were employed. In the first, external radiation from a line source was focussed so as to go through a small region between the electrodes either near the anode, in the middle or near the cathode. In the second arrangement a ring-shaped discharge tube was placed around the discharge volume. The radiation was difficult to focus but better conversion was obtained. Only the experiments using the first arrangements will be described here.

The discharge through the tube was maintained steady, and the side light pulsed. The current was found to rise immediately on application of the side light and then to decrease slowly. When the side light was cut off the current dropped suddenly and then returned slowly to its steady state value. The side light had two effects: that of increasing the number of photons striking the cathode, and that of decreasing the metastable density in the region through which the light was passing.

The sudden increase in current when the light was switched on was due to the increase in the incidence of photons at the cathode. The slow decrease was caused by the diminution of the number of metastables available to diffuse to the cathode. The net reduction of current with the light on showed that photons were less effective than metastables in producing electron liberation at the cathode.

The time constant of the slow component was measured with and without the side light, and τ_1 computed for the two cases. Now $(\pi^2/d^2)D_m$ includes the contribution of diffusion losses to $1/\tau_1$, and G the effect of volume destruction. With the light off, G includes only the normal volume loss, G_c. With the light on G also includes the volume loss caused by radiation, G_s. Therefore, the difference in $1/\tau_1$ for the two cases gives a measure of G_s. The quantities $\pi^2 D_m/d^2$ and G_c and G_s are also, to a first approximation, a measure of the rate at which the metastables are destroyed at the electrodes, in the gas by collision and in the gas by radiation. It is assumed that half of the photons released by either type of volume destruction will

will go to the cathode. Thus the quantities

$$\frac{\pi^2 D_m/2d^2}{(\pi^2 D_m/d^2)+G_c} \text{ and } \frac{G_s/2}{(\pi^2 D_m/d^2)+G_c} \tag{2.10}$$

represent the fractions of the excitation energy of the metastables which without the side light reach the cathode by metastables and photons respectively. Immediately after the side light is turned on the rate of arrival of metastables remains unchanged but the rate of arrival of photons changes suddenly by the factor $\frac{G_c+G_s}{G_c}$. Then, gradually, a new steady-state is set up for which the fractional carriers of energy are given by the above expression, except that G_c is replaced by G_c+G_s.

The measurement of γ_r/γ_m is made using the amplitude of the slow component either immediately the light is turned on or using the value of this component after the new equilibrium has been obtained. Molnar employed the former method.

The quantities $\pi^2 D_m/d^2$, G_c and G_s are established from time constant studies. The magnitude of the slow component just before the side light is turned on, s, and its value just afterwards, $s+\delta s$, is measured. Both s and $s+\delta s$ will be directly proportional to the electron currents leaving the cathode due to the combination of metastables and photons from converted metastables striking the cathode, i.e.

$$\delta s/s = G_s\gamma_r/\gamma_m(\pi^2 D_m/d^2) + \gamma_r G_c \tag{2.11}$$

Therefore,

$$\gamma_r/\gamma_m = (\delta s/s)(\pi^2 D_m/d^2)/(G_s-(\delta s/s)G_c) \qquad (2.12)$$

All the quantities on the right hand side are measurable and γ_r/γ_m can be evaluated directly, to an accuracy of about ±20%, the main source of error being the electrical noise induced in the Townsend current by the operation, in close proximity, of the light source. The average value of γ_r/γ_m was 0.40 for tantalum, 0.08 for molybdenum and 0.10 for a barium oxide cathode.

α_i was determined by a trial and error method. A value of α_i was assumed and together with the ratio of i_+/i_o taken for different values of electrode separation, d, at constant E/p_o, α_+ was computed from the Townsend equation. The values of α_i which made α_+ constant with d were accepted as the 'best' values. Values of γ and γ_+ were computed from i/i_o and i_f/i_o data, and γ_s obtained from the relation $\gamma=\gamma_f+\gamma_s$.

Molnar was further able to show that the following relation held:

$$f_{esc}\left(\alpha_m\gamma_m+\alpha_m\gamma_r(Gd^2/\pi^2D_m)\right)$$

$$= \{\alpha_i i_o i_{s_1}/i_f(i_{s_1}+i_f)\}\ (1+Gd^2/\pi^2D_m)H \qquad (2.13)$$

where H is a function of α_i, α and $\alpha_i\alpha_o$. Thus if the right hand side of the expression is plotted as a function of Gd^2/π^2D_m then a straight line with slope $\alpha_m\gamma_r f_{esc}$ and an intercept of $\alpha_m\gamma_m f_{esc}$ results. Thus if f_{esc} is known, $\alpha_m\gamma_m$ can be determined.

The quantity f_{esc}, in the expression for γ, is evaluated by making detailed measurements of the current at low voltages, and was determined

as 2.56×10^{-8} amps, the value observed for an E/p_o of 400 in the region of 8 to 14 volts. The fraction of this value at 14 volts for other values of E/p_o was assumed to be a measure of f_{esc}.

Molnar was thus able to measure f_{esc}, α_i, γ_+, γ_s, $\alpha_m\gamma_m$ and γ_r/γ_m. The quantities α_m and α_r could not be measured, and were taken from Kruithoff (29), who evaluated the ratio $(\alpha_m+\alpha_r)/\alpha_i$ as a function of E/p_o for the rare gases. γ_m values were then calculated from α_m and $\alpha_m\gamma_m$. γ_r was then computed from the ratio γ_r/γ_m. Finally, $(\alpha_r/\alpha_i)f_{rk}\gamma_r$ was computed, assuming $f_{rk}=0.4$ (the grounds for this assumption are not made clear), from which γ_i could be computed from γ_+ and f_{esc}. The values of γ_i and γ_m were accurate to about 20% and were found to be similar in magnitude.

2.4 The Approach of Davidson. Formative Time Lags

The total time taken between the application of a potential difference greater than or equal to the breakdown potential, and breakdown is known as the total time lag, t. The time, t_s, which elapses between the application of the voltage and the appearance of an initiatory electron is called the statistical time lag, since the appearance of such electrons is statistically distributed. After the appearance of such an electron the time, t_f, taken for the gap to break down, is called the formative time lag. Thus

$$t = t_s + t_f$$

In practice, the statistical time lag can be eliminated by irradiating the cathode with ultra-violet light, thus ensuring an adequate supply of initial electrons at all times. The total time lag can

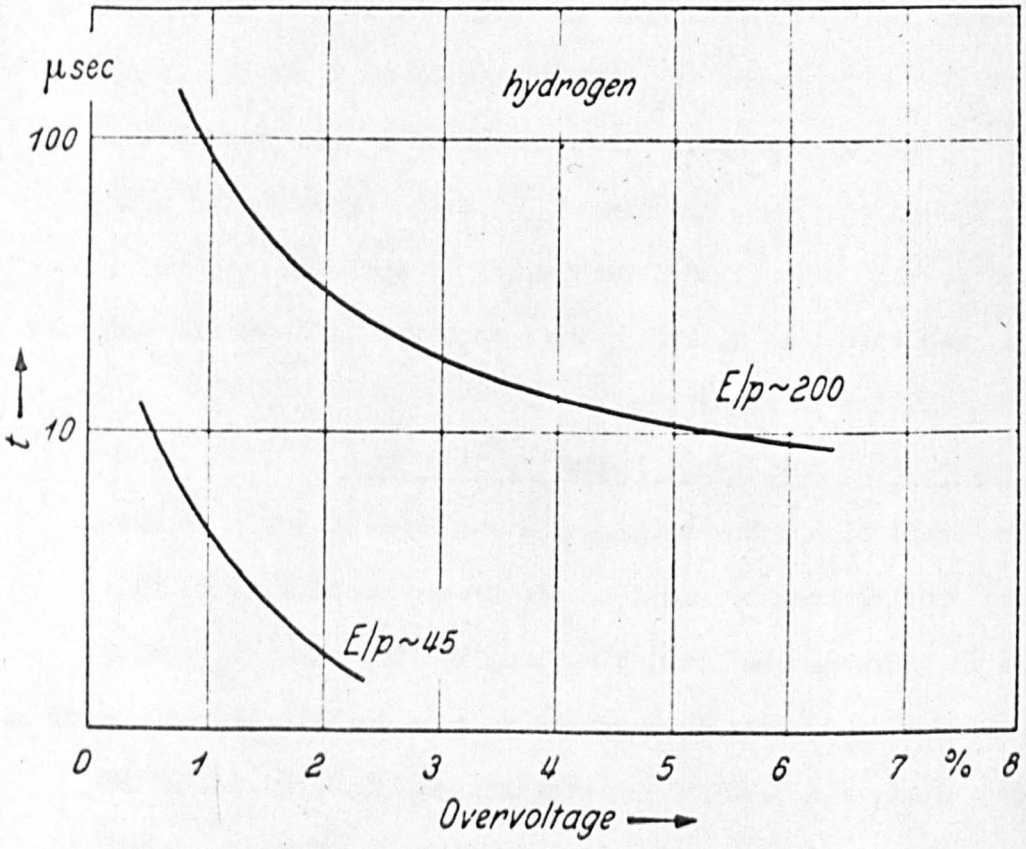

Formative time lags in hydrogen.

fig 18

then be equated with the formative time lag.

The formative time lag at any given E/p_o will be related to the speed of the various secondary processes. Hence a study of formative time time lags should make it possible to estimate the relative importance of the different processes. The method is that of assuming values for the coefficient of each process as a fraction of ω/α and using these to calculate a theoretical curve of formative time lag against per cent overvoltage. These curves can then be compared with those obtained by experiment. Typical experimental curves for hydrogen, where only two processes are possible, those of positive ion action and photon action at the cathode, are shown in fig. (18).

The original theory by Davidson (30), gave an exact solution to the problem of ionisation growth involving the primary, α, process and the action of positive ions, (γ process) and undelayed photons, (δ process) at the cathode. The later theory (28) given below takes into account the action at the cathode of metastable atoms, (ε process) and scattered resonance radiation (δ_3 process).

The scattered radiation process is treated as a diffusion process. Photons emitted by atoms which have been excited by the electron current may be strongly absorbed by ground state atoms and after a mean time interval, τ, re-emitted with scattering. They thus proceed to the cathode by a process of diffusion due to repeated scattering. Since metastable atoms are uncharged, their motion is entirely due to diffusion and may reach the cathode by this process if not destroyed in the gas with the liberation of an active photon.

The formulae employed to represent the diffusion of repeatedly scattered photons resenble the formulae which represent the diffusion of metastable atoms and advantage is taken of this fact. The two cases were referred to as cases (b) and (a) respectively.

To investigate the spatial and temporal growth produced by processes depending on diffusion, it is assumed that initially the only process operating is of this type. It is further assumed, both in case (a) and case (b), that the internal destruction produces no active photons capable of reaching the cathode either directly or by diffusion. The treatment was then generalised to include the case where all possible secondary processes are acting simultaneously.

Two plane parallel electrodes, of separation d, with the cathode (x=0) being exposed to a constant radiation producing a photo-electric current I_o, are considered. At time zero the potential difference of the plates is increased to a value V above the breakdown potential V_s and maintained. A region of the gas at distance x from the cathode is then considered, and the diffusion equation which the active particles satisfy is given as

$$\partial n(x,t)/\partial t = -\partial j(x,t)/\partial x + \alpha_1 e^{\alpha x} i_-(t-x/w_-) - n(x,t)/\tau_i \qquad (2.14)$$

where n(x,t) is the spatial density of the active particles, j(x,t) is their current density in the x direction, α the first Townsend ionisation coefficient, α_1, the number of active particles generated by an electron moving unit distance in the x direction, w_- the electron drift velocity, $1/\tau_1$ the fraction of active particles in any region

which are destroyed per unit time by collision with ground state atoms and i_- the electron current density at the cathode. i_- and n are assumed so small as to justify neglect of quantities proportional to their product (e.g. the destruction of metastable atoms by electrons). The current density, j, is related to the diffusion coefficient by

$$j = -D\, dm/dx$$

As D is taken to be constant in space, $-\partial j(x,t)/dx$ becomes $D\partial^2 n(x,t)\partial x^2$. Thus the diffusion equation becomes

$$\frac{\partial n}{\partial t}(x,t) = D.\frac{\partial^2 n}{\partial x^2}(x,t) + \alpha_1 i_- e^{\alpha x}(t-x/w_-) - \frac{n(x,t)}{\tau_1} \qquad (2.15)$$

The diffusion coefficient D is defined differently for cases (a) and (b). In case (a), $D=D_m$ which is an ordinary atomic or molecular diffusion coefficient and is given approximately as $\frac{1}{3}\ell_m\bar{v}$ where ℓ_m is the mean free path of the metastables and $\bar{v}$ their mean kinetic velocity. In case (b), $D=D_p$ which is given approximately by

$$D_p = \frac{1}{3}\ell_p/\left[\tau + (\ell_p/c)\right](1-F) \qquad (2.16)$$

when the current density of bound photons is neglected. F is the fraction of the original momentum retained by the photons on re-emission from the bound state, ℓ_p is the collision mean free path of the photons, τ the mean time for which a photon remains bound and c/ℓ_p the fraction of free photons which become absorbed per unit time. Since the current of photons is not accurately monochromatic and since the absorption of photons is a resonance phenomenon, any spatial

variation in their frequency distribution will be accompanied by a spatial variation in ℓ_p and hence in D_p. Thus it is not certain on inserting D_p into the diffusion equation that an accurate equation is obtained with D_p constant in space and time. Thus the diffusion equation with constant D may not apply to trapped radiation with the same accuracy as it does to metastable atoms.

Davidson next considers the boundary conditions of the diffusion equation. Assuming that the fraction, g, of the number, N, of active particles striking the cathode per unit time destroyed in so doing is not greater than 1/5 the resulting asymmetry in the directional distribution of the active particles near the cathode can be ignored. Thus for $g < 1/5$, Davidon writes, in case (a),

$$N = \tfrac{1}{4}\, n\bar{v} \text{ and } D(\partial n/\partial x) = g.\tfrac{1}{4}.n\bar{v} \qquad (2.17)$$

that is $n = h\partial n/\partial x$ at $x=0$, where

$$h = 4D/g\bar{v} = \frac{4}{3} \cdot \frac{\ell_m \bar{v}}{g\bar{v}} = \frac{4}{3}\, \ell_m$$

If G is the fraction of active particles destroyed on striking the anode, then

$$n = -H.\partial n/\partial x \qquad \text{at } x=d \qquad (2.18)$$

where

$$H = \frac{4}{3}\, \ell_m/G$$

At the cathode a fraction of the active particles destroyed, g_1,

will cause the emission of an electron. If there is an externally maintained electron current density at the cathode, I_o, then

$$i_- = I_o + g_1 D(\partial n/\partial x) \quad \text{at } x=0 \tag{2.19}$$

Consideration is now given to case (b). The D in the last equation must be replaced by

$$D = \tfrac{1}{3}\, \ell_p^2/\left[\tau + (\ell_p/c)\right](1-F)$$

and N by

$$N = \tfrac{1}{4}\, nc/\{(c\tau/\ell_p) + 1\}$$

Thus at x=0, it can be written that

$$D(\partial n/\partial x) = \tfrac{1}{4}\, g.n.c./\{(c\tau/\ell_p) + 1\}$$

In the expressions for n (equations 2.17 and 2.18) h now becomes

$$h = \frac{4\ell_p}{3} / (1-F)G \qquad \text{and} \qquad H = \frac{4\ell_p}{3} /(1-F)G$$

If n and i_- are constant in time, a steady state is attained and the diffusion equation can be written as

$$D\, \partial^2 n/\partial x^2 + \alpha_1\, i_-\, e^{\alpha x} = n/\tau_1 \tag{2.20}$$

with the boundary conditions as defined above, that is

$$n = h\partial n/\partial x \qquad \text{at } x=0$$

$$n = -H\, \partial n/\partial x \qquad \text{at } x=d$$

$$\text{and } i_- = I_o + g_1\, D(\partial n/\partial x) \text{ at } x=0$$

The equation is integrated to give

$$i_-/I_o = 1/\{1 - \frac{X}{\alpha^2-\mu^2}\left(\frac{e^{\alpha d}-\cosh \mu d - \alpha(\sinh \mu d)/\mu}{\sinh \mu d/\mu}\right)\} \qquad (2.21)$$

providing g and G are large enough to make h=H=0

$$X = g_1\alpha_1, \qquad \mu = 1/\sqrt{D\tau_1}$$

When μd (but not αd) is a small fraction, the ratio i_-/I_o becomes

$$i_-/I_o = 1/\{1 - \frac{X}{\alpha^2 d}\left(e^{\alpha d} - \alpha d - 1\right)\} \qquad (2.22)$$

After considering the steady state Davidson turns his attention to the problem of current growth in time. The gas is assumed to be free from active particles and electrons up to the time, t=0, at which the externally generated cathode current I_o is established. Concerning the quantities n(x,t) and $i_-(t)$ the following conditions are given as sufficient to determine these quantities at all times

(i) at $t < 0$, $n(x,t) = i_-(t) = 0$

(ii) at $t > 0$, $i_-(t) = I_o + g_1 D\, \partial n(x,t)/\partial x$ at $x=0$ (2.23)

(iii) at $t > 0$, $n(0,t) = n(d,t) = 0$

(iv) at $t > 0$ the differential diffusion equation holds throughout the gas

The folbwing contour integrals are given as a solution to this equation satisfying the above four conditions.

$$\frac{n(x,t)}{I_o} = \frac{i\alpha_1}{\pi D}\int_c \frac{Z\, e^{D(Z^2-\mu^2)t}}{(Z^2-\mu^2)\theta}\left[(1-e^{-2Zd})e^{\psi x} + (e^{(\psi-Z)d})e^{-Zx} + (e^{-2Zd} - e^{(\psi-Z)d})e^{Zx}\right] dZ \qquad (2.24)$$

$$\frac{i_-(t)}{I_o} = \frac{i}{\pi}\int_c \frac{Ze^{D(Z^2-\mu^2)t}(Z^2-\psi^2)(1-e^{-2Zd})dZ}{(Z^2-\mu^2)\theta} \tag{2.25}$$

where $\psi = \alpha - D(Z^2-\mu^2)/w$ (2.26)

$$\theta = \xi + \{2XZe^{(\psi-Z)d} - (2XZ+\xi)e^{-2Zd}\} \tag{2.27}$$

$$\xi = \{Z+\psi\}\{(Z-\psi)F-X\} \tag{2.28}$$

$$F = 1 \tag{2.29}$$

The purpose of introducing the symbol F which in the present case is unity is explained later.

It is further shown that at all positive times i_-/I_o is the real part of

$$A + \sum \frac{2\lambda(\lambda^2-\psi^2)(1-e^{-2\lambda d})e^{D(\lambda^2-\mu^2)t}}{(\lambda^2-\mu^2)(\partial\theta/\partial Z)\lambda} \tag{2.30}$$

where A is given by the right hand side of equation (2.21) and is shown to be given by

$$i_-/I_o \; 1/\{1 - \frac{X}{\alpha}(e^{\alpha d}-1)\} \tag{2.31}$$

if volume destruction can be negelcted. The summation extends over all values of λ of Z (other than θ or μ) which satisfy $\theta(Z)=0$ and which lie on the positive real or positive imaginary axes or in the quadrant bounded by them. The character of λ, all values of which lie on the axes, depends on the sign of the quantity, A. At large times and A positive a steady state is established and the ratio reduces to A. If A is negative, the case when the breakdown potential is exceeded, one of the values of λ is real and greater than μ and thus contributes to the current A term which increases exponentially with time.

The treatment can be generalized to include the secondary action at the cathode of positive ions and unscattered photons. To the boundary condition (ii) in (2.23) is added the integral expressions which represent these secondary actions, viz.

at $t > 0$,

$$i_- = I_o + g_1 D\, \partial n(x,t)/\partial x + \gamma\, I_+(0,t) + \delta \int_o^d i_- e^{-\mu x} dx \qquad (2.32)$$

where μ is an absorption coefficient. To satisfy these modified boundary conditions, the quantity F, which was previously taken as unity, has to be replaced by

$$F = 1 - (\delta/\psi)(e^{\psi d}-1) - (\alpha\gamma/\phi)(e^{\phi d}-1) \qquad (2.33)$$

where

$$\phi = \alpha - D(Z^2-\mu^2)/w \qquad (2.34)$$

and

$$\frac{1}{w} = \frac{1}{w_-} + \frac{1}{w_+} \qquad (2.35)$$

The expression

$$\frac{i_-}{I_o} = 1/\{1 - \frac{X}{\alpha}(e^{\alpha d}-1)\}$$

represents the condition of a normal pre-breakdown Townsend discharge and can be replaced by

$$\frac{i_-}{I_o} = 1/\{1-\omega/\alpha(e^{\alpha d}-1)\} \qquad (2.36)$$

Thus the complete solution can be written as

$$\frac{i_-}{I_o}(0,t) = 1/\{1-\omega/\alpha(e^{\alpha d}-1)\} + \frac{2\lambda(\lambda^2-\psi^2)(1-e^{-2\lambda d})_d D(\lambda^2-\mu^2)t}{(\lambda^2-\mu^2)(\partial\theta/\partial Z)} \qquad (2.37)$$

If there is negligible volume loss of the diffusing particles,

$\mu = 1/\sqrt{D\tau_1}$, can be neglected since $1/\tau_1$ is zero. If the time lag is of the same order as the transit time of the diffusing particles, w_- can be considered infinite. Therefore, the expression $i_-(t-x/w_-)$ in the original diffusion equation can be replaced by $i_-(0,t)$. ϕ and ψ may now be replaced by α since

$$\psi = \alpha - D(Z^2-\mu^2)/w_- \qquad \phi = \alpha - D(Z^2-\mu^2)/w$$

The complete modified solution then becomes

$$\frac{i-(o,t)}{I_o} = \frac{1}{\{1-\omega/\alpha(e^{\alpha d}-1)\}} + \frac{2(\lambda^2-\alpha^2)(1-e^{-2\lambda d})e^{D\lambda^2 t}}{\lambda\ (\partial\theta/\partial Z)} \tag{2.38}$$

where

$$\partial\theta/\partial Z = 2\lambda F - X - 2X(\lambda d-1)e^{(\alpha-Z)d} - e^{(-2\lambda d)}\{2Fd(d^2-\lambda^2)+2dX(\alpha-\lambda)+2\lambda F+X\} \tag{2.39}$$

λ is given the real value satisfying $\theta(Z)=0$, i.e.

$$(\alpha-Z)\{(\alpha+Z)F+X\}e^{-2Zd}+2\lambda Ze^{(\alpha-Z)d}-(\alpha+Z)\{(\alpha-Z)F+X = 0 \tag{2.40}$$

where $F = 1 - (\gamma+\delta/\alpha)(e^{\alpha d}-1)$ (2.41)

Thus by applying the above formulae to particular gases the rate of current growth due to the simultaneous action of metastable atoms, trapped radiation, undelayed photons and positive ions at the cathode can be calculated when the various coefficients are known. The calculated rate of growth may then be compared with that measured experimentally. Values of α corresponding to different per cent overvoltages are substituted and t calculated. The results are then conveniently plotted as formative time lags aginast $\Delta V\%$ overvoltage.

The Apparatus of Llewellyn-Jones & Galloway

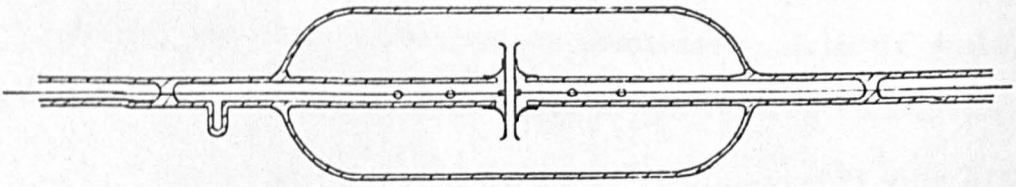

fig 19

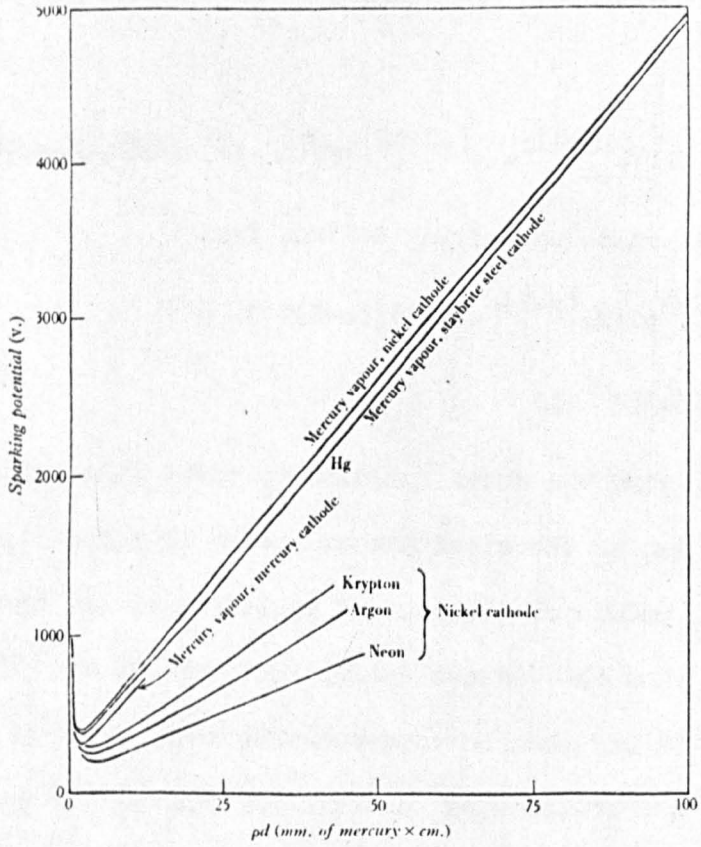

The Results of Llewellyn-Jones & Galloway

fig 20

CHAPTER 3

PREVIOUS WORK

3.1 Introduction

Llewellyn-Jones and Galloway (31) and Grigorovici (32) carried out work on breakdown potentials in mercury vapour using alien metal electrodes. The first measurements of ionisation coefficients were made by Badareu and Bratescu (33) in 1944, and more recently by Smith (34) in this laboratory. The experiments and results of the above will be discussed in this chapter.

3.2 The Work of Llewellyn-Jones and Galloway

These experiments were confined to the measurement of breakdown potentials in mercury vapour. The apparatus used was of simple design, consisting of two polished metal electrodes, 3.8 mm. in diameter, one of nickel and the other of 'Staybright' steel, both 1 mm. thick, with bevelled edges to reduce field distortion in these regions, enclosed in a glass envelope. A fixed electrode separation of 2.5 mm. was used. The ratio of electrode separation to electrode diameter was 1/15, so that the field between the electrodes could be assumed uniform. A diagram of the apparatus is shown in fig. (19).

The electrodes were degassed at 750°C in vacuum before being sealed in the tube. When the tube was complete it was maintained at 400°C whilst being evacuated by a diffusion pump. There is no mention of the ultimate pressure reached or of how and in what condition the mercury was introduced into the tube.

The vapour pressure of the mercury was raised by heating the tube

in an electric furnace, the temperature of the vapour being indicated by a mercury thermometer placed as near as possible to the electrodes.

Initial experiments showed that the Paschen curves taken while the temperature of the tube was rising did not coincide with those obtained while the temperature of the tube was falling. The difference was attributed to a temperature lag between thermometer reading and the actual temperature of the tube. It was assumed that the temperature lag was the same when the tube was being heated as when it was being cooled, so that for any given sparking potential the corresponding temperature for the vapour was obtained by taking the mean of the two temperatures recorded during the heating and cooling. A less ambiguous procedure would have been to change the temperature by small amounts allowing at each change sufficient time for the mercury to reach a steady temperature before measuring the breakdown potential.

It was observed that the minimum sparking potential was about 80 volts lower when the temperature was rising than when it was falling. The difference was attributed to the condensation of mercury on the electrodes, presumably due to the temperature lag between the outer and inner parts of the tube. If the temperature of the walls was slightly greater than that of the electrodes, mercury would be expected to condense on the latter. If the reverse condition was operative, i.e. when the tube was being cooled, then the electrodes would be expected to be free from mercury. Smith (34) has criticised this interpretation saying that any sudden change in cathode surface due to condensation of mercury would result in a change of slope of

the Paschen curve. However, it can be seen that condensation would occur only at the point when the walls of the tube were warmer than the electrodes, i.e. at the onset of the experiment, before the measurements were taken.

The results obtained are shown in Fig. (20). The minimum sparking potential with a mercury-covered nickel and a mercury-covered steel cathode was found to be 305 volts in both cases. The values for the clean surfaces were found to be 400 volts for the nickel cathode and 380 volts for the staybright steel cathode. The results were reproducible to 3% for several different tubes. The difference was attributed to the difference in work function of the two metals.

The electric furnace employed to raise the vapour pressure is not described in full. Temperature gradients would almost certainly exist to an appreciable extent if the furnace were a simple box with heating elements on the inside. These, together with the doubtful experimental procedure for determining vapour temperatures, could lead to serious errors in pressure measurement. The work was, however, useful in that it was established that mercury vapour has the same general sparking characteristics as the true gases.

3.3 The work of Grigorovici

Grigorovici's measurements were confined to the breakdown potentials in mercury vapour, with the object of deducing conclusions as to the phenomena taking place on sparking in the gas and at the electrodes.

A diagram of the apparatus is shown in fig. (21). The electrodes

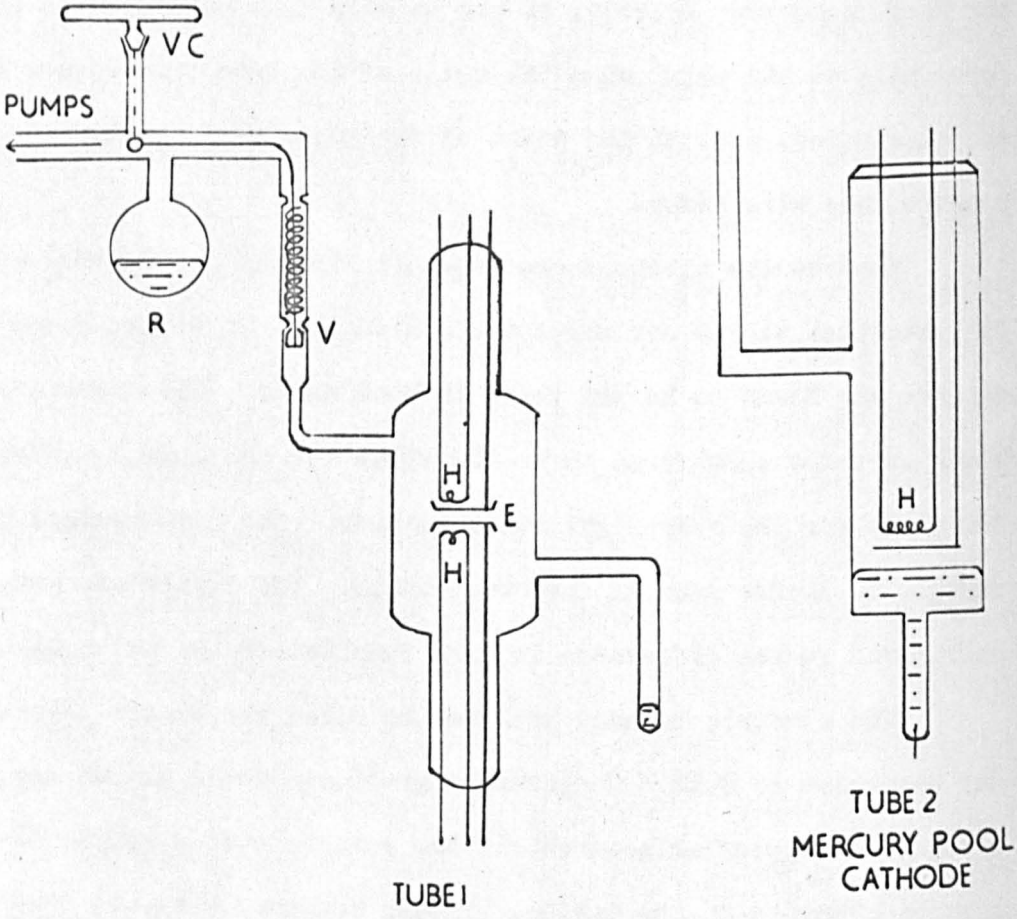

VC VALVE CONTROL
V VALVE
R RESERVOIR
E ELECTRODES
H HEATERS

(a)

The Apparatus of Grigorovici

fig 21

consisted of thin metal foils of platinum, aluminium and iron, mounted on an iron base, the whole being held in position by iron stays. The iron bases contained heating coils so that condensed mercury could be removed by evaporation if necessary. The mercury was contained in a small side-arm of the main tube containing the electrodes, while another side-arm led via a valve to the pumping system. The valve was so designed that it could be operated from outside the surrounding electric furnace.

The mercury was introduced to the tube after distillation under vacuum. The heating coils were outgassed by heating to white heat and the tube by heating in an electric oven to about 400°C. The electrodes were heated by passing an abnormal glow discharge in mercury vapour and the escaped gases were pumped off. The platinum and aluminium cathodes could not be subjected to this treatment since the surface was affected by the discharge. An impurity content of 0.01% could not be avoided because the valve allowed some gas to leak back from the pumps. The high excitation potential for some of the states for nitrogen could thus have influenced the discharge.

The temperatures were measured by calibrated mercury in glass thermometers placed on the sides of the tube where mercury was condensing. There is no description in Grigorovici's paper as to how the temperature of the vapour was maintained, but the fact that condensation was occurring on the tube walls implies that temperature gradients were present, which would make the accurate determination of vapour pressure difficult.

Breakdown potentials were measured with three different cathodes. The minimum sparking potentials obtained were 565 volts for a platinum cathode, 437 volts for an iron cathode, 390 volts for an aluminium cathode, and for a mercury pool cathode used in a second tube (fig. (21b)), 295 volts.

It was noticed that after running a discharge for some time using an iron cathode the sparking potential was lowered until it was 3 to 10 volts higher than for a pure mercury cathode. The lowering was attributed to the formation of a mercury layer on the cathode, since on heating the cathode the potential returned to its former value. The other two metals, platinum and aluminium, chosen because of their large difference in work function, (about 1.5 volts), gave different results. The surfaces of these cathodes took on a spongy structure, a result attributed to the incidence of singly charged mercury ions. The mercury was found difficult to remove, indicating that some form of strong binding existed between mercury and cathode. Grigorovici has suggested that this may simply be due to the increased absorptive power of the irregular surface. A similar effect, but to a lesser extent, was observed with the iron cathode. The minimum breakdown potentials for the mercury-covered cathode were 300 volts for iron, 245 volts for aluminium and 200 volts for platinum. The mercury layer was invisible to the naked eye but could be detected with a microscope. Further experiments indicated that the minimum breakdown potentials were dependent on the thickness of the film, such that the thicker the film the lower the minimum breakdown potential. It is well-known that when a

film is sufficiently thick it takes on the properties of the metal of which it is composed. Llewellyn-Jones and Davies (35) revealed that a decrease in the work function of a surface when a thin film of electro-positive metal was deposited on one of lower electro-positivity resulted in a lowering of the sparking potential. Mercury occupies a lower position in the electro-chemical series than iron but lies above aluminium and platinum. The change in breakdown potential can therefore be explained on this basis.

From the value of η_{min}, the minimum energy required to form an iron pair, given by Langmuir and Jones (36) for mercury vapour, Grigorovici calculated the second Townsend coefficient. The value given for η_{min} was 38 eV, to which Grigorovici added 15% to give η_{min} = 44 eV as an upper limit. If the energy which is spent by an electron in the field for the production of an ion pair is known then from the relation

$$Vs_{min} = \eta_{min} \ln (1 + \frac{1}{\gamma})$$

γ can be calculated. The values of γ obtained for Vs_{min} and η_{min} are shown in the following table reproduced from Grigorovici's paper.

Gamma as a function of Cathode Melting Point

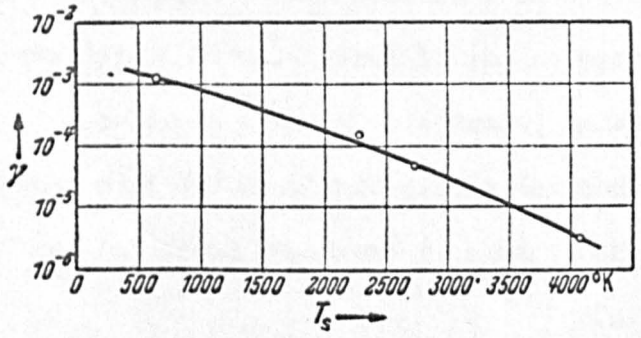

fig 22

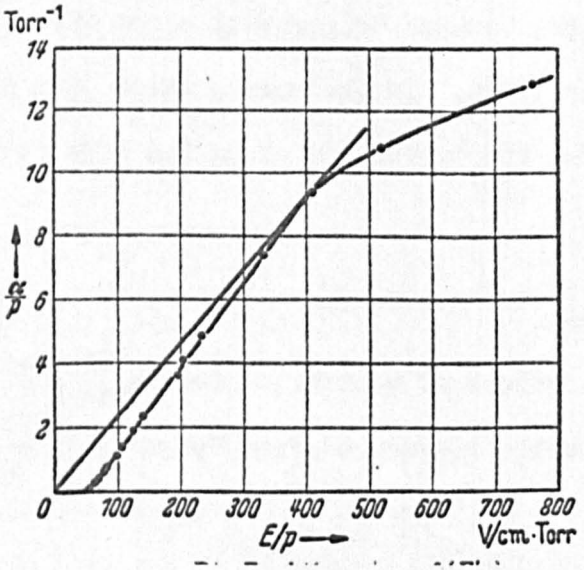

Primary Ionization Coefficients.(Grigorovici)

fig 23

Cathode Material	$\gamma\%$	ϕ	$V_i-2\phi$	T_s
Pt	3.2×10^{-4}	5.5	-0.6	4073
Fe	4.8×10^{-3}	4.5	+1.4	2723
Al	1.5×10^{-2}	3.0	+4.4	2273
Hg	1.2×10^{-1}	4.5	+1.4	630

Comparisons of the excess energy of the Hg^+ ion ($V_i-2\phi$) and the boiling point of the cathode, T_s, with the value of γ, led Grigorovici to the conclusion that the boiling point of the cathode was the more significant factor. The kinetic energy of the ions is therefore assumed to be responsible for electron emission from the cathode, the mechanism being that suggested by Kapitza (21) in which intense local heating is produced resulting in thermionic emission. By plotting γ as a function of T_s, which is proportional to the critical temperature, a smooth curve was obtained, fig. (22). The slightly high point corresponding to an aluminium cathode is explained by assuming that in this case, where $(V_i-2\phi) \simeq 4.4$ eV, the potential energy of the ion may play some part. The possible effects of metastable and photon action at the cathode are ignored, i.e. γ is not considered to be a composite parameter. At the values of E/p in question ($\sim$500), this assumption may be valid. Evidence will be given in Chapter 6 to the effect that at values of E/p less than 500 V/mmHg. metastable and photon effects become the dominant factors in electron liberation.

From the value of γ calculated from the relation

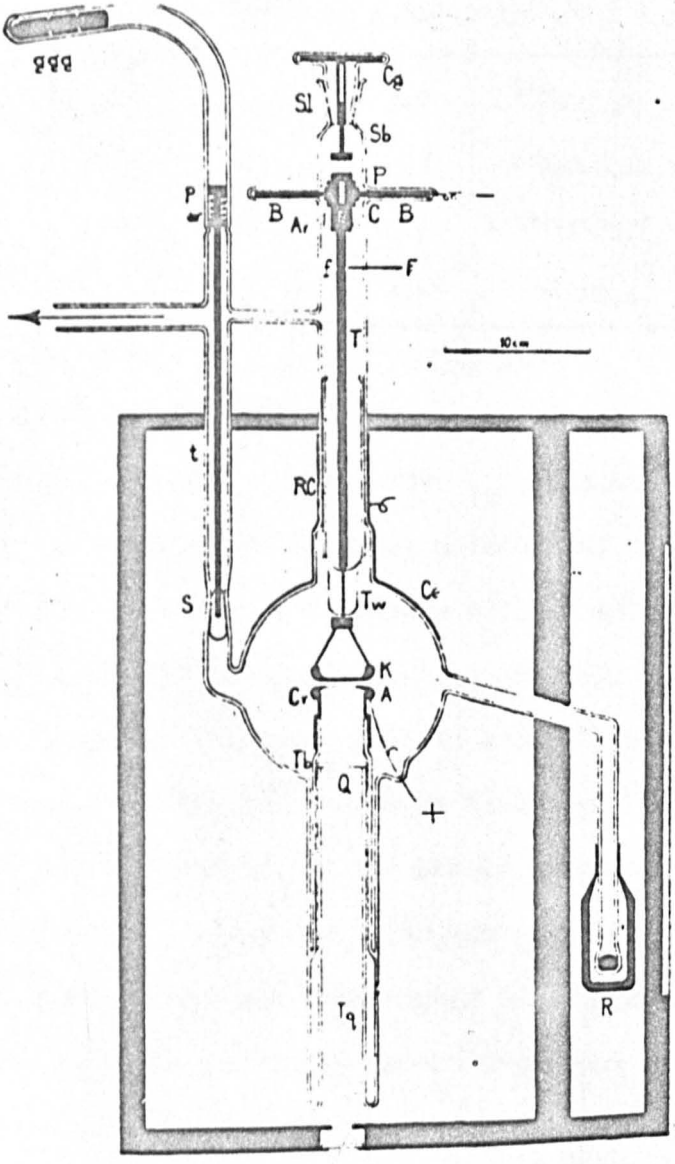

The Apparatus of Badareu & Bratescu.

fig 24

$$V = \eta(1 + \frac{1}{\gamma})$$

Grigorovici calculated $\alpha/p = f(E/p)$, assuming γ constant with E/p , an assumption that is in contradiction to his postulate that γ was primarily the result of the kinetic energy of the Hg^+ ion, a contradiction which he recognises. α/p is calculated from the relation where $V/pd=E/p$. The result is shown in fig. (23). The values of α/p are noted to be high compared to those of the rare gases, a result attributed to the low ionisation potential and small electron mean free path. It is recognised that the uncertainty of the absolute values of V, and the assumption regarding γ probably makes α/p too high, with a maximum error of 15%. However, as will be shown later, the values of α/p calculated by Grigorovici show remarkable agreement with experiment up to an E/p of 500 volts/cm.mm.Hg.

3.4 The work of Badereu and Bratescu

The aim of this work was to determine α/p as a function of E/p by measuring pre-breakdown currents, i, and plotting $\log_e i$ as a function of electrode separation, d. A diagram of the apparatus used is shown in fig. (24).

The main discharge chamber was of 'Duran' glass and was spherical in shape with a long side-arm containing a mercury reservoir. This side-arm was maintained at 20° to 70°C. below the main discharge chamber to avoid condensation of mercury on the electrodes. The temperature difference was achieved by splitting the electric furnace into two compartments, one containing the reservoir and the other the

main discharge chamber. The electrodes were mounted on glass tubes set centrally in the main chamber. The tube supporting the anode contained a quartz window through which ultra-violet light could be transmitted through small holes in the anode on to the cathode to provide an initial photo-electric current. The cathode was attached to a screw mechanism which could be operated from outside the oven, so altering the electrode separation. A fourth side-arm led via a valve to the pumping system. The electrodes used were of iron with Rogowski profiles to reduce field distortion.

The mercury was distilled thrice in vacuum before being distilled into the experimental tube. In order to reduce oxides present the tube was pumped and then flushed with hydrogen at atmospheric pressure, and baked at 400°C. for several days. The ultimate pressure reached was 10^{-5} mm.Hg. After isolation from the pumping system the pressure reached 10^{-4} mm.Hg. in 24 hours but did not increase above this value. At one mm.Hg. of vapour pressure, therefore, the impurity concentration was about 0.01% and the values of a/p measured could have been influenced by the high concentration of nitrogen. Temperatures were measured by mercury in glass thermometers and the pressure (reduced to 0°C.) was calculated from the temperatures of both compartments. This experimental arrangement, designed to keep mercury off the electrodes, probably produced disturbed thermal conditions. It would therefore have been difficult to gauge the pressure between the electrodes accurately. Thermal non-equilibrium also implies that temperature gradients were present, another factor complicating pressure measurement.

Primary Ionization Coefficients. (Badareu & Bratescu)

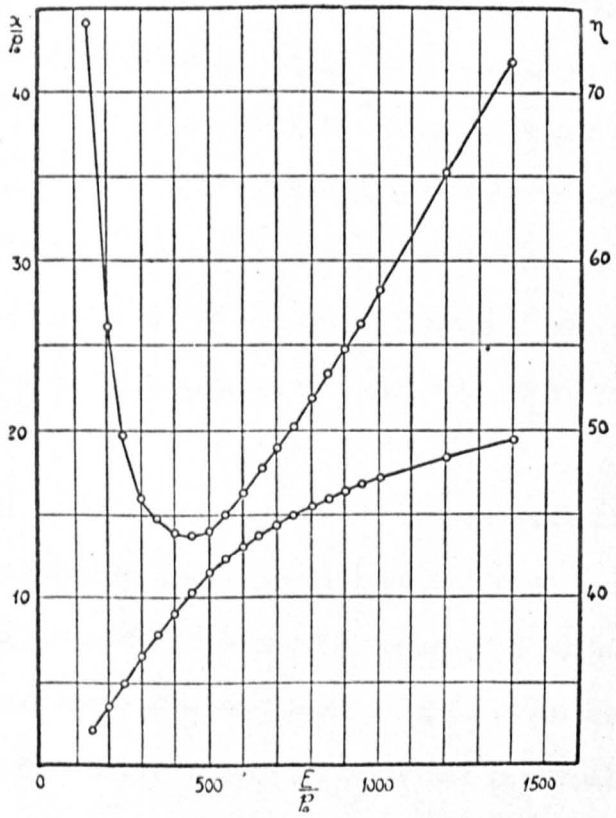

fig 25

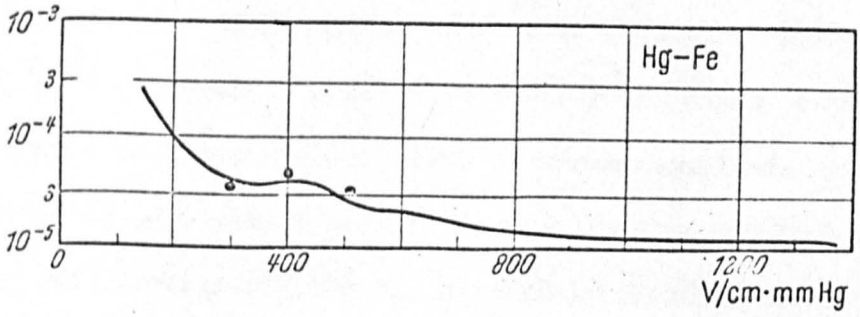

Values of γ as a function of E/p for Hg vapour with Fe electrodes.
(Badareu & Bratescu)

fig 26

Several graphs of $\log_e i = f(d)$ were plotted and values of α/p obtained from the slopes. It was found that even with the ultra-violet radiation switched off considerable current was flowing, presumably around the walls of the tube. To allow for this, current measurements were taken with the radiation on and with it off. The gas current was then taken as the difference in the two readings. A curve of $\alpha/p_o = f(E/p_o)$ was then plotted for a range of E/p_o from 150 to 1400 volts/cm.mm.Hg. A curve of η ($=E/\alpha$) as a function of E/p_o was also plotted. These results are shown in fig. (25). The values of α/p_o obtained were of the same order as those calculated by Grigorovici and the minimum value of η was 43.8 eV occurring at an E/p_o of 445, in good agreement with the value estimated by Grigorovici.

From their curve of α/p_o as a function of E/p_o Badareu and Bratescu calculated the constants of the Townsend relation

$$\alpha/p_o = A \exp B\ (p_o/E)$$

as A = 26.1 and B = 414. These values for the constants apply over the range of E/p between 200 and 1200 volts/cm.mm.Hg. A further discussion of these constants will be given in the final chapter of this thesis.

Assuming that the energy distribution of electrons was narrow, Badareu and Bratescu related α/p_o to the ionisation efficiencies of Smith (37) and Arnot (38). This enabled them to relate E/p_o to electron energy. Thus at an E/p_o of 200 the mean electron energy is quoted as 13.5 eV, the average between the values of Smith and Arnot.

Knowing the electron energy and using excitation functions, assuming an excitation potential of 7 volts (reference is not given) the authors calculate that at an E/p_o of 200, or a mean electron energy of 13.5 eV, there will be an average of 3.6 (value of α/p_o at 1 mm. pressure at $0^oC.$) ionisations and 17 excitations. Thus for every ion pair produced there are on average 4.7 excited atoms, assuming only one excited state. For an E/p of 1000, with $\alpha/p = 17.2$, the value of the mean electron energy is 33 eV and 9.6 exciting collisions are on average calculated to occur. The method of calculation unfortunately is not given, neither is the source of the excitation function, and thus it is not possible to check the calculations. An alternative method of arrivingeat the number of excitations per ionisation is one first suggested by Smith (34) in which use is made of the values of $\eta = E/\alpha$ which represents, at a given E/p, the energy an electron must gain from the field before ionisation takes place. The energy required to ionise, V_i, is in the case of mercury 10.4 volts. The amount of energy $(\eta-10.4)$ must then have been absorbed in elastic and exciting collisions. The fractional energy loss on an elastic collision between an electron and mercury atom, $\Delta\varepsilon$, is very small since

$$\Delta\varepsilon = \frac{2m}{M} \simeq 5 \times 10^{-6}$$

and, therefore, losses to excitations only need be considered. Knowing E/p as a function of electron energy, use can now be made of the excitation functions. These were made available by Penney (1) in 1932 for the four P states of mercury. For a given electron energy the ratios of the

probabilities of excitation give the ratios of the numbers of atoms in each state. Multiplying the ratios by the energies of the states, summing, and equating to the energy value (η-10.4) at the value of E/p equivalent to the electron energy in question allows the number of atoms in each state per ion pair produced to be calculated for that value of E/p. Smith (34) made some use of this method assuming only two states were important, and more detailed use is made in the final chapter of this thesis. It is surprising, however, that Badareu did not make use of η in this way, particularly as Penney's excitation functions had been available for some years. The secondary coefficients, for an iron cathode, were determined from Grigorovici's measurements of breakdown potentials, using the relation

$$V = \eta \log \left(1 + \frac{1}{\gamma}\right)$$

Three values of γ were also obtained from the upcurving parts of the $\log_e i$ versus d curves. The values calculated by the two methods were found to be in good agreement. The values of γ as a function of E/p_o are shewn in fig. (26).

Between the range of 800 to 1400 for E/P_o the secondary coefficient was found to be constant, leading the authors to the conclusion that the potential energy of the ion was the more important factor in electron liberation. At lower values of E/P_o the higher values of γ were attributed to a combination of the photo-electric effect and the potential energy of the ion. The role of metastable atoms in electron liberation was considered negligible compared to that of the other

elementary processes, the reason given being that the high temperatures involved favour the creation of normal excited states rather than metastable states. In a second paper Bratescu (39) cites the two resonance 'p' states as the most important. Any metastables produced are considered to have negligible probability of reaching the cathode, their destruction being achieved in the volume, with the resultant photon having a photo-electric effect at the cathode. Thus at values of $E/p_o < 800$ the principal secondary process is thought to be a photo-electric action and at values of $E/p_o > 800$ the principal secondary processes are thought to be a combination of photon effects and the singly charged positive ion, acting by virtue of its potential energy.

The currents used by Badareu and Bratescu lay between 10^{-9} and 10^{-5} amps. Although space charge effects are thought to become important at 10^{-5} amps (5) the use of such currents would not affect the values of α/p since the large currents would be confined to the upcurving part of the $\log_e i$ versus d curves. The lack of an analysis to correct for secondary effects also would not affect their values of α/p since the secondary coefficients determined are about 10^{-4}. The main criticism of their work lies in the poor vacuum techniques where the residual air pressure could not be reduced below 2.4×10^{-4} torr. thus introducing a possible Penning effect and in the design of the electric furnace which probably introduced non-equilibrium conditions and consequent difficulty in determining the vapour pressure. Further, although the apparatus was flushed with hydrogen and baked at $400^{\circ}C$, no effort was made to outgas the bulk iron electrodes, either by Eddy-current heating

The Apparatus of Smith.

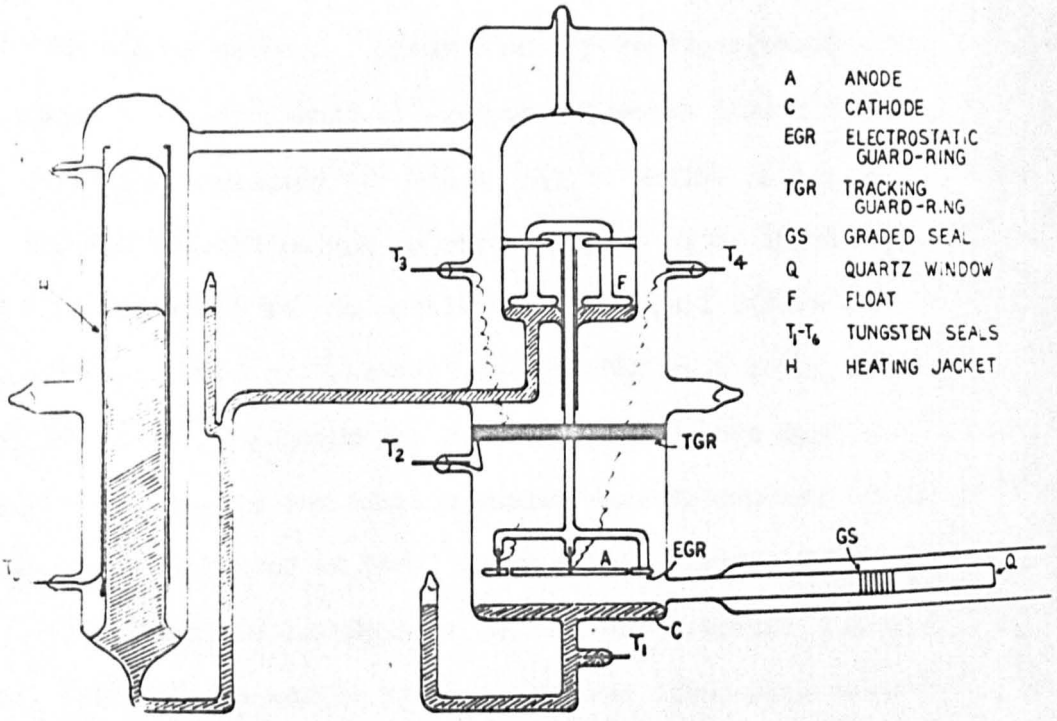

fig 27

or by passing a glow discharge. The probable out-gassing of these electrodes under the experimental conditions would increase the impurity content.

3.5 The experiment of Smith

The aim of this work was the measurement of α/p_o as a function of E/p_o by measuring pre-breakdown currents as a function of electrode separation. A diagram of the apparatus used in shown in fig. (27).

The electrode system consisted of a mercury pool and a glass anode. The anode, 4 cm. in diameter, was surrounded by a glass guard-ring, making the total diameter of the anode assembly 6 cm. Both anode and guard ring were ground smooth and coated with graphite on the under-sides to give conducting surfaces. Electrical connections to these surfaces were made by tungsten seals.

The anode assembly was connected to a glass float in a subsidiary chamber. This subsidiary chamber was connected to an external mercury reservoir surrounded by a heating coil, so that by heating the mercury the vapour pressure in the reservoir was increased, forcing mercury into the float chamber and consequently raising the anode assembly.

A graphite ring was painted on the inside of the discharge chamber in order to by-pass currents travelling between anode and cathode along the walls of the tube. Ultra-violet radiation was admitted through a quartz window arranged so that radiation struck the cathode at glancing incidence.

The apparatus was baked for 24 hours at 450°C. while being pumped by a diffusion pump and a rotary pump arranged in series. The mercury

α/p_o as a function of E/p_o in Mercury Vapour. (Smith)

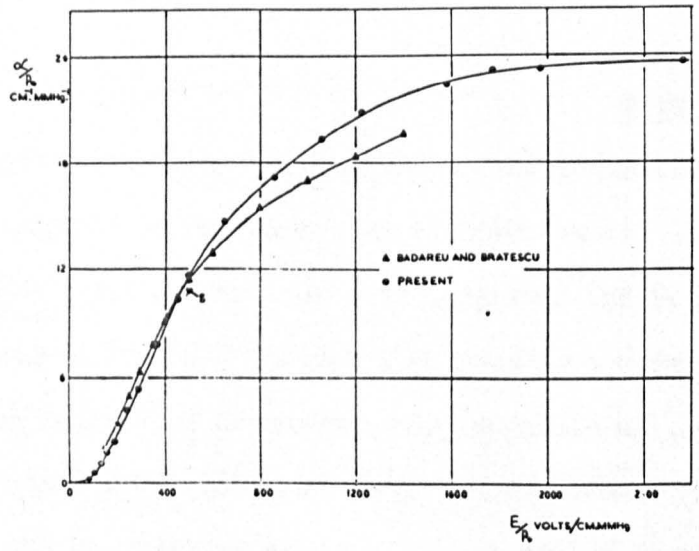

fig 28

The Present results for α/p_o compared to the similar results of Bleakney. (Smith)

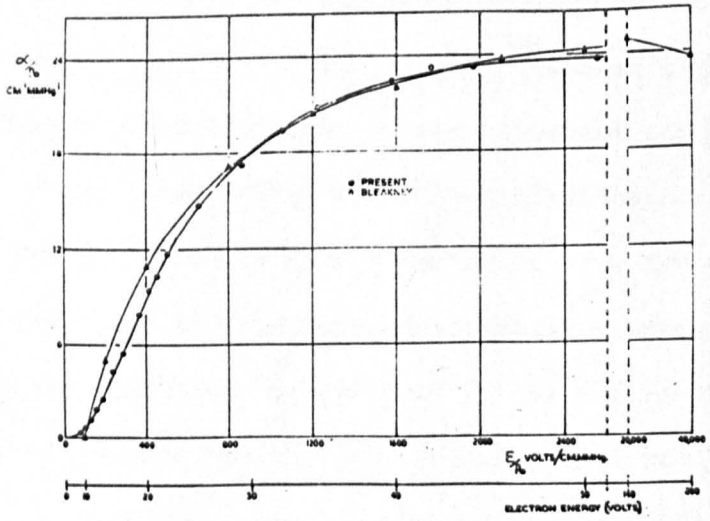

fig 29

was twice distilled under vacuum before being admitted to the tube, which by the use of ion-gauge techniques had previously been evacuated to an ultimate pressure of 10^{-7} mm.Hg.

The type of oven used was developed in conjunction with the present author and will be described more fully in Chapter 4. Basically it consisted of a massive iron chamber in which the experimental tube was placed, heated by elements placed on the inner walls of an outer chamber which completely enclosed the iron box. Temperatures were measured by thermocouples and a maximum difference in temperature of 1°C. could be detected between any two extreme points (1 metre) in the inner enclosure.

Using currents between $10^{-7}$and 10^{-11} amps Smith obtained values of α/p_o as a function of E/p_o for a range of $80 < E/p_o < 2500$ volts/cm.mm.Hg. His results, together with those of Badareu and Bratescu are shown in fig. (28). The curve shows a levelling at high E/p_o, a result which is to be expected from theoretical considerations. The detection of this levelling is attributed to the application of the Davies-Milne (40) analysis, which corrects for secondary effects. This point will be discussed further in chapter 6 in relation to the present results.

The curve crosses that of Badareu and Bratescu at an E/p_o of 480 volts/cm.mm.Hg. The point at which the curves cross is the Stoletow point. The corresponding Stoletow constant, which is the minimum value of $\eta = E/\alpha$ is quoted as 44 volts, which agrees with that of Grigorovici and of Badareu and Bratescu. Smith attributes the crossing of the two curves to errors in pressure measurement on the part of Badareu and

Bratescu. An error of 3% in temperature measurement would result in the observed 20% error in pressure which would explain the difference. The error in temperature measurement is thought to be a result of temperature gradients occurring as a result of non-thermal equilibrium conditions. This explanation becomes more clear when plots of η (which is a function of E/p_o only) against E/p are considered.

The value of the constants of the Townsend equation relating α/p_o to E/p_o were obtained by plotting $\log_{10} \alpha/p$ as a function of E/p_o. The equation was found valid over a range of $250 < E/p < 1800$ volts $cm.^{-1}mm.Hg.^{-1}$, being

$$\alpha/p_o = 30 \exp \left[\frac{-500}{E/p_o} \right]$$

Following the idea of Badareu and Bratescu Smith compared his values of α/p_o with the ionisation efficiencies of Bleakney (3) and showed there was reasonable agreement between the two sets of results. These are shown in fig. (29). It was considered significant that both curves level off at approximately the same value, in the case of Bleakney's results 25 $cm.^{-1}mm.Hg.^{-1}$ and in Smith's case 24 $cm.^{-1}mm.Hg.^{-1}$. Further, by fitting the two curves to give a reasonable agreement over the maximum range of E/p_o, Smith concluded that the mean electron energy, ε, in volts was related to E/p_o by

$$\varepsilon = (E/p_o)^{\frac{1}{2}}$$

The fact that the maximum value of α/p_o obtained was less than the value for the ionisation efficiency of Bleakney is surprising. It would be expected that the α/p_o of a Townsend discharge would be greater than the

corresponding ionisation efficiency in the experiment where mono-energetic beams are considered because of the electrons in the high energy tail of the distribution function with energies above that corresponding to the mean energy, E/p_o, in question.

It will be noticed that the best fit between the curves of $\alpha/p_o = f(E/p_o)$ and the ionisation efficiency curve is obtained at high E/p_o, i.e. at values greater than that at the Stoletow constant. It will be remembered that at values of E/p_o greater than this value, the coefficient $\eta=\alpha/E$ decreases i.e. the electrons no longer completely dissipate their energy by collisions in the gas, but deliver a large part of their energy to the anode. Under these conditions the electrons are no longer in equilibrium with the field and the drift velocity and energy increase with distance from the cathode. Thus, at values of E/p_o greater than the Stoletow point, α/p_o no longer has a precise meaning, since the mean energy, E/p_o, no longer has a precise meaning. Thus the comparison on ionisation efficiency with α/p_o, in order to relate E/p_o with electron energy, should be confined to values of E/p_o which do not exceed the Stoletow point by any great amount. If this is done with Smith's values of α/p_o the relation between E/p_o and electron energy $\bar{\varepsilon}$ is found to be linear and is given by

$$\bar{\varepsilon} = \frac{k}{42}(E/p_o) + 6$$

where k is a dimensional constant of the order of unity. This point is discussed further in relation to the present results in Chapter 6. Using the method outlined in the discussion of the work of Badareu and

Secondary Ionization Coefficients as a function of E/p
(Smith)

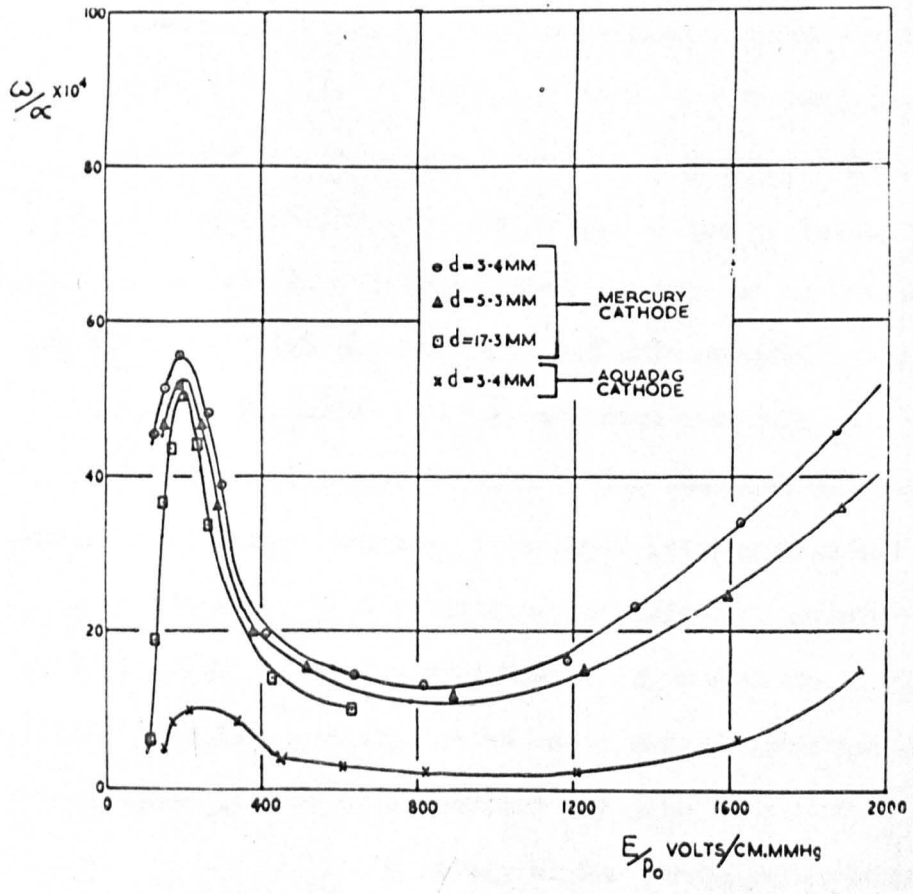

fig 30

Bratescu, Smith calculated the number of excitations per ionisation at the E/p_o corresponding to η_{min}. Assuming that the two resonance levels of energy 4.8 eV and 6.7 eV to be the only ones of importance, the ratio of exciting to ionising collisions was found to be 6:1.

Using his values of α/p_o and of sparking potentials, curves of the second coefficient, ω/α, as a function of E/p_o, were obtained for three different electrode spacings. The three curves show the same trends with a high peak at low values of E/p_o, which is attributed to photon action at the cathode. Increased loss of photons from the discharge volume is given as an explanation of the displacement of the curves along the ω/α axis. Using a graphite cathode it was found that the values of ω/α were much lower than those obtained for a mercury cathode, fig. (30). This is accounted for by the higher work function of graphite. The increase in ω/α at higher values of E/p_o is ascribed to the emission of secondary electrons due to the incidence of doubly charged mercury ions on the cathode surface. It is thought that the large potential energy, 30 eV, rather than the kinetic energy of the ion, is the more important factor. The ion would be expected to occur at a value of E/p_o of about 900 volts $cm.^{-1}mm.Hg.^{-1}$ if the electron energy were equivalent to $(E/p_o)^{\frac{1}{2}}$. This is where the curve begins to rise again. However, Kovar (41) when determining the mobility of mercury ions in mercury vapour, was unable to detect Hg^{++} although his range of E/p_o extended as far as 1500 volts/cm.mm.Hg. The only fast ion detected, with a mobility of approximately twice that of the singly charged ion,

was Hg_2^+, which could not be detected above an E/p_o of about 100 volts $cm.^{-1}mm.Hg.^{-1}$. However, an alternative explanation of the increase in ω/α at high E/p to that of the ion Hg^{++} must be found. This point will be discussed further in Chapter 6.

By plotting breakdown potentials as a function of p_od, Paschen curves were obtained for different gap distances, d. It was found that the minimum sparking potential could be related to the ratio of d/D where D is the electrode diameter, by the expression

$$Vs_{min} = 282 + 20(d/D)$$

to an accuracy of 1 volt. Such a relationship cannot be determined unless the work function, and hence the emissive properties of the cathode surface, remain constant. It therefore appears that a mercury pool will provide such a surface under low current conditions.

3.6 Conclusion

It can be seen from the above review that knowledge of the electrical properties of mercury vapour is incomplete. Values of the primary and secondary coefficients have been established to an order of magnitude and the general behaviour of mercury vapour under controlled discharge conditions is established as being very similar to that of the rare gases. Further measurements are required of the first ionisation coefficient in an attempt to resolve the discrepancy between the results of Badareu and Bratescu and Smith. The interpretation of the curve $\omega/\alpha = f(E/p)$ is in doubt, and temporal studies of the growth of ionisation are required to facilitate the solution of this problem.

The work of Llewellyn-Jones and Galloway and of Grigorovici has shown that with the use of bulk metal electrodes, surface effects become important to the discharge, either through amalgamation or condensation. Smith has demonstrated that a mercury pool will provide a clean, reproducible surface of constant work function suitable for use as a cathode under the gas discharge conditions concerned. Such a cathode is used in the experiments described in this thesis.

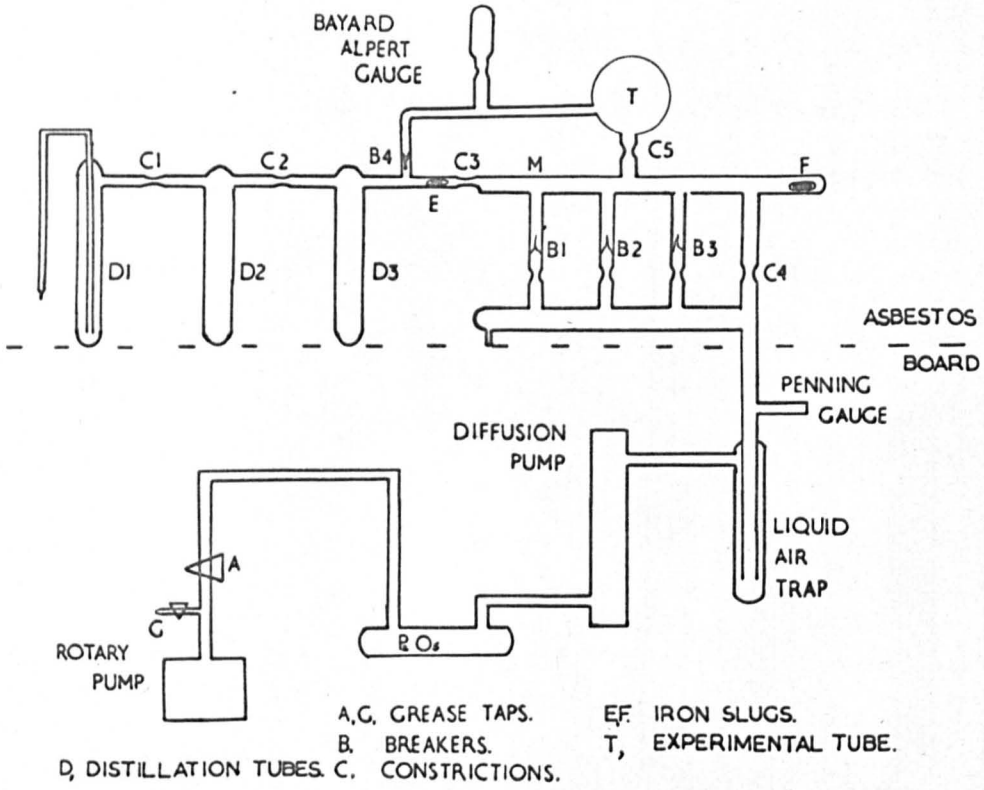

First Vacuum System.

fig 31

CHAPTER 4

APPARATUS

4.1 Vacuum System

A line diagram of the vacuum system used to process the first two experimental tubes is shewn in fig. (31). The system, apart from the rotary pump was made of Pyrex glass and mounted on a Dexion frame.

The system was divided into two parts by an asbestos board. Those components mounted below the board made up the main pumping system, those parts above the board the manifold and experimental tubes. The purpose of the board was to act as a support for an electric furnace used to bake the manifold and tubes in order to assist in outgassing them.

The pumping system consisted of a rotary pump in series with a two stage mercury diffusion pump, separated from the latter by a vessel containing phosphorous pentoxide, included to protect the rotary pump from moisture. The diffusion pump in turn was connected to a liquid air trap in order to condense any mercury vapour on the high vacuum side and prevent it reaching the manifold.

There were two grease taps, A and G. The function of A was to isolate the rotary pump from the rest of the system; that of G to let the rotary pump up to atmospheric pressure after isolation. No grease taps were present on the high vacuum side of the pumping system.

The manifold consisted of three distillation tubes, D_1, D_2, D_3, connected together in series and separated from each other by constrictions C_1 and C_2. The constriction C_3 separated these tubes from the

VACUUM SYSTEM AND MANIFOLD

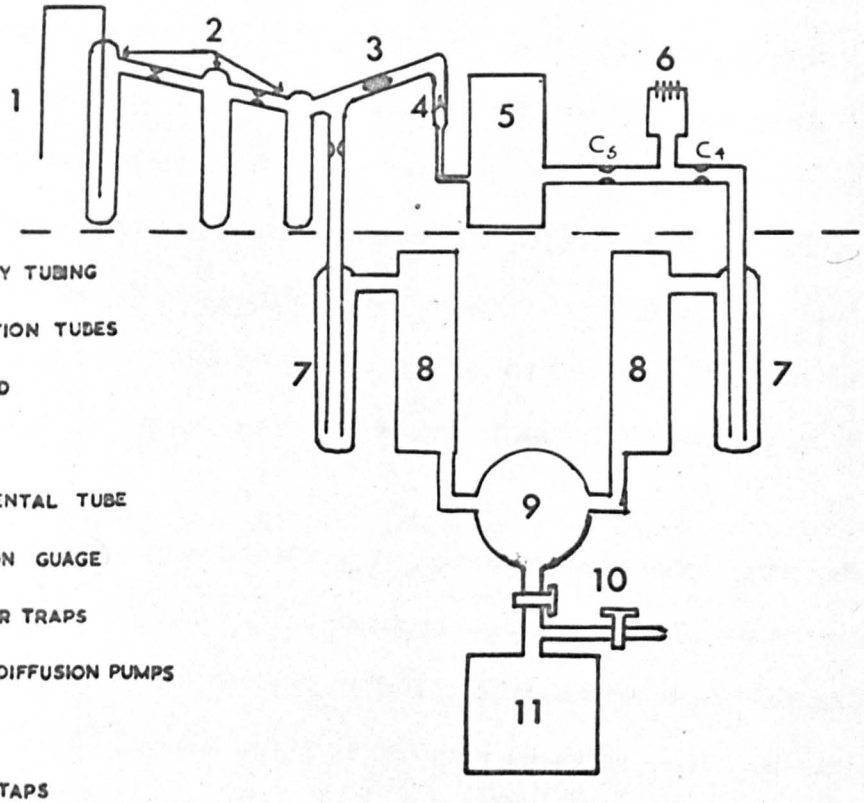

1 CAPILLARY TUBING
2 DISTILLATION TUBES
3 IRON ROD
4 BREAKER
5 EXPERIMENTAL TUBE
6 IONISATION GUAGE
7 LIQUID AIR TRAPS
8 MERCURY DIFFUSION PUMPS
9 P_2O_5
10 GREASE TAPS
11 ROTARY PUMP
C CONSTRICTIONS

fig 32

main arm of the manifold,M. This arm was joined to the pumps via a constriction, C , and three pigstail breakers B_1, B_2 and B_3. The breaker B_4 served to isolate the experimental tube T from the distillation tubes. The tube was connected to the main arm of the manifold by a constriction C_5. Iron rods, completely surrounded by glass, were placed at E and F in order that the breakers might be smashed when required.

A Penning gauge was constructed and mounted on the mercury free side of the liquid air trap in order that the pressure could be measured while the manifold was being baked. A Bayard-Alpert type gauge was also constructed and mounted between the experimental tube, T, and the breaker B_4. When the constriction C_5 was closed, it served both as a measuring and a pumping device.

The vacuum system was modified for use with the third and fourth experimental tubes. A diagram of the modified system is shewn in fig. (32). The breakers B_1, B_2, and B_3 were dispensed with. The distillation tubes were pumped separately from the experimental tube by a second diffusion pump. The experimental tubes were connected via constrictions C_5 and C_4 to the original diffusion pump. The ion gauge was mounted between C_5 and C_4, so that it could pump the tube after the closure of C_4. This arrangement was found to give a better pumping speed, and greatly simplfied glass blowing problems.

4.2 The First Experimental Tube

The electrode system of the first experimental tube, fig. (33),

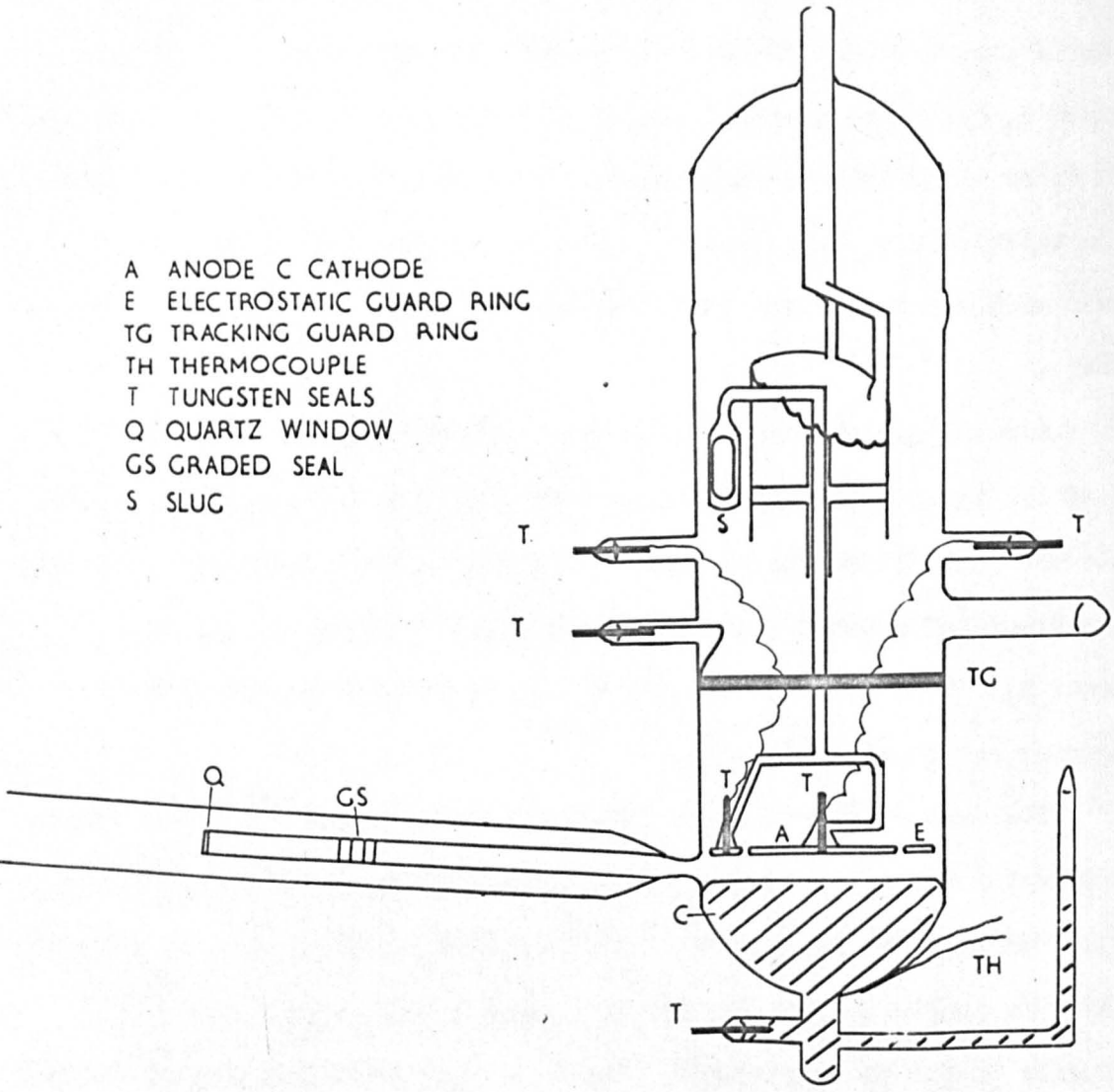

First Experimental Tube.

fig 33

consisted of a mercury pool cathode and a glass anode and guard-ring. The diameter of the cathode and that of the anode and guard-ring taken together, were approximately equal, measuring about 6 cm. The anode and guard-ring were made by melting glass rod in a carbon mould. Both electrodes were then ground smooth using successively finer grades of carborundum powder. Finally, a thin layer of graphite was sprayed on the smooth surfaces to render them conducting. Electrical contact to these surfaces was made through tungsten rods embedded in the elctrodes and fine nickel wire attached to tungsten seals in the walls of the tube. The anode and guard-ring were connected mechanically by joining the glass surrounds of the tungsten rods together by means of thin glass rods. Joined to the latter was a second glass rod which passed upwards immediately above the centre of the anode, through the inner of two concentrically placed glass tubes. The upper edge of the outer tube was sloped and serrated, so that the glass rod, on emerging from the inner tube, could be bent over and held in one of the notches, thus being held in position. The glass tubes in turn were fixed by glass rods to the roof of the discharge chamber. Thus, by selecting different notches to hold the central glass rod, the height of the anode assembly above the mercury pool could be altered. A metal rod enclosed in glass was included so that a magnet could be used to select the appropriate notch. The mercury pool itself rested in the base of the discharge chamber. The amount of mercury was sufficient to bring the surface level above the curvature of the base, so that measurements of the electrode separation were not complicated by refraction effects. The electrical

connection to the pool was through a tungsten seal in the base of the tube.

A graphite ring was painted on the inside of the discharge chamber, in order to intercept currents travelling along the walls of the tube. Connection to the ring was made by nickel wire joined to a tungsten seal in the wall of the tube and a connection was then made to the appropriate side of the electrometer. A quartz window was joined to the tube through a graded seal and positioned at such an angle that ultra-violet radiation transmitted through it would strike the cathode at almost grazing incidence and provide an efficient source of photo-electrons.

The main body of the discharge chamber was made by sealing together two glass envelopes. This obviated the need for tungsten-glass pinches normally used to seal such envelopes and reduced the amount of foreign metal in the tube. A thermocouple was strapped to the outer wall of the base of the discharge chamber so that the temperature of the pool could be determined.

The tube was connected to the distillation apparatus via a breaker and a length of narrow bore tubing which could easily be collapsed after the mercury had been distilled into the tube. A tube of wider bore containing a constriction served as a pumping arm. The experimental tube could be removed from the manifold after sealing the constriction.

4.3 The second experimental tube

The first experimental tube suffered from the disadvantage that

A ANODE C CATHODE
E ELECTROSTATIC GUARD RING
TG TRACKING GUARD RING
TH THERMOCOUPLE
R RESERVOIRS
H HEATERS
T TUNGSTEN SEALS
Q QUARTZ WINDOW
W GLASS WINDOW
GS GRADED SEAL
F FLOAT
B BULB
O POINT OF ROTATION

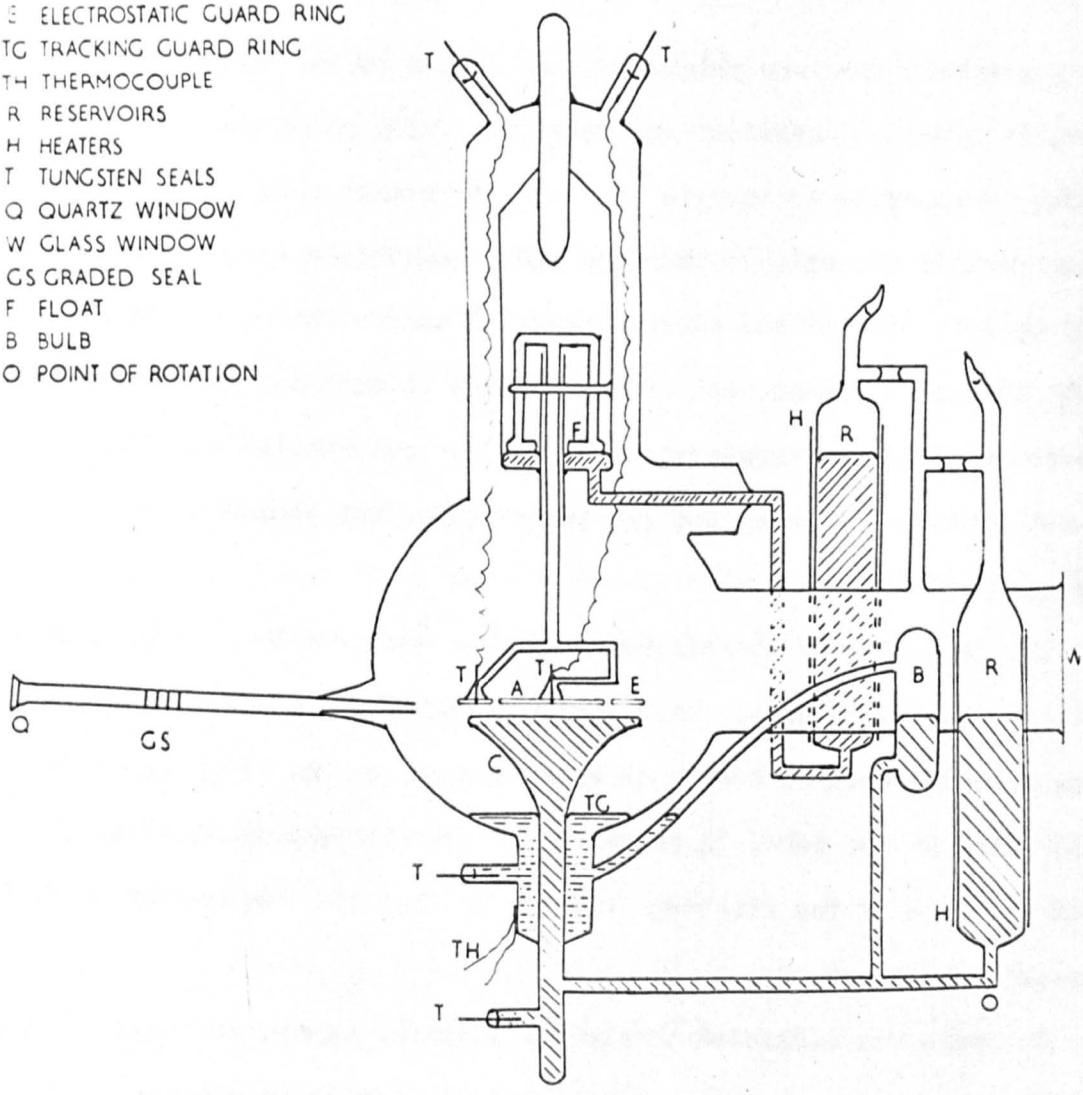

The 2nd & 3rd Type of Experimental Tube.

fig 34

the inter-electrode distance could not be varied when the tube was in position in the furnace. All measurements had to be taken at constant electrode separation, the pressure being the variable parameter. Since sufficient time had to be allowed for the temperature to reach a steady level, a single Paschen curve often took as long as a week to complete, as did a curve to evaluate η. (The process used to determine these results will be described in the next chapter). Accordingly, a second tube was built to incorporate the device used by Smith (34) to vary the electrode separation. A diagram of the tube is shown in fig. (34).

Experiments with the first experimental tube indicated that appreciable currents were flowing on the walls of the tube, as noticed by Badareu and Bratescu and by Smith. These currents may have influenced the distribution of the field. In order to approximate more closely to the original conditions on which Townsend's theory of the spatial growth of current were based, it was decided that the walls of the main discharge chamber should be as far away as possible from the electrode system. This could have been achieved by blowing out the walls of a glass envelope of the type used in the construction of the first tube. However, no such envelopes could be obtained. Eventually it was decided to use a 500 c.c. Pyrex boiling flask for the main body of the tube. The neck of the flask unfortunately limited the total diameter of the anode plus guard-ring to 4.5 cm. These were made in exactly the same way as the electrodes which were used in the first tube.

The anode and guard-ring were joined to a glass rod which in

turn was fixed to a flat glass annulus. This annulus floated on mercury contained in a subsidiary chamber in the main ionisation discharge tube. A length of narrow bore glass tubing linked the subsidiary chamber to a mercury reservoir external to the main discharge chamber. A heating coil was passed around this reservoir so that on passing electricity through the coil the vapour pressure of the mercury in the reservoir was increased, so forcing mercury along the small bore tubing into the subsidiary chamber, and raising the annulus and anode assembly.

The mercury forming the cathode was contained in a conical cup attached to the base of the discharge chamber by an internal seal whence it was joined to a second mercury reservoir by a length of small bore tubing. This reservoir was also surrounded by a heating coil so that fine adjustments to the cathode level could be achieved if so desired. A wall current guard-ring was formed during the distillation process by allowing mercury to overflow from the full cathode and accumulate at the base of the cathode support. Electrical connection to the pool so formed was by the usual method of a tungsten seal.

In order to allow for excessive depletion of the cathode by evaporation, a length of small bore glass tubing was placed between the wall electrode and the cathode reservoir via a glass bulb, B. Mercury evaporated from the cathode would eventually condense in the pool forming the wall electrode. This could then be returned to the cathode by rotating the whole tube about the point O, thus first filling the bulb B, then, on lowering the tube back to its original position, the mercury

could then flow from the bulb to cathode and reservoir.

The above mechanism also served the additional purpose of keeping the cathode surface clean and free from small particles of graphite removed from the other electrodes. A small number of such particles was observed on the surface of the cathode of the first experimental tube. An examination of Smith's cathode revealed the presence of graphite there also.

F 'h reservoirs were placed on the same side of the tube so that rotation of the tube always resulted in a flow of mercury away from the tube into the reservoir.. This prevented mercury from spilling from the subsidiary chamber into the main ionisation chamber. The reservoirs were supported by tubes containing sealed constrictions, the tubes being joined to a wide side arm attached to the main chamber. This side arm was terminated by a flat plain glass window, facilitating the observation and measurement of electrode separation. Such a window was a necessity because of the distorting effect of the wall curvature.

A smaller side arm was attached to the chamber at right angles to the viewing arm. A quartz window was attached to this arm via a graded seal and an internal seal. The tube containing the quartz window was drawn out to form a tube of narrower bore, enabling a narrow beam of ultra-violet radiation to be directed at grazing incidence at approximately the centre of the cathode, and also preventing obstruction of the light by the anode.

The experimental tube was connected to the manifold in a similar

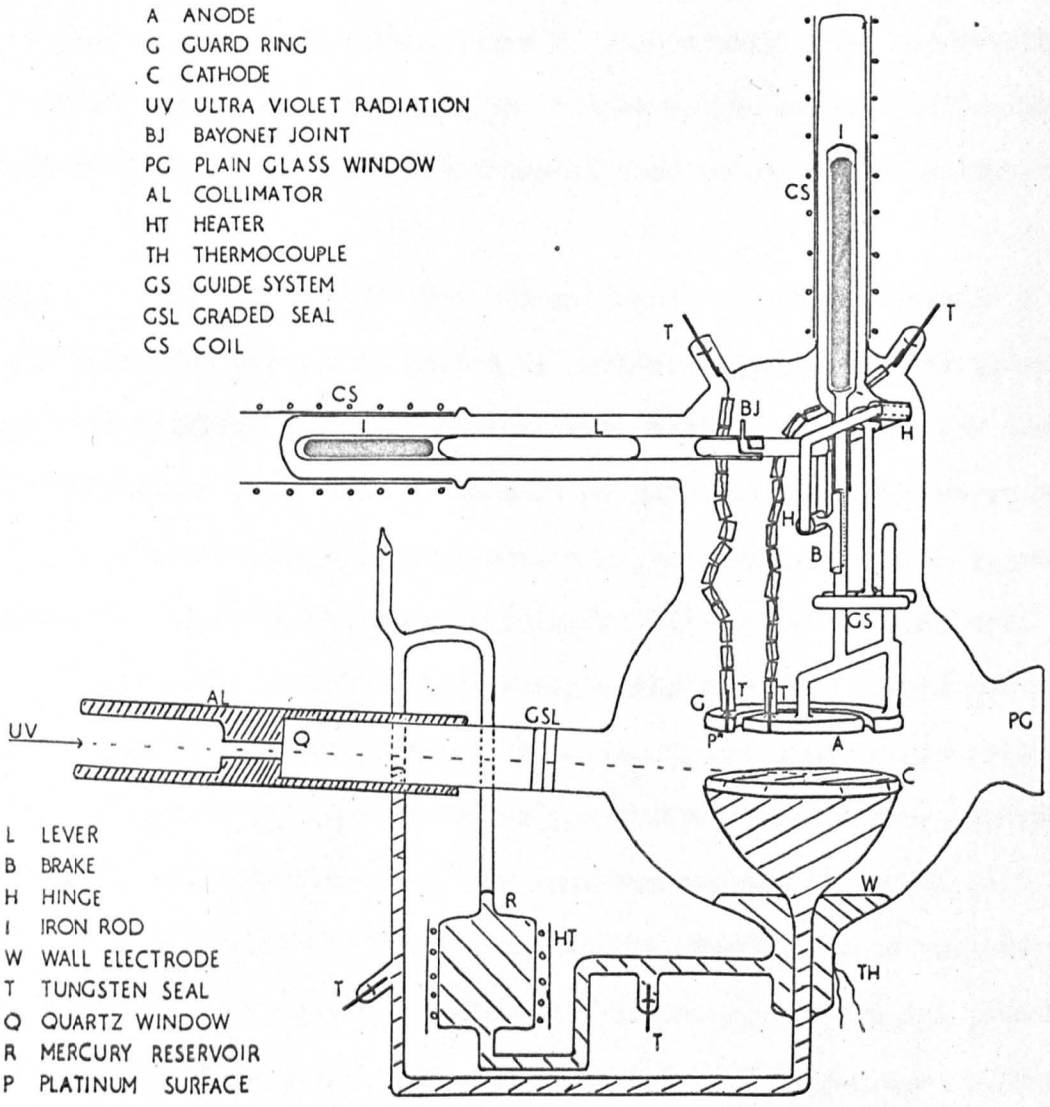

The Fourth Type of Experimental Tube.

fig 35

way to the first tube.

4.4 The third experimental tube

This tube was built to a similar plan as the second tube, the main difference being that electrodes of diameter 6 cm. were used instead of those of 4.5 cm. The use of larger electrodes was made possible by having the main body of the tube built by a prefessional glass-blower.

4.5 The fourth experimental tube

The method employed to raise the anode assembly in the second and third tubes, although it enabled the electrode separation to be varied when the tubes were in situ, was only suitable for measurements of α/P_o where the separation was not required to be constant for any great length of time. Temporal studies, however, require the electrode separation to remain constant for indefinite periods. Accordingly another method of changing the electrode separation was devised.

A diagram of the complete tube is shown in fig. (35). The anode and guard-ring, total diameter 6 cm., were made in the same way as the electrodes formerly described, with the graphite undersurface replaced by platinum, which, it was found, had better adhesive properties. The anode and guard-ring were joined by thin glass rod. To this was connected another rod in a place normal to the anode assembly. This rod passed through a close-fitting tube and was joined at its other end to a glass tube completely surrounding a length of iron rod. The close-fitting tube, which served to maintain the anode assembly in the

correct plane, was widened at the end furthest from the electrodes and joined to a tube surrounding the tube containing the iron rod. The tube was joined to the main body of the discharge chamber by an internal seal.

The tube was sufficiently long to allow considerable vertical movement of the iron rod and electrode assembly. This movement was achieved by activating a coil, C, placed around the tube. The coil was wound on glass tubing and the wire was glass covered to maintain insulation at the high temperatures of operation.

A rectangular frame of glass rod was hinged at a point a little above that at which the guide tube was widened. This was achieved by joining a short length of tubing to the guide tube in a horizontal plane, and threading through it a rod which was then bent on either side. The ends of the rod were then bent and joined in a further length of short tubing, making a second hinge in a horizontal plane. To this short tubing was joined, in a vertical plane, a further piece of tubing which was later sliced in half longitudinally. This was allowed to rest on the rod supporting the anode assembly and thus acted as a brake, preventing vertical movement of the anode, when a load was applied. This was achieved by mounting a horizontal lever on the second hinge. This lever consisted of a glass rod, joined to the hinge, with a small glass peg sealed normal to its surface. A glass tube, with an appropriate notch at one end, was slipped over and hooked on to this rod. To the other end of the tube was sealed a rod

to which was attached a tube completely enclosing a length of iron rod The weight and position of the rod were such that sufficient frictional force was exerted between the brake and rod supporting anode to prevent movement when contact was made. The frictional force was increased by roughening rod and brake with coarse carborundum powder. The point of the peg and notch system in the lever was to facilitate construction of the tube, the main body of the lever being hooked on after t. · anode assembly had been fixed in position. A coil, C_2, could be used to lift the brake from the rod.

The cathode, as in the second and third tubes, was contained in a glass support fixed by an internal seal in the base of the discharge chamber. A wall guard-ring was formed at the base of the chamber during the distillation process. This electrode was connected to the cathode (though electrically separate) via the rsservoir, B. This was surrounded by a heating coil so that mercury could be distilled from the wall electrode to the cathode thus maintaining the required cathode level. This level was proud of the edge of the containing cup by about 2 mm. This method of maintaining the correct amount of mercury in the cathode was simple and convenient as no mechanical disturbance of the tube was required and the level could be restored without cooling and removing the electric furnace.

A wider diameter ($\frac{1}{2}$") quartz window was attached to the discharge chamber at such an angle that radiation of the cathode at grazing incidence by ultra-violet radiation could be achieved. A wide diameter tube was used so that if necessary the radiation from an air spark-gap

could be focussed on the cathode. For steady state experiments an ordinary high pressure mercury lamp was used as a source of radiation, collimation being achieved by an appropriately machined cylinder of aluminium, mounted over the quartz tube.

Electrical contacts were made by tungsten seals and nickel tape, which was surrounded by lengths of glass tubing to minimise contact with the chamber walls. Observations of electrode separation were made through a plain glass window.

4.6 The Electric Furnace

Previous workers in the field of low pressure discharges in mercury vapour have used air furnaces with apparent satisfaction. They have the advantage over oil baths in that there is no mechanical vibration to disturb the mercury surface, and that convection currents do not introduce difficulties in measuring electrode separations to the same extent. An air oven was therefore decided on and was developed in conjunction with Smith (34).

Preliminary experiments were carried out with a furnace consisting of an iron box approximately 1' × 6" × 6" and with a thickness of plate of about $\frac{1}{4}$". A flanged plate of the same material served as a lid. Holes were drilled in this lid and thermocouples mounted in it in such a way that when the lid was in place the tips of the thermocouples at various points of different height along the length of the box. A thermocouple was mounted in a tube which passed along the centre of the box. The position of the thermocouple could then be altered by the manipulation of the tube from outside the oven. Thus assembled, the box

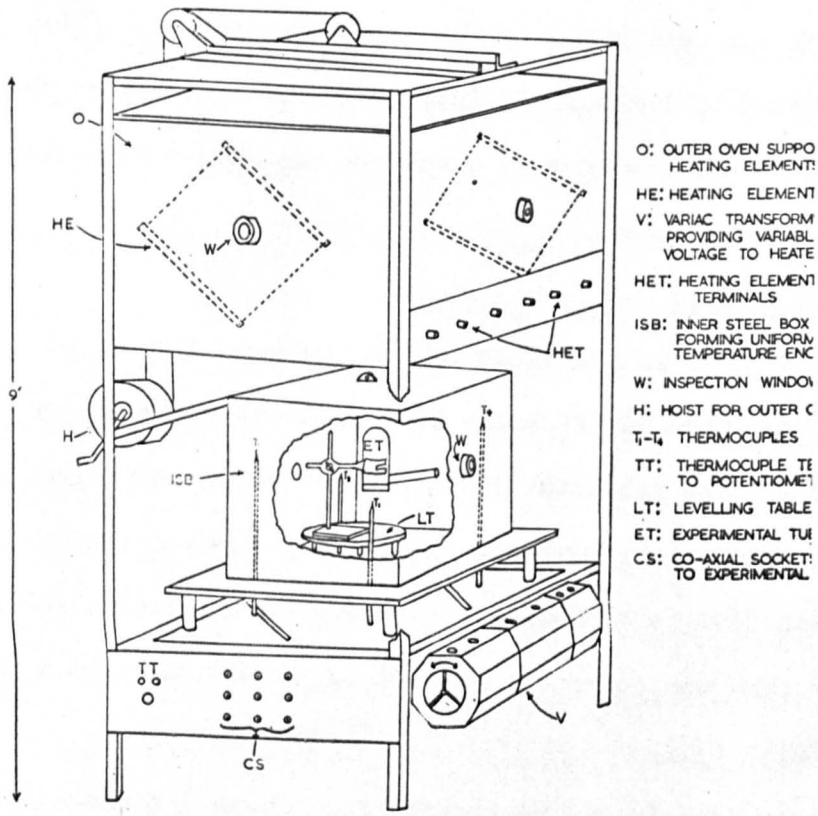

The Electric Furnace.

fig 36

was mounted inside another in such a way that a free flow of air all round the box was possible. This outer container was fitted with electric elements on two of its faces. It was hoped that the high conductivity of the iron would produce six faces all at the same temperature, thus reducing temperature gradients within the inner box. It was found that no appreciable difference in the thermocouple readings occurred if the temperature was increased slowly.

On the strength of this result, an improved and larger furnace was constructed on the same principles, fig. (36). In this case the inner enclosure consisted of a cube of side 2'3" and was constructed from $\frac{1}{2}$" thick steel plate. The base was detachable, and by the use of a winch the main body of the enclosure could be lifted clear providing easy access to the experimental tube. The base plate was mounted clear of the underside of the outer container, allowing air to circulate freely. The outer container was a cube of side 4' made from hard asbestos and lined on its outer faces with polished aluminium sheet to reduce heat losses. It was made on the same plan as the internal enclosure so that by use of a winch it could be raised clear of its base exposing the inner iron box. The amount of air space between the inner faces of the outer box and the outer faces of the inner box was about 6" all round. Windows 2" in diameter were drilled in the centre of each lateral face of each container. These were necessary for the illumination and inspection of the electrode space, and also to allow the irradiation of the cathode by ultra-violet light.

The heating system consisted of twelve five hundred watt elements

mounted two to each of the inner faces of the outer box, providing a total power of 6 kilowatts. The elements were mounted obliquely across each face to assist the even distribution of heat. The heaters were connected to the mains through three eight amp Variac transformers ganged together so that they could be operated simultaneously. The transformers enabled the temperature of the furnace to be adjusted to any desired value up to a maximum of 200°C. Four calibrated thermocouples were used to test the furnace for temperature gradients. These were mounted at different parts and at different heights inside the inner box. The maximum difference in temperature that could be detected between the extremes of the furnace was 1°C. This meant that the variation in temperature in the centre, in the region of the ionisation chamber, was about 0'1°C.

Leads to the thermocouples and to the various electrical connections to the experimental tubes were taken out through the base of the furnace through glass tubes and attached to coaxial sockets on a panel fixed to the main frame. In the case of the anode and cathode leads the glass tubing was encased in copper conduit piping and fixed rigidly in position. This reduced vibration and the production of small charges by friction and also provided an efficient electrostatic screen. Both these conditions are essential for the measurement of currents of the order of 10^{-11} amps.

The large thermal capacity of the inner iron enclosure ensured that small changes in power supply produced negligible fluctuations in temperature unless the change was maintained for long periods of time.

VOLTAGE SOURCE

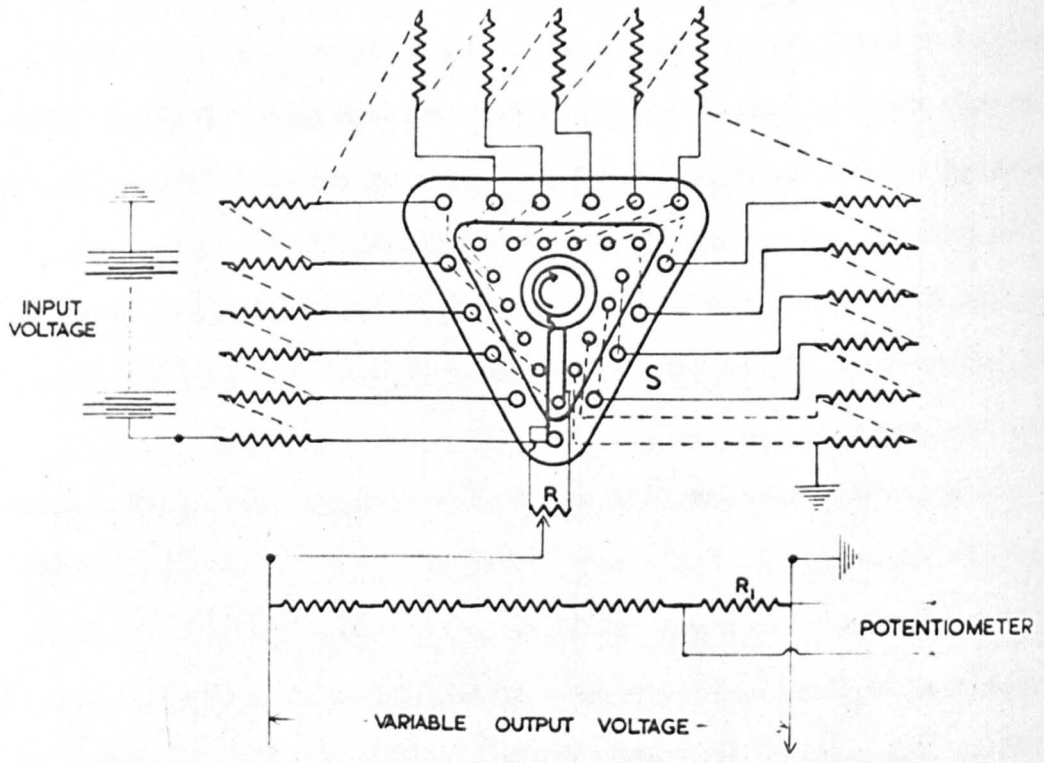

fig 37

Furthermore, the large overall mass, about 10 cwt., ensured almost pefect mechanical stability.

4.7 The voltage source

The D.C. voltages were obtained from a bank of dry cells connected in series through a chain of 500 kΩ resistors. These resistors were wired to a double bank selector switch, S, (fig. (37), enabling various voltages to be tapped.

A 250 kΩ wire-wound potentiometer, R, was connected across the output of the switch. The centre terminal of this potentiometer was used as the high tension output, enabling the voltage to be varied by less than 0.1 volts.

The output voltage was measured by applying it across a chain of calibrated resistances, each of the order of a megohm. This chain was wired in series with a calibrated wire-wound 15 kΩ resistor, R_1, and the voltage drop across this resistor measured with a potentiometer. The multiplication of this voltage by the appropriate factor gave the value of the output voltage.

The apparatus described above was used in the measurement of breakdown potentials, first ionisation coefficients and formative time-lags. The techniques used in obtaining these measurements will be described in the following chapter.

CHAPTER 5

EXPERIMENTAL PROCEDURE

5.1 The production of high vacuum and distillation of mercury

The method of evacuating the experimental tubes was basically the same in all cases. All grease and dust particles were removed from the glassware before it was assembled by washing it thoroughly, first in nitric acid, then in distilled water. As each stage was assembled it was tested for leaks by pumping with the rotary pump and using a high frequency tester. Once it was established that the system was free of leaks large enough to be detected by this method the mercury diffusion pumps were switched on, liquid nitrogen added to the liquid air traps to condense any mercury vapour and the system pumped down until the micro-ammeter of the Penning gauge showed no deflection. The pressure on the high vacuum side of the pumps was then taken to be about 10^{-6} torr.

The metal parts of the Bayard-Alpert gauges were outgassed by simultaneously heating the filaments to red heat by passing a large current through them, and heating the grid to roughly the same temperature by means of an eddy current heater. The whole manifold was then baked at 480°C. overnight in an electric furnace. In the third and fourth experimental tubes, where commercial Bayard-Alpert gauges of Kodial were used, the maximum bake-out temperatures were limited to 450°C. Above this temperature the gauges began to soften. After baking the Bayard-Alpert gauges were again treated as previously described and the constriction, C_4 (figs. 31, 32) closed. The manifold then being

completely isolated from the pumps, the Bayard-Alpert gauge was used to indicate the pressure in the manifold. For the first few attempts the gauge indicated that the system was not leak-free. One of the breakers, $B_1 \ldots B_3$, was then opened, the leak found and the whole procedure repeated until the gauge, after showing a small initial rise in pressure, probably from a slight outgassing of the system, showed a steady decrease in pressure. This indicated that the system was leak-free and that the gauge was acting as a pump. Another of the breakers was then opened, the gauge again outgassed and the system baked continuously at the maximum possible temperature for 120 hours.

The experimental tubes could then be isolated from the manifold by slowly collapsing the constriction on the pumping arm (C_5), thus allowing the gas to be released by the heat to be pumped away.

In the case of the third and fourth experimental tubes, where the distillation apparatus was pumped continuously, the Bayard-Alpert gauge was used to test and pump the experimental tubes alone. The constriction, C_4, was replaced after each test. The tubes were pumped for about three weeks by the gauge, the ultimate pressure being between 10^{-7} and 10^{-8} torr.

While the gauge was pumping, the distillation of the mercury was begun. 99.9% pure mercury was admitted to the first distillation tube by breaking the fine tip of the capillary tube submerged in the mercury and drawing the mercury into the tube under the action of the vacuum. The purpose of the capillary tubing was to reduce the speed and violence of the entry of the mercury into the first distillation tube and so

prevent the apparatus from shattering. When sufficient mercury had been admitted the capillary tube was softened and sealed at a point just beneath that at which it was drawn out. Distillation from the first to the second tubes was then begun. This was achieved by means of an electric heating coil surrounding the tube, in series with the variable resistance. The resistance enabled the selection of convenient distillation rates. Heating braids were also used when the distillation rate was too slow.

When about three quarters of the mercury had been distilled the constriction, C_1, was closed and the distillation from the second tube effected in the same way as from the first tube. Again, after about three quarters of the mercury had been evaporated the constriction, C_2, was closed.

Since it was probable that the distillation of the mercury was effective in outgassing the mercury, the glass between the third distillation tube and the experimental tube was heated by a gas flame to drive off any absorbed gas on the walls of the tubing. The mercury in in third tube was then heated, the intention being that the vapour, acting as a pump, would drive at least some of the gas liberated through the constriction, C_3. After this had progressed for some time, the constriction, C_3, was closed and the Bayard-Alpert gauge removed from the experimental tube by collapsing the narrow tubing that attached it to the latter, or, as in the case of the third and fourth tubes, the constriction, C_5. This was to prevent the mercury atoms from dislodging gas from the walls of the gauge on opening the breaker, B_4. This breaker

was then smashed by means of the glass encased iron rod, and the final distillation of the mercury into the experimental tubes completed. The tubes were then removed after sealing the tube through which the mercury had been admitted. In the case of the third and fourth experimental tubes, the distillation tubes were made progressively smaller so that the volume above the surface of the mercury in the third distillation tube was small compared to the volume of the experimental tube. The volumes differed by approximately a factor of 20. Any residual air at a pressure of 10^{-6} mm. mercury in the final distillation tube would not then increase the residual air pressure in the experimental tube by an appreciable amount.

After the tubes had been removed from the manifold, they were mounted on a tripod table with adjustable supports. The tubes were then positioned in the inner enclosure of the furnace in such a way that the electrodes were above the centre of the base plate and on a level with the windows of the enclosures. After the electrical connections had been made the electrodes were checked for parallelism by measuring the inter-electrode spacing between the diametric extremes in two directions at right angles by means of a cathetometer. Parallelism was achieved by tilting the cathode surface in the desired direction by adjusting the appropriate supports of the tripod. The enclosures were then lowered into position and the variacs set to give the required operating temperature.

5.2 The measurement of breakdown potentials

The circuit used in the determination of breakdown potentials is

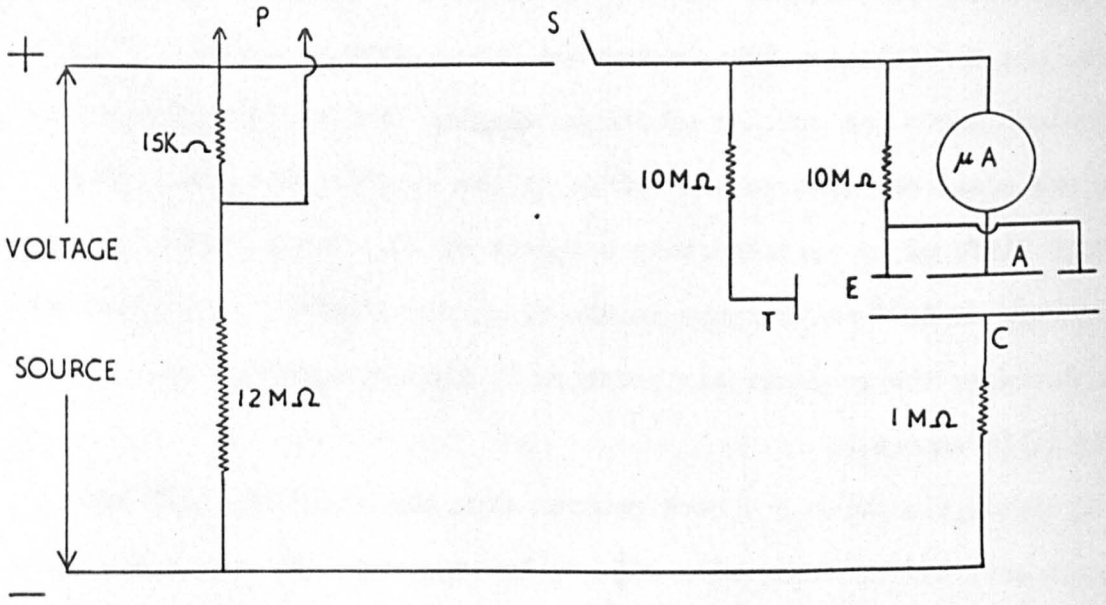

P POTENTIOMETER A ANODE
E ELECTROSTATIC GUARD RING
T TRACKING GUARD RING
C CATHODE S TAPPING KEY

Circuit for the Determination of Breakdown Potentials.

fig 38

shown in fig. (38). The breakdown potential was taken as the potential just sufficient to maintain the discharge without external radiation. The current flowing under these conditions was observed to be 10^{-6} amps, measured by a micro-ammeter. In the case of the first and second experimental tubes the breakdown potentials were taken by varying the vapour pressure for the different electrode separations, the results being plotted in the form of Paschen curves. The temperature of the vapour, taken as that of the cathode, was determined by a calibrated copper-constantan thermocouple strapped to the walls of the tube adjacent to the cathode. No measurements were taken until identical readings between this thermocouple and the others measuring the air temperature of the furnace were observed. This condition meant that there was no temperature difference between the inside and outside of the experimental tubes. Preliminary experiments had shown that, even after the air temperature had become steady, considerable differences in temperature between the air and cathode existed often for periods of up to one hour.

When it was certain that the temperature measured was that of the mercury, the electrode separation was measured with a cathetometer and the breakdown potential taken. This was done by increasing the voltage by small amounts until the micro-ammeter showed the required deflection. The pressure, reduced to the vapour pressure at $0^{o}C.$, was then determined from a graph of pressure and thermal e.m.f. plotted from the tables in the Handbook of Chemistry and Physics. The measurement of breakdown potentials was facilitated by the irradiation of the cathode by ultra-violet light from a high pressure mercury source. Smith (34)

has demonstrated the suitability of such a lamp to these experiments. The radiation was trasmitted from the exterior of the furnace to the quartz window through glass tubing of progressively narrower bore which acted as a wave guide and concentrated the radiation on the cathode. The power to the oven was then increased to give a small increase in temperature and the process repeated. In the case of the fourth experimental tube, a length of metal pipe with polished interior surface was used as a 'wave guide' since it was found to have better transmitting properties.

In the case of the second and third experimental tubes, Paschen curves were obtained by measuring the breakdown potentials for different electrode separations at a given pressure. Sufficient current was passed through the coils surrounding the reservoirs to raise the level of the anode by an appropriate amount. When it was clear that the electrode was stationary, the breakdown potential and electrode separation were measured. The current through the coil was then increased slightly to produce a small change in electrode separation, and the process repeated. Identical precautions were taken as to the determination of vapour pressure as those exercised when using the first and fourth tubes. It was found that the heat developed by the various coils used in tubes 2, 3 and 4 had a negligible effect on the air temperature of the furnace.

A sufficient number of curves could be taken with the third experimental tube to enable curves at given electrode separations to be extracted. These could then be compared with the results from the

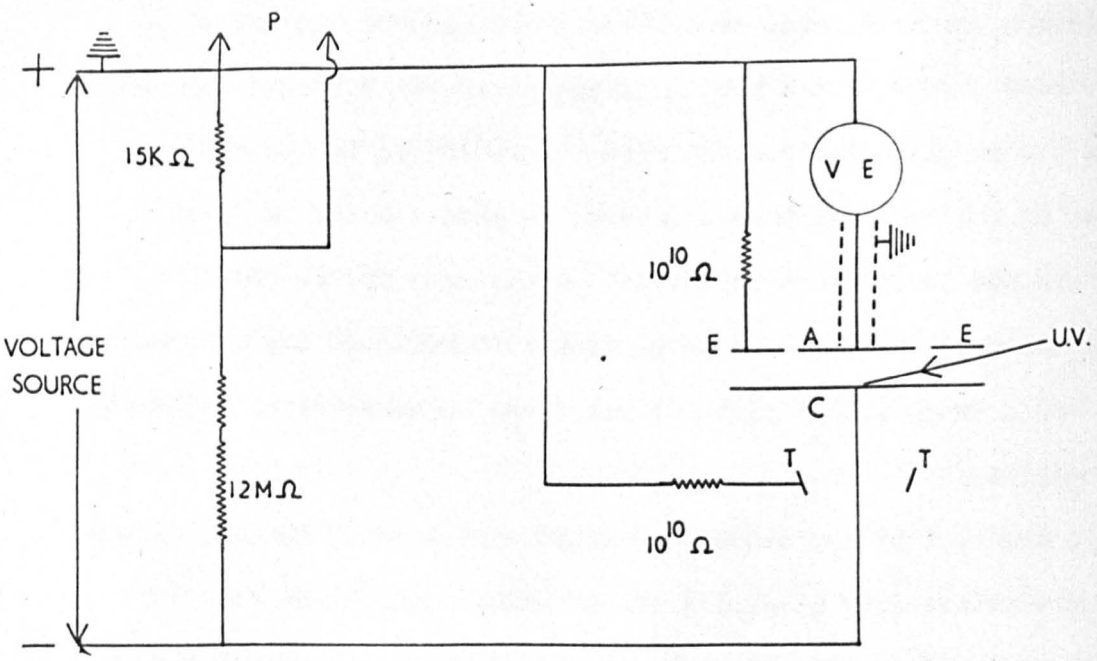

P POTENTIOMETER A ANODE
E ELECTROSTATIC GUARD RING
T TRACKING GUARD RING
C CATHODE
VE VIBRON ELECTROMETER
UV ULTRA VIOLET RADIATION

Circuit for the Determination of Primary Ionization Coefficients.

fig 39

other tubes.

5.3 The measurement of first ionisation coefficients

The circuit used in the determination of first ionisation coefficients for all experimental tubes is shown in fig. (39). In the case of tube 1, it was found that the furnace acted as an excellent electro-static screen when earthed, but with later tubes the anode lead in the oven had to be screened to eliminate pick-up from the various coils.

The high pressure mercury lamp used as a source of ultra-violet light was tested over a period of several days. It was found that constant photo-electric currents could be obtained over this length of time, indicating that the cathode did not suffer from photo-electric fatigue and that the output from the lamp was invariant. Using 'wave-guides' as explained above photo-electric currents of the order of 10^{-11} amps were obtained with all tubes.

Using tube 1, values of the coefficient $\eta=\alpha/E$ were obtained by plotting $\log_e i$ as a function of voltage for different values of E/p_o. The power to the furnace was regulated to give a convenient operating pressure. When agreement between the reading of the thermocouple at the tube and those measuring air temperature had been reached the pressure and electrode separation were measured. These were then used to calculate the voltage required to give a chosen E/p_o. This was then applied by setting the potentiometer to the required value and increasing the voltage until no deflection was observed on the galvanometer of the instrument. Although a wall electrode was included in the tube,

appreciable currents flowed when the ultra-violet radiation was intercepted by a metal shutter. At low values of E/p_o, these currents were of the same order of magnitude as the gas current. The gas current was taken as the difference between the current measured with and without the radiation. The currents were measured in terms of the arbitrary units of the Vibron electrometer.

Using the second, third and fourth experimental tubes, values of the coefficient α were obtained by measuring the slopes of the semi-log plots of current, i, against electrode separation, d, for different values of E/p_o. The pressure was maintained at a constant value, the electrode separation being increased by appropriate amounts. The value of the pressure and electrode separation were used to calculate the necessary voltage to give the required E/p_o. This was applied by using the potentiometer as described previously. The gas current was again taken as the difference between the current flowing with and without the ultra-violet radiation. In general, in order to measure currents of the required order of magnitude at high E/p_o, smaller pressures were necessary than those used at lower values of E/p_o. This limitation, imposed by the conditions of the experiment, will be discussed further in relation to the results obtained, in Chapter 6.

5.4 The measurement of formative time-lags

Using the second experimental tube preliminary measurements of formative time-lags were taken and plotted as a function of E/p_o. The tube was unsatisfactory in that adequate control of the electrode separation could not be maintained. All the useful measurements of

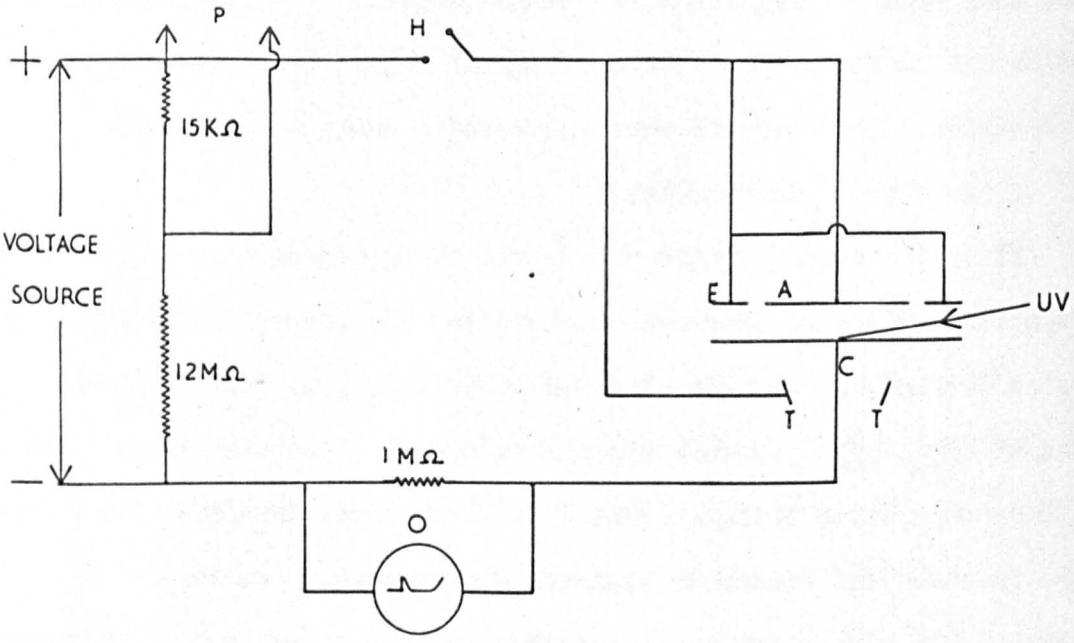

P POTENTIOMETER H MERCURY SWITCH
E ELECTROSTATIC GUARD RING
A ANODE C CATHODE
T TRACKING GUARD RING
UV ULTRA VIOLET RADIATION
O OSCILLOSCOPE

Circuit for the Determination of Formative Time Lags.

fig 40

formative time-lags were taken with tube 4, in which the electrode separation could be maintained at a given value indefinitely.

The overvoltages were limited to a maximum of about 3% so that E/P_o could be taken as sensibly constant. The maximum increase in E/P_o was about 5 volts/cm.$^{-1}$mm.Hg.$^{-1}$. The statistical time-lag was eliminated by supplying initial electrons provided by the irradiation of the cathode by ultra-violet light.

Using a generator giving a rectangular pulse to trigger the time base of an oscilloscope, initial experiments were performed on the measurement of the time-interval between the application of the pulse and the beginning of the fall of the voltage applied to the gap. These attempts were unfruitful because it was not possible to obtain a signal generator which could give pulses of sufficient length to produce breakdown. A more simple circuit was constructed, fig. (40), whereby the times taken for the current to grow from zero to the desired value, 10^{-6} amps, from the instant of application of the pulse could be measured directly. The pulse in this case consisted of the output voltage from a bank of dry batteries. The pulse was applied by means of a mercury switch with a rise time of the order of a micro-second, which enabled pulses of any required length to be applied to the gap. The time taken for the gap to break down and the magnitude of the current flowing were measured by a Tektronix Type 545A oscilloscope, the probes of which were connected across the megohm resistance, R, in the cathode circuit. The voltage drop across the resistance was used to trigger the time base of the oscilloscope. The resistance also served to limit the current flowing in the circuit.

After the pressure and electrode separation had been measured, the breakdown potential (that required to produce a current of one micro-amp) was measured with both micro-ammeter and oscilloscope. The values obtained by these two methods were identical, and for later measurements the oscilloscope only was used. The height of the pulse, equal to the breakdown potential plus the required percentage of this amount, was controlled by giving the appropriate setting to the potentiometer and increasing the voltage output until no deflection on the galvanometer of the instrument was observed. The mercury switch was then closed, and the time taken for 10^{-6} amps to build up in the circuit measured. Several measurements of the formative time-lag were taken for a given percent overvoltage and the average taken. The gap distance was then altered to give a different value of E/p_o and the process repeated. The results of these measurements, together with those on breakdown potentials and first ionisation coefficients are presented and discussed in the following chapter.

Paschen Curves: First Tube.

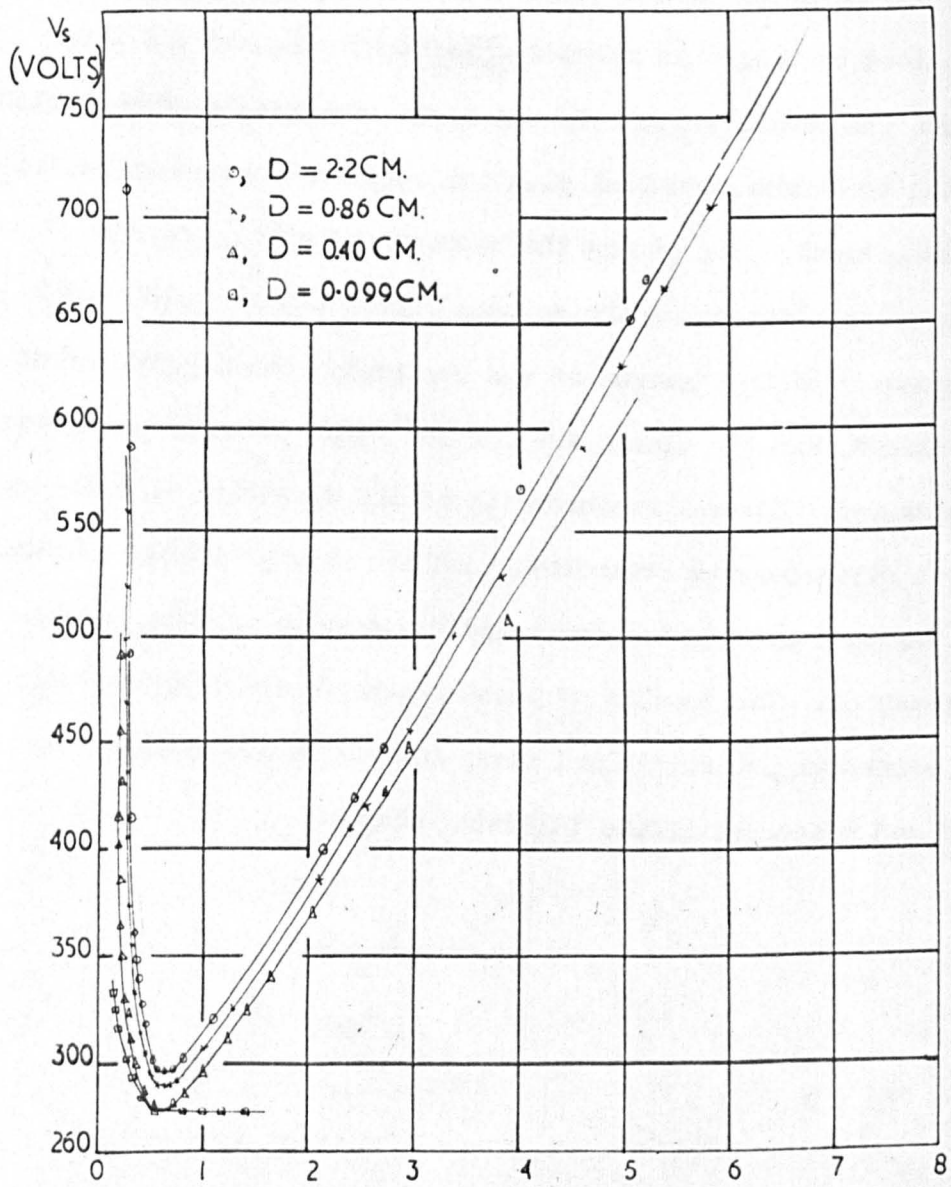

fig 41

CHAPTER 6

DISCUSSION OF THE RESULTS

6.1 Breakdown Potentials

Preliminary measurements of breakdown potentials as a function of the product $p_o d$ were taken for different electrode separations during the rise and fall of temperature. Similar displacements of the two curves along the $p_o d$ axis to those found by Llewellyn-Jones and Galloway (31) and Smith (34) were observed. In order to obtain more accurate results measurements were subsequently taken only after the thermocouple on the tube gave the same thermal e.m.f. as those in the surrounding air. The results obtained in this way with the first tube are shown in fig. (41).

It can be seen from the curves that Paschen's law was not strictly obeyed. For any given value of $p_o d$ over the range plotted the breakdown potential was lower for smaller electrode separations. The divergence from Paschen's law was more pronounced at the minimum. A reduction in electrode separation of 1.34 cms. dropped the minimum breakdown potential by 6 volts. Calculations of the generalised secondary coefficient from these curves, using the sparking criterion, should, therefore, show noticeable differences with electrode separation. This will be discussed further in the section on secondary coefficients.

A similar deviation from Paschen's law was observed by Smith, a reduction in electrode separation of 1.39 cms. produced a drop in

Pasohen Curves: Second Tube.

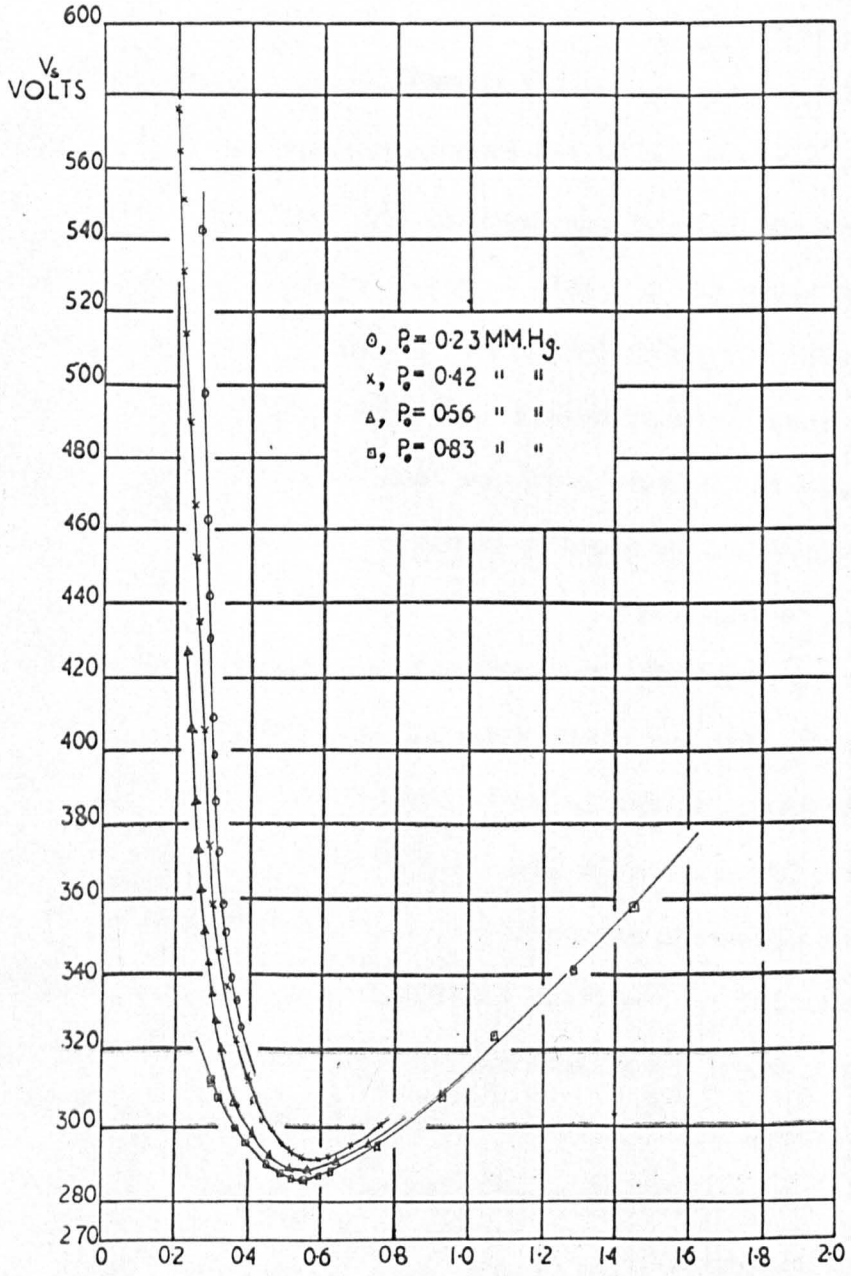

fig 42

the minimum breakdown potential of 9 volts. However, the results obtained for the electrode separation of 0.4 cms. and 0.099 cms. were surprising. There was no change in minimum breakdown potential (277 volts) on decreasing the separation through the difference of 0.3 cms. Smith had shown that the minimum breakdown potential should tend to 282 volts at very small electrode separations. Since the breakdown potential could be determined to within half a volt the difference of 5 volts was hard to explain on the basis of experimental error. Close examination of the cathode surface, however, revealed the presence of a few minute grains, probably of graphite, floating on the surface of the cathode. The particles could have been dislodged either from the anode assembly or from the wall electrode painted on the inner surface of the experimental tube. Assuming a diameter of the order of 10^{-3} cms. with a voltage of 277 and an electrode separation of 0.099 cms. the field applied to the particles would be of the order of 10^{6} volts/cm. which may be just sufficient to produce field emission. Such a mechanism would be independent of pressure and would explain the level nature of the Paschen curve on the right hand side of the minimum. In effect a gas discharge device was produced with a breakdown potential independent of pressure. Such a device may have industrial applications.

The Paschen curves obtained with the second experimental tube are shown in fig. (42). These curves were obtained by keeping the pressure constant while the electrode separation was varied. Unfortunately, the number of curves and the range of $p_o d$ over which the range of breakdown potentials could be measured was restricted by the

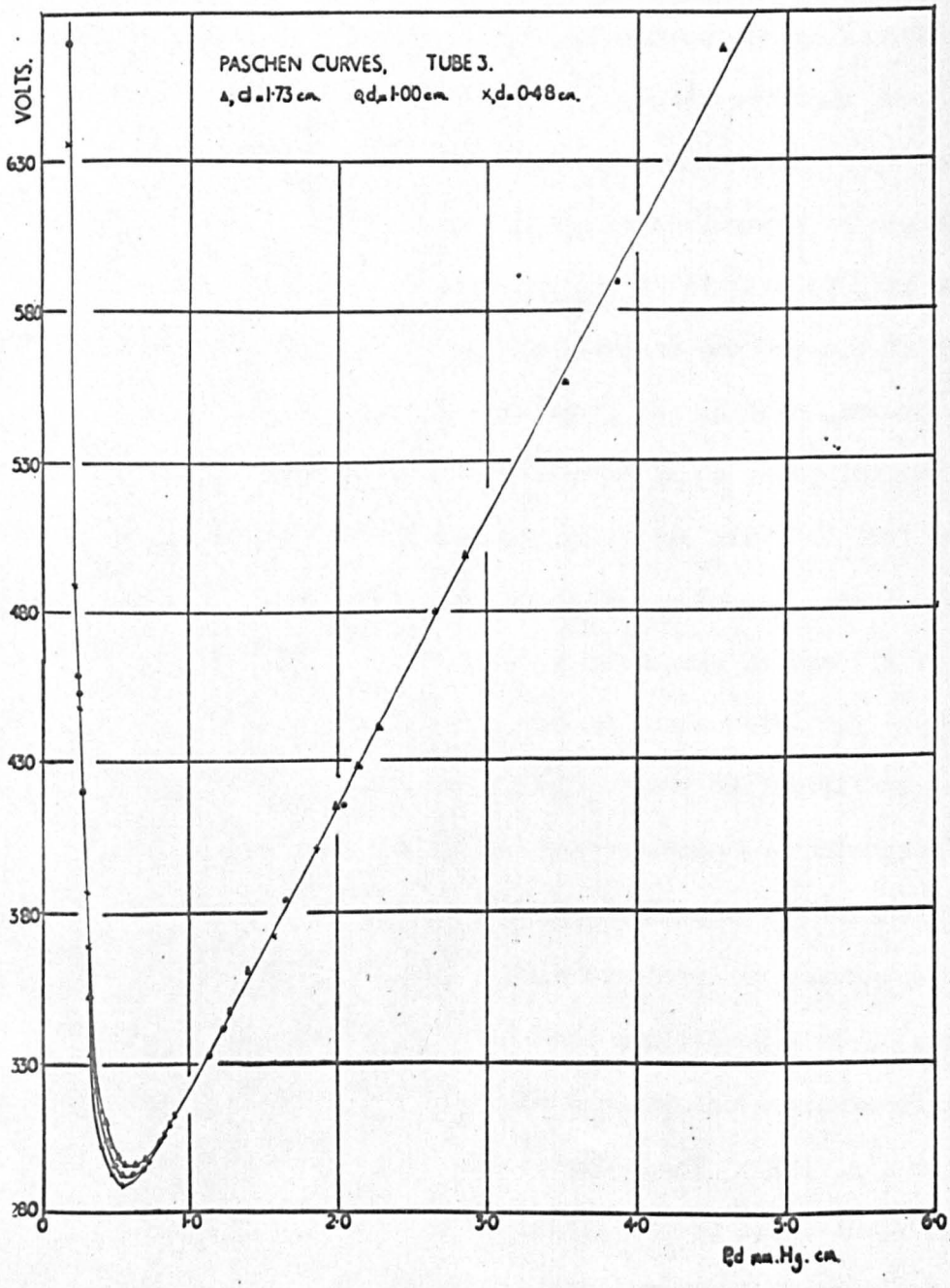
PASCHEN CURVES, TUBE 3.
Δ, d = 1·73 cm. ○ d = 1·00 cm. × d = 0·48 cm.
VOLTS.
630
580
530
480
430
380
330
280
0
1·0
2·0
3·0
4·0
5·0
6·0
pd mm. Hg. cm.

fig 43

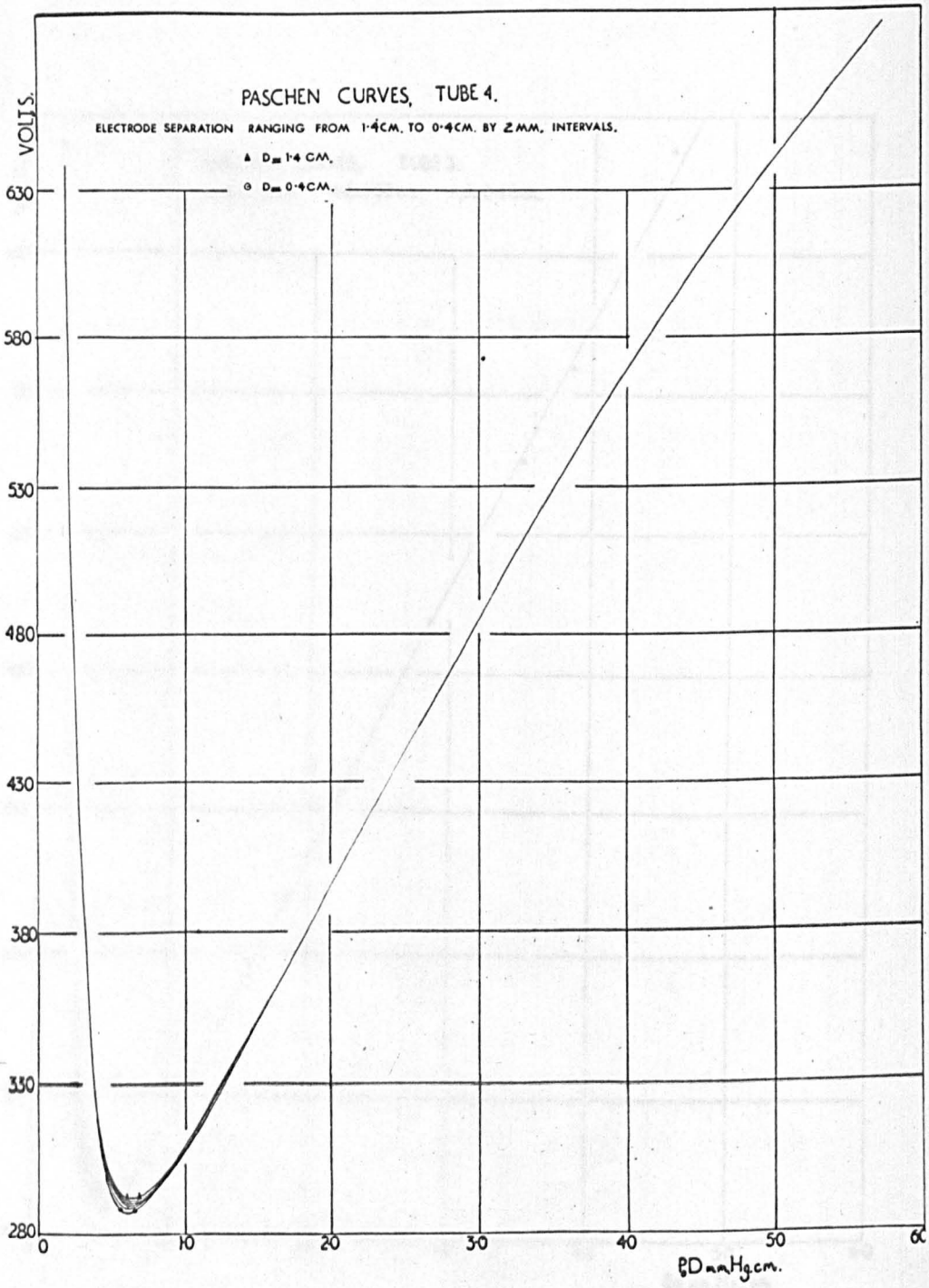
PASCHEN CURVES, TUBE 4.
ELECTRODE SEPARATION RANGING FROM 1·4CM. TO 0·4CM. BY 2MM. INTERVALS.
▲ D= 1·4 CM.
⊙ D= 0·4CM.
VOLTS.
630
580
530
480
430
380
330
280
0
10
20
30
40
50
60
pD mm Hg cm.

fig 44

fact that the minimum electrode separation was 4 mm. This limited the choice of pressure required to give the value of $p_o d$ at the minimum.

Deviations from Paschen's law were again apparent. For any given value of $p_o d$ the breakdown potential was lower for higher values of p. The curve $V = f(pd)$ has the same shape as the curve $V = f(\frac{d}{\lambda})$ where λ is the mean free path of electrons. At lower pressures $\frac{d}{\lambda}$ is smaller because λ is larger. Hence that will be fewer collisions and higher voltages will be required to produce breakdown. This would explain the displacement of the curves along the voltage axis.

Paschen curves obtained with the third and fourth tubes are shown in fig. (43) and fig. (44) respectively. The curves obtained with the third tube for the three electrode separations 1.73 cm., 1.0 cm. and 0.48 cm. were extracted from several curves taken by varying the electrode separation for a given pressure. The curves obtained with the fourth tube were taken in a similar manner to that used with the first experimental tube.

It can be seen that as with the first tube, deviations from Paschen's law occur in both cases at the minima, viz. between the range for $p_o d$ of 0.3 and 1.6 torr.cm. A decrease in electrode separation again reduces the minimum breakdown potential. With tube 3 a reduction of electrode separation from 1.78 to 0.48 cm. lowers the breakdown potential by 7.5 volts and with tube 4 a reduction in electrode separation from 1.4 to 0.4 cm. lowers the breakdown potential by about 5 volts. Outside this range of $p_o d$ one curve describes the variation of the breakdown potential, V_s, with $p_o d$ irrespective of the value of

the electrode separation. The fact that the deviation, more pronounced at the minimum, is maintained at higher values of $p_o d$ in the case of tube 1 and in the case of Smith has to be explained. In both these tubes the electrode geometry was identical and the electrodes had little clearance from the walls of the tubes. The third and fourth tubes had electrodes of the same diameter as tube 1 but the clearance of these from the tube walls was greatly improved. These facts suggest that in some way the proximity of the tube wall was affecting the discharge. McCallum and Klatzow (40), working in argon, neon and helium, demonstrated that the breakdown potential depended on the ratio D:d and to some extent on the distance between the walls of the tube and the electrodes. The effect of the proximity of the walls was found to be important in those cases where the diffusion rate of electrons was great. The effect was investigated by measuring the photo-electric currents between the electrodes. It was found that a small current of electrons to the wall of the tube occurred. It was proposed that the proportion of electrons lost in this manner would be greater for an apparatus of which the value of D:d is small than for one in which the ratio is large, and consequently it would be expected that the breakdown potential would be greater in the former apparatus although the value of pd is the same. The effect of the lateral diffussion of electrons is to negatively charge the glass walls. This may affect the uniformity of the field and also cause loss of positive ions on contact with the glass, an increase in potential being required to compensate for the loss. It should be remembered that the

potential of the tube wall would be slightly positive with respect to the cathode since the wall electrodes were maintained at anode potential. This would have the effect of increasing the lateral diffusion of electrons. However, in a mercury discharge it is to be expected that the metastable atoms and photons will be to some extent important to the breakdown mechanism. Collision of metastables with the walls may result in the production of a photon or in simple reflection. The probability of volume destruction of metastables on reflection would be smaller the smaller the volume and the probability of contact with the cathode greater. Thus the smaller the electrode separation the lower the breakdown potential expected if this mechanism were operative. The fact that at high $p_o d$, for any $p_o d$ the breakdown potentials are lower in in tube 1 and that of Smith than the potentials found with tubes 3 and 4, suggests that reflection may be operative and may be more important than lateral electron diffusion.

In tubes 3 and 4 the Paschen curves suggest that the similarity principle is obeyed except for the range of $p_o d$ between 0.3 and 1.6 torr.cm. However, since the rate of change of V_s with $p_o d$ is zero at the minimum any influence of electrode geometry on the breakdown potential due to the loss of active particles should be most noticeable at this value. The next section deals in more detail with this region of the Paschen curve.

6.2 The minimum breakdown potential

McCallum and Klatzow pointed out the importance of taking into consideration the ratio D:d in monatomic gases when comparing breakdown

MINIMUM BREAKDOWN POTENTIAL AS A FUNCTION OF ELECTRODE SEPARATION.

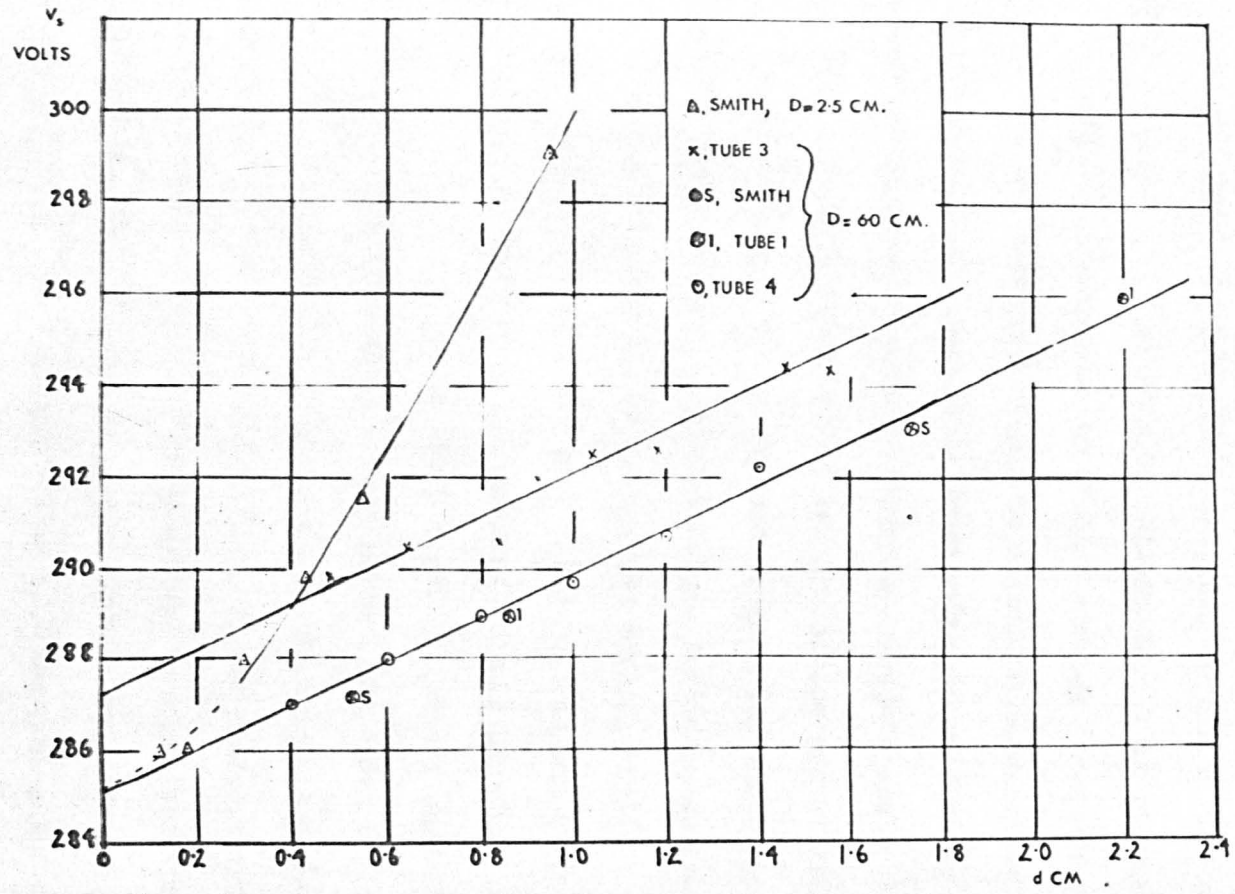

fig 45

potentials obtained with different apparatus. Smith, using the results of one tube with an electrode diameter of 2.5 cms. and another with diameter 6 cms. showed that the minimum breakdown potential could be related by the equation

$$V_{s(volts)} = 282 + \left(\frac{d}{D}\right) 41 \mp 1 \text{ volt}$$

Thus, as d tends to zero, V_s tends to 282 volts. The present results do not fit this expression to the nearest volt, but are often 2 or 3 volts out. The present equation relating V_s to D:d is

$$V_{s(volts)} = 285 + 29 \left(\frac{d}{D}\right) \mp 0.5 \text{ volts}$$

The reason for this discrepancy becomes apparent when the minimum breakdown potential, V_s, is plotted as a function of d alone. Such a plot is shown in fig. (45).

The results obtained with tubes 1 and 4, and those of Smith with a tube of the same electrode diameter, 6 cms., show that a linear relationship exists between the minimum breakdown potential and electrode separation given by

$$V_s = 285 + 5d \mp 0.5 \quad \text{where d is in millimetres.}$$

The results obtained by Smith with a tube containing an anode of smaller diameter, 2.5 cms., and a cathode of about 6 cms. diameter show a steeper relationship, which, when extrapolated, intercepts the voltage axis at about 282 volts. However, the minimum breakdown voltages at the smallest electrode separations indicate that in fact this curve is bending to give an intercept of 285, in agreement with the results

obtained from the previously mentioned tubes.

The results from the third experimental tube again indicate a linear relationship between V_s and d, with a slope of 5d as found with the other tubes of the same electrode diameter. However, the intercept is no longer at 285 volts but at 287. For a given electrode separation the minimum breakdown potential is 2 volts higher than previously obtained with electrodes of the same diameter. The vacuum and mercury purifying techniques were similar to those used in the manufacture of the other tubes and the ultimate pressure, no higher than 10^{-7} mm.Hg. was the same. The higher voltages could not be due to any difference in these techniques. It was noticed, however, that when the constriction C was being closed when making tube 3, gas was evolved in sufficient quantities to raise the pressure by an order of magnitude. Although the constriction was not finally sealed until this gas had been pumped away by the Bayard-Alpert gauge and the pressure had returned to its initial lower value, quantities of gas may have been adsorbed on the walls of the tube. It seems possible that some of this gas, a fair proportion of which would be oxygen, would desorb under experimental conditions and rest on the cathode. Smith has shown that an air impurity with a partial pressure of 10^{-4}mm.Hg. was sufficient to raise the breakdown potential by 40 volts. It is well known that the adsorption of gas on to a cathode can markedly change the breakdown characteristics. A thin layer of oxygen would effectively raise the work function and explain the increase in the breakdown potentials. To produce a change in breakdown potential of two volts, the change in work function would

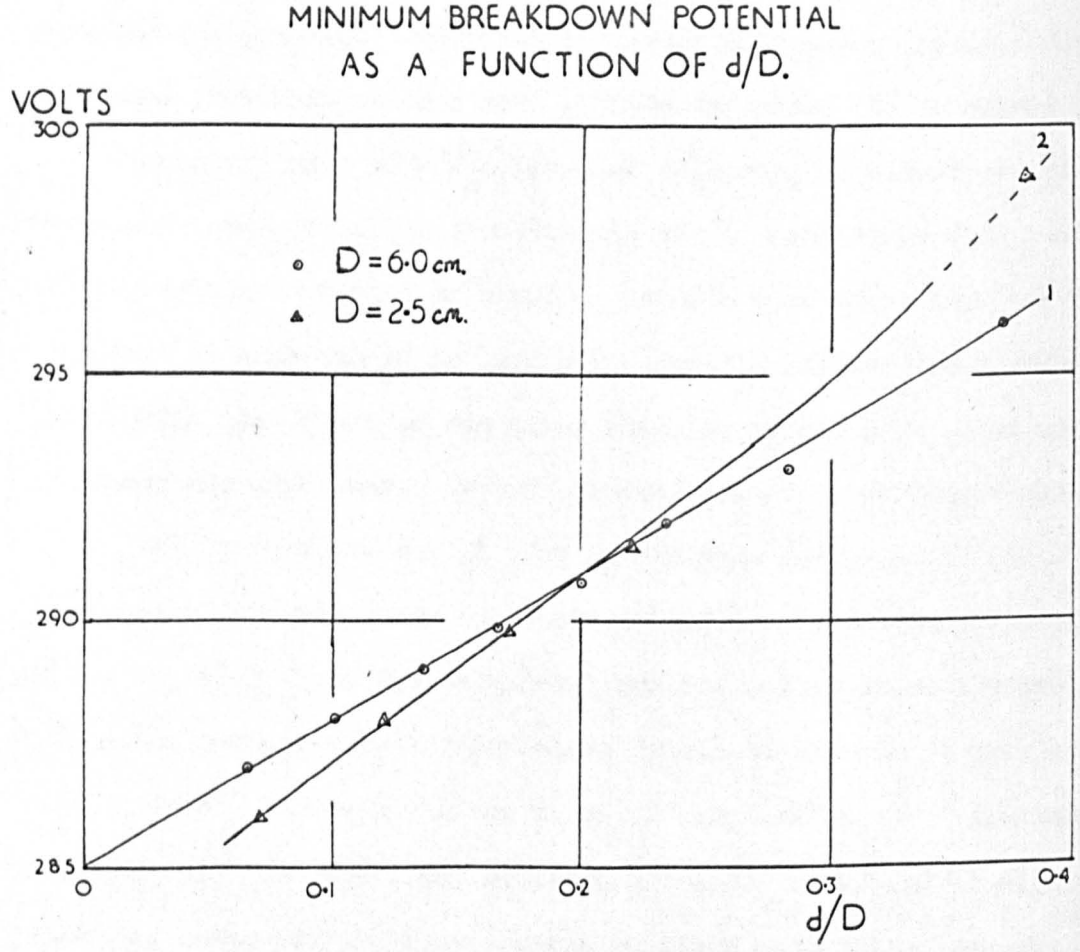
MINIMUM BREAKDOWN POTENTIAL
AS A FUNCTION OF d/D.
VOLTS
300
295
290
285
D = 6·0 cm.
D = 2·5 cm.
1
2
0
0·1
0·2
0·3
0·4
d/D

fig. 46.

not necessarily have to be very great. Gozna (43) has shown that with copper surfaces an increase in work function of 1/50 volt is sufficient to raise the breakdown potential by 1 volt. Any misgivings that this impurity content, though small, would effect the gaseous ionisation process were dispelled when the values of α/p obtained with this tube were reproduced with the fourth tube, where the rise in pressure during the sealing of the constriction C_5 was not observed, and an ultimate residual pressure of not greater than 10^{-8} torr was attained.

When V_{smin} is plotted as a function of the ratio d:D two distinct curves emerge, fig. (46). Curve (1) represents the results taken with tubes with electrode diameter of 6 cm. and curve (2) those taken by Smith with an anode dimaeter of 2.5 cms. Ideally, if V_s is a function of d:D alone these two curves should be coincident. However, the geometry used by Smith in this tube was poor and would not result in uniform field conditions. Direct comparison is therefore not justified in this case.

The values of the minimum breakdown potentials obtained with the second experimental tube cannot be compared directly with those obtained by keeping the electrode separati n constant and varying the pressure since an insufficient number of curves was obtained at constant p and variable d for curves at constant d and variable p to be extracted. However, the minimum values of 286, 288 and 292 volts fall within the range obtained with other tubes. The value of 295 volts as obtained by Grigorovici also falls within this range. The close agreement between the results is remarkable on consideration of the

Current as a Function of Voltage.

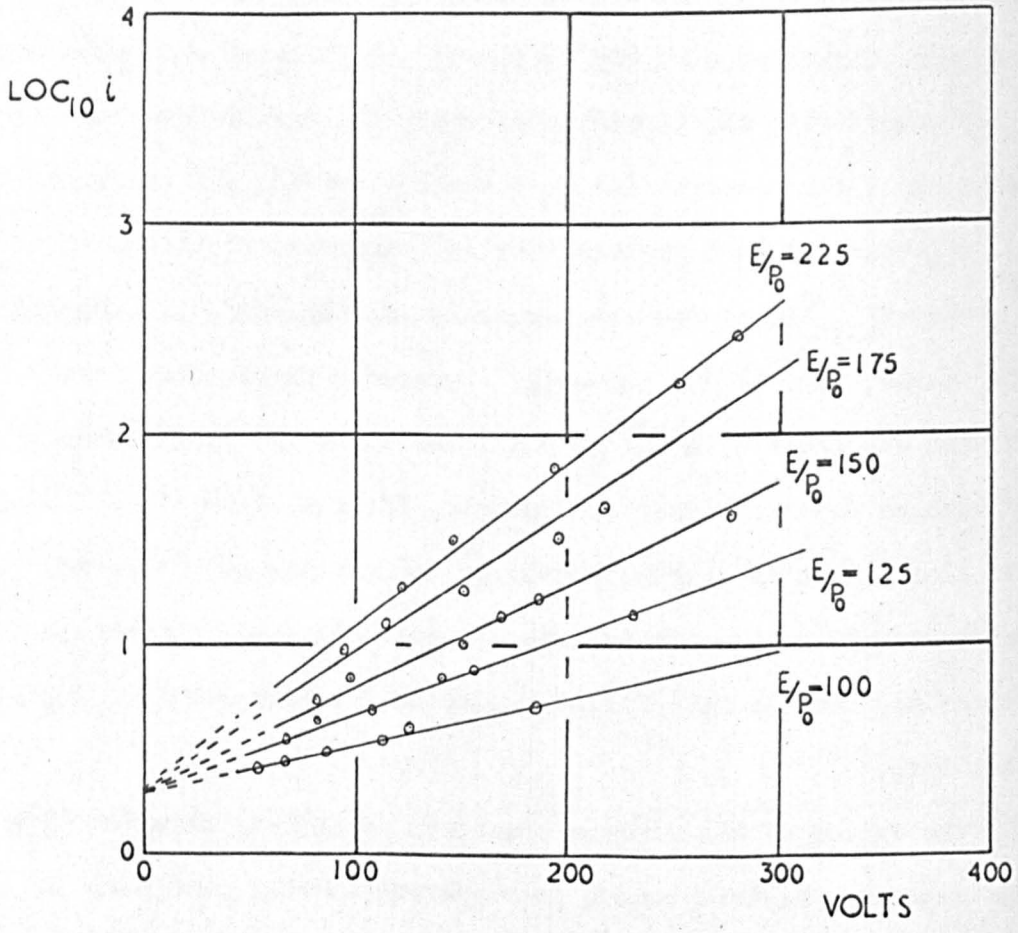

fig. 47.

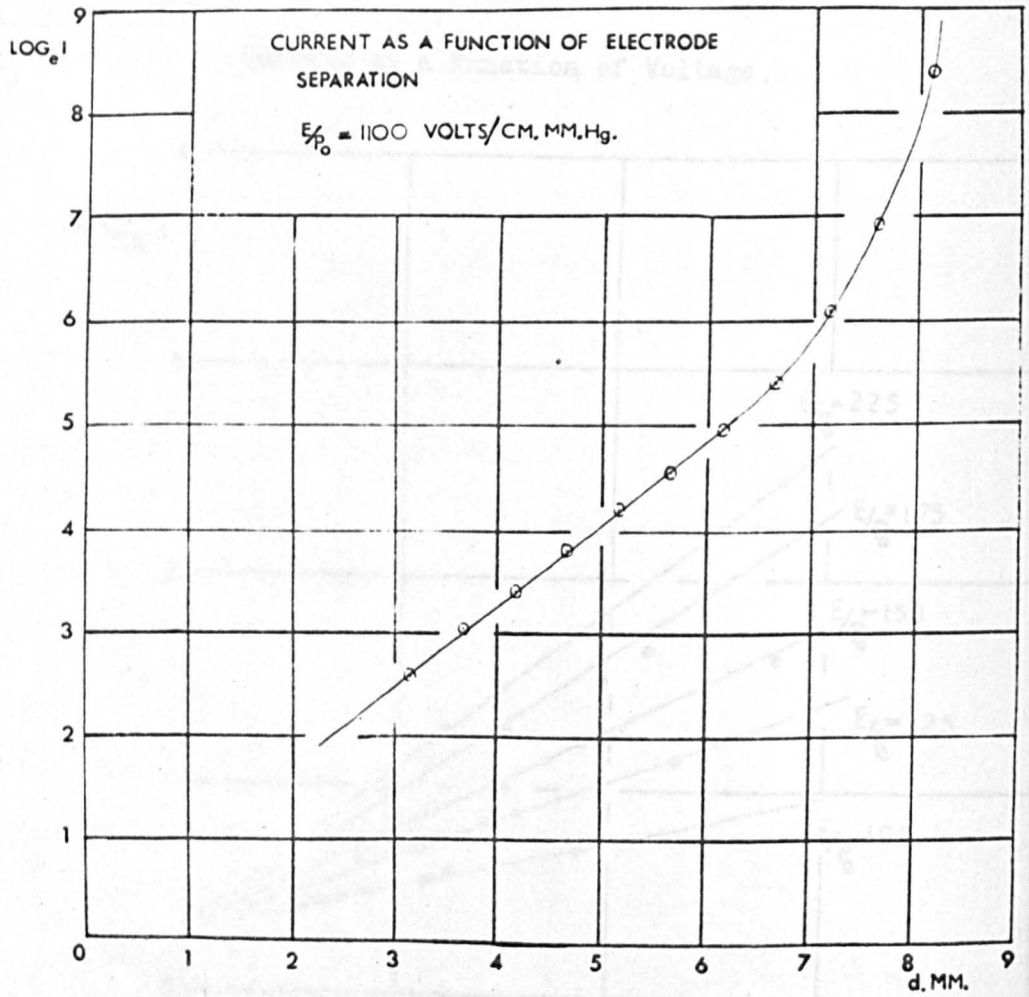
CURRENT AS A FUNCTION OF ELECTRODE SEPARATION
E/p₀ = 1100 VOLTS/CM. MM. Hg.
LOG_e I
9
8
7
6
5
4
3
2
1
0
1
2
3
4
5
6
7
8
9
d. MM.

fig. 48.

wide divergences that have been demonstrated to occur by Llewellyn-Jones and Galloway and by Grigorovici when alien metals are used as cathodes. Such agreement indicates that by using a properly prepared mercury pool cathode a surface of constant work function can be obtained. This condition is only likely to hold for low current discharges. When arc discharges are involved the possible evaporation of anode material and consequent contamination of the cathode will alter the discharge characteristics.

6.3 First Ionisation coefficients

Using currents between 10^{-12} and 10^{-8} amps, values of α/p as a function of E/p_o were obtained with all experimental tubes. In the case of the first tube the method consisted of plotting $\log_e i$ as a function of voltage for different values of E/p_o by varying the pressure and keeping the electrode separation constant. Some of the curves are shown in fig. (47). In this way values of $\eta=\alpha/E$ were obtained for a range of E/p_o from 100 to 300 volts $cm.^{-1}mm.Hg.^{-1}$. Pursuit of measurement beyond this range was prevented by a break occurring inside the tube in the electrical lead to the electro-static guard-ring. A few measurements were taken with the electro-static guard-ring floating, in the hope that some indication might be given as to the actual importance of the guard-ring in the discharge. It was found that the values of α/p for a given E/p_o were about 6% higher with the guard-ring floating. At the electrode separation used the ratio of D:d was about 2, which meant that some field distortion was probably present, apparently increasing the values of α/p.

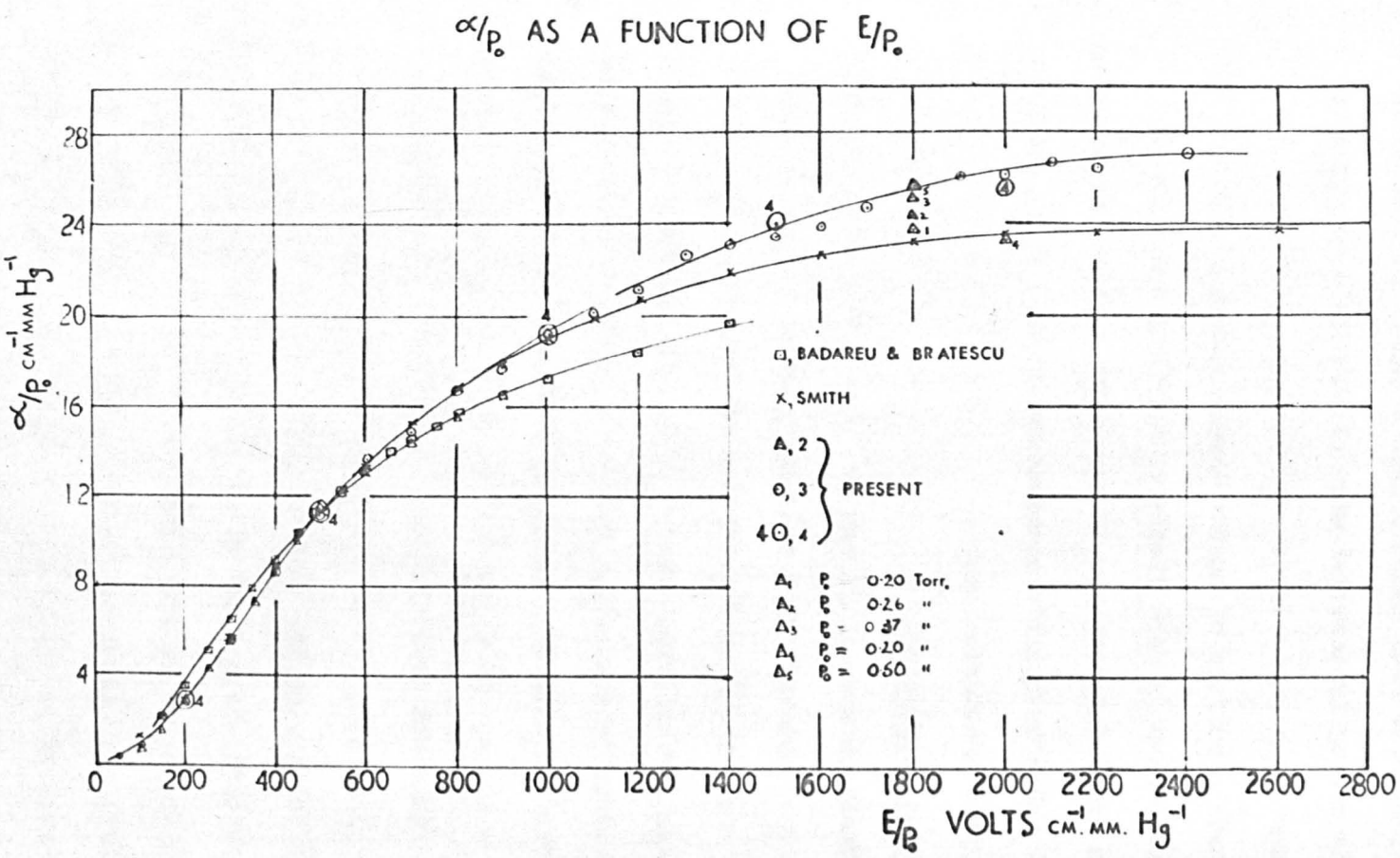
α/p₀ AS A FUNCTION OF E/p₀
α/p₀ CM⁻¹ MM Hg⁻¹
E/p₀ VOLTS CM⁻¹. MM. Hg⁻¹
□, BADAREU & BRATESCU
×, SMITH
▲, 2
⊙, 3
⊙, 4
PRESENT
▲1 p₀ 0·20 Torr.
▲2 p₀ 0·26 "
▲3 p₀ = 0·37 "
▲4 p₀ = 0·20 "
▲5 p₀ = 0·60 "

Fig. 49.

Values of α/p as a function of E/p_o were obtained with tubes 2, 3 and 4 by plotting curves of $\log_e i$ as a function of electrode separation, d, for a given E/p_o. A typical curve is shown in fig. (48).

Although the second tube allowed measurements to be taken over a greater range of E/p_o than was possible with the first tube the range was limited to a maximum of 800 volts $cm.^{-1}$ $mm.Hg.^{-1}$ by the small electrode diameter and large minimum electrode separation which restricted the possible range of electrode separation. These facts also limited the range of pressure, very low pressure being required at high E/p_o. The use of larger electrodes in the later tubes enabled measurements to be extended over a much greater range.

The curves of α/p_o as a function of E/p_o obtained with the second, third and fourth tubes together with those of Badareu and Bratescu and Smith are shown in fig. (49). The results obtained with the first tube were few and are omitted from the graph for the sake of clarity. These results are listed in Appendix (3). It is convenient to discuss the present results in relation to those of Smith first.

It can be seen that the present results from all tubes are practically coincident with those of Smith up to a value for E/p_o of about 480 volts $cm.^{-1}$ $mm.Hg.^{-1}$, the value of the Stoletow constant. Above this point the values obtained with the second experimental tube lie well below those of Smith and approach those obtained by Badareu and Bratescu. The results obtained with the third experimental tube

are coincident with those of Smith up to about an E/p_o of 1000 volts $cm.^{-1}mm.Hg.^{-1}$. Above this value of E/p_o the two sets of results diverge, the values of Smith levelling off at an E/p_o of 24 $cm.^{-1}mm.Hg.^{-1}$ and those obtained with the third experimental tube appearing to level at about 27 $cm.^{-1}mm.Hg.^{-1}$. The levelling is to be expected from the shape of the probability of ionisation curve, which shows a maximum of about 100 volts electron energy. That the levelling was observed in Smith's case was attributed to the application of the Davies-Milne analysis for the correction of secondary effects. This analysis has been found to be effective in hydrogen (44) where the values of the second ionisation coefficient are high, of the order of 10^{-2}. The values for this coefficient in mercury vapour are small, of the order of 10^{-4}. It would therefore be expected that the correction factor would be small. When the Davies-Milne analysis was applied to the present results it was found that the correction factor was negligible. At an E/p_o of 2,400 volts $cm.^{-1}mm.Hg.^{-1}$ correction was less than 0.1 $cm.^{-1}mm.Hg.^{-1}$. The analysis would be expected to be most effective at low values of E/p_o where ω/α reaches its maximum value. The correction is found to be negligible here also. It seems unlikely, therefore, that the analysis of $\log_e i$ versus d curves can account for the levelling, the experimental error, about 5%, probably being greater than the correction factor.

The fact that the curves are coincident at low E/p_o and diverge only at high E/p_o offers a clue as to a possible explanation of the

divergence. At values of E/p_o greater than that which makes $\eta=\alpha/E$ a maximum the electrons no longer reach equilibrium with the applied field. The electrons gain more energy from the field than can be dissipated in collisions and the excess energy is ultimately delivered to the anode. Thus the concept of a mean electron energy no longer applies because the average electron energy and consequently the electron drift velocity will vary with distance from the cathode. Thus because there is uncertainty in the meaning of E/p_o, α/p has little meaning at these high values of E/p_o. Under conditions of fairly low E and high p, however, electrons can reach terminal energy after travelling a distance, d_o, which is generally taken to be about $\frac{1}{\alpha}$ (45). At high values of E/p_o, d_o cannot be attained and the use of low pressures can only aggravate the situation. At these high values of E/p_o Smith used pressures $\sim 0.1 \rightarrow 0.2$ torr. The electron mean free path at this pressure is 0.05 cm. as calculated from kinetic theory. Assuming Smith's relation

$$\bar{\varepsilon} = (E/p_o)^{\frac{1}{2}}$$

the probability of ionisation is calculated as 0.2, i.e. one in every five m.f.p.'s results in ionisation, or an ionisation occurs on average every 2.5 mm., a distance equivalent to about half the electrode separation. At pressures of 0.5 torr, those used in the present investigation, the ionisation distance corresponds to about one-twentieth of the electrode separation. Thus although equilibrium at high E/p_o (values of E/p_o greater than that given by the Stoletow

constant) is not attained in either case, the values determined by Smith represent a greater diversion from the ideal equilibrium condition than the present results. An explanation of the higher values of α/p as determined with tube 3 in terms of the Penning effect is eliminated since the results obtained at these high values of E/p_o with tube 4, in which the residual air pressure at no time during processing rose above 10^{-8}torr, show excellent agreement. This effect would, in any case, be expected to be most noticeable at low E/p_o where the density of metastables is likely to be greatest. Furthermore, measurements with the third tube using low pressures used by Smith resulted in values of α/p_o showing good agreement with those of Smith. For example, at an E/p_o of 2000 volts $cm.^{-1}mm.Hg.^{-1}$ the value of α/p_o obtained by Smith is 23.5 $cm.^{-1}mm.Hg.^{-1}$. At the same value of E/p_o and with a pressure of 0.2 torr the value obtained with the third tube is 23.2 $cm.^{-1}mm.Hg.^{-1}$. The value of α/p_o at an E/p_o of 1800 volts $cm.^{-1}mm.Hg.^{-1}$ is given by Smith as 23.2 $cm.^{-1}mm.Hg.^{-1}$. Determinations carried out with the third experimental tube at this value of E/p_o for a range of pressures showed an increase in α/p_o with increasing pressure, as shown in the table below.

P_o torr	α/p_o
0.20	23.5
0.26	24.2
0.37	25.1
0.50	25.6

This trend is to be expected under non-equilibrium conditions, where an

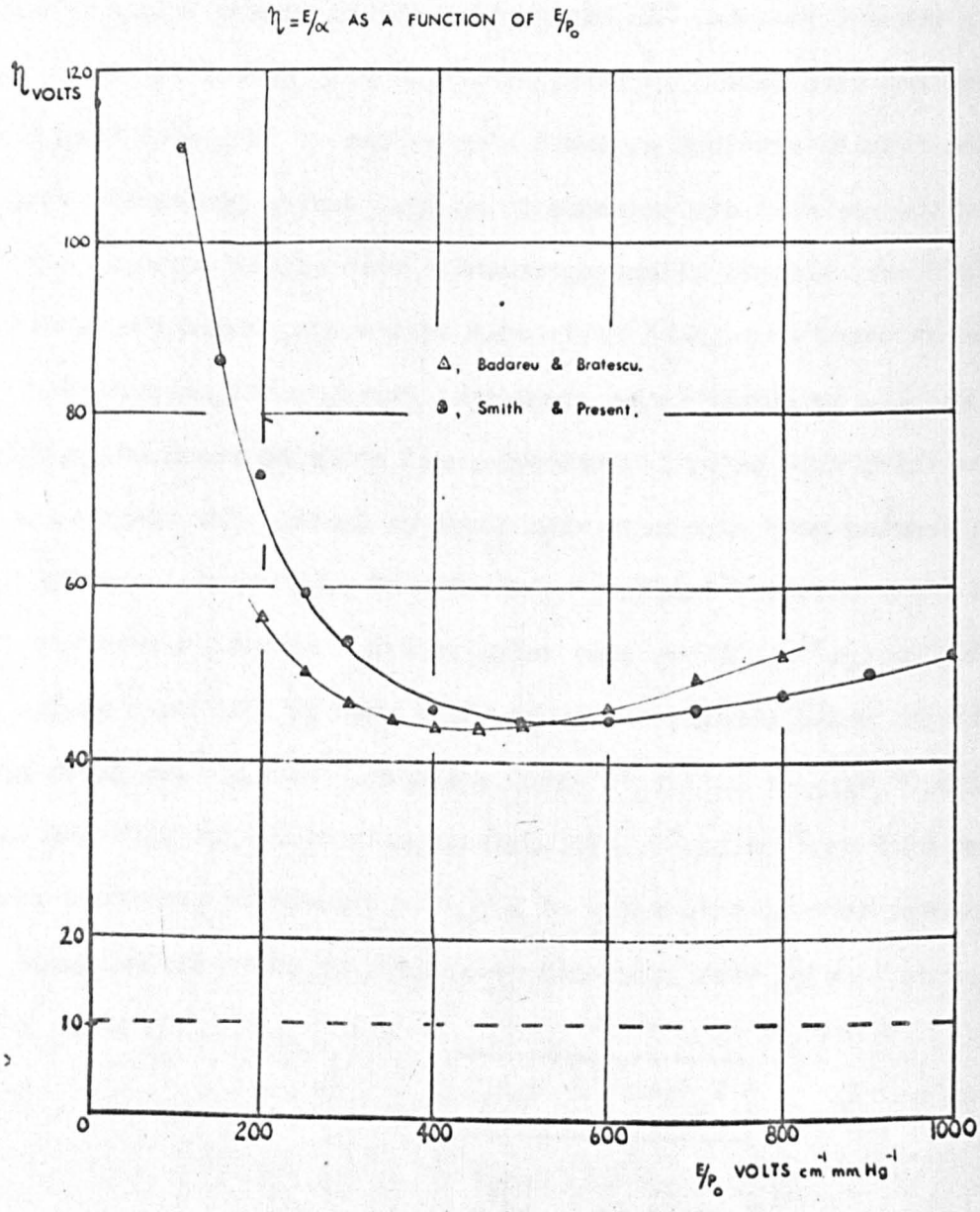
η = E/α AS A FUNCTION OF E/P₀
η VOLTS
120
100
80
60
40
20
10
0
200
400
600
800
1000
Δ, Badareu & Bratescu.
●, Smith & Present.
E/P₀ VOLTS cm⁻¹ mm Hg⁻¹

fig. 50.

increase in pressure will result in greater dissipation of electron energy in the gas and consequently greater ionisation. If the use of higher pressure with the third and fourth tubes had been possible it is probable that even higher values of α/p_o would have been obtained. It is likely that for all practical purposes a maximum value of α/p_o for a given E/p_o will be attained when the closest possible approach to equilibrium is reached. The determination of this value would necessitate the use of electrodes greater in diameter than those used in the present investigations.

The divergence of the curve $\alpha/p_o = f(E/p_o)$ as determined with the second experimental tube can be explained in a similar manner to the above. The comparatively small diameter of the electrodes together with the large minimum electrode separation necessitated the use of low pressures ($\sim$ 0.15 torr) at values of E/p_o from 600 to 800 volts $cm.^{-1}mm.Hg.^{-1}$.

The shape of the curve obtained by Badareu and Bratescu, however, cannot be explained on this basis since the pressures used ranged from 1.26 torr to 3.18 torr and it is therefore likely that a closer approximation to equilibrium conditions at high E/p was obtained by them than was obtained either by Smith or by the present investigator. A possible explanation forthe discrepancy was suggested by Smith when the curves of $\eta=E/\alpha$ as a function of E/p_o are considered. Fig. (50) shows η plotted as a function of E/p_o.

The minimum value of η given by the Stoletow constant represents the minimum amount of electr[illegible]ergy needed to produce an ion pair in

the gas concerned. The values of η at the minimum are 43.8 eV as determined by Badareu and Bratescu and 44.5 eV as determined by Smith and the present author. The agreement is well within experimental error. Since the coefficient η is independent of pressure it would be expected, providing the current measurements had been determined accurately, that the minimum values of η would be the same. However, if some consistent error in the pressure measurements occurred the curves would be expected to show some displacement along the E/p_o axis. It can be seen from fig. (50) that the maximum difference for any two values of E/p_o between the present curves with that of Smith and that of Badareu and Bratescu, for a given value of E/p, is about 20% which represents a difference of 20% in pressure measurements, corresponding to a difference in temperature of 3^oC.

Such a large error in temperature measurement is not likely to have occurred in any of the experiments. The more probable cause is an actual difference in temperature resulting from temperature gradients. A constant check for temperature gradients was maintained in the present case and in the case of Smith. The maximum difference in temperature that could be detected across the extremities of the furnace ($\sim$ 1 metre) in both the above cases was 1^oC. There is no mention in their paper that similar precautions were taken by Badareu and Bratescu. The position of the electric elements in the furnace is not described but it seems most likely that these were mounted on the inner faces of the compartment, in which case temperature gradients are almost certain to have been present. The probability of this would be increased by the

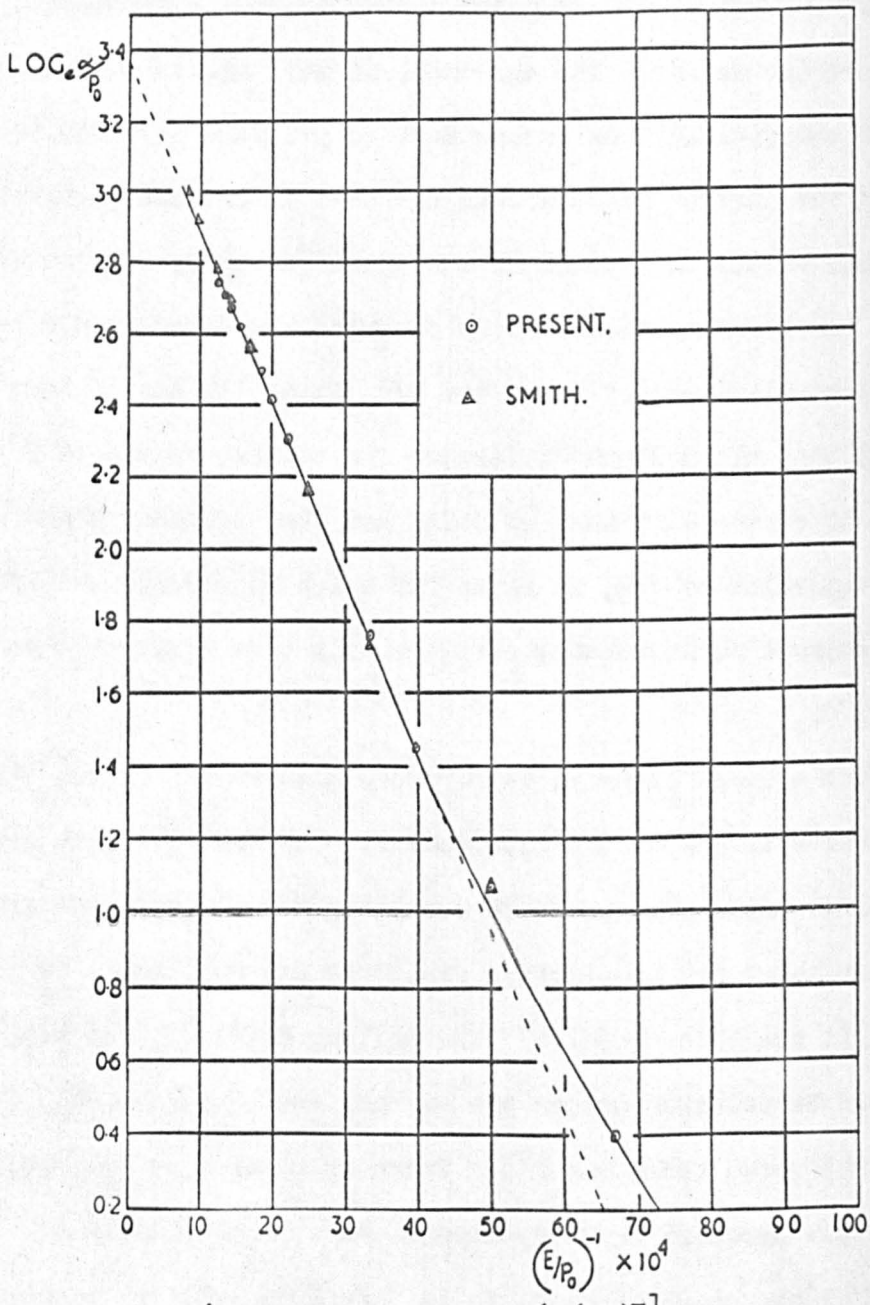

Log$_e$ α/p_0 as a function of $(E/p_0)^{-1}$ for Mercury Vapour.

fig. 51.

practise of maintaining a maximum difference of 70°C between the two compartments (see fig. (24)). The heat losses through the walls would then be unequal. It therefore seems likely that temperature gradients across the tube of Badareu and Bratescu were present on a larger scale than those occurring in the present determinations and those of Smith. Errors due to such gradients, together with a probable experimental error of 5% would explain the relative positions of the curves.

The range of validity of the Townsend equation relating α/p_o to E/p_o was investigated by plotting $\log_e \alpha/p_o$ as a function of $(E/p_o)^{-1}$. The curve is shown in fig. (51). The line departs from linearity at an E/p_o of about 250 volts cm.$^{-1}$mm.Hg.$^{-1}$. The value of the constant, A, representing the saturation value of α/p, obtained from the intercept on the $\log_e \alpha/p$ axis is 29.1, about 2 cm.$^{-1}$mm.Hg.$^{-1}$ higher than that found in practice. The value is in good agreement with that quoted by Smith of 30 and in reasonable agreement with that of Badareu and Bratescu, which was 26.1. The theoretical value, given by $A = \frac{1}{\lambda P}$ is 36.5. The low value of A is in accordance with the general trend for the experimental values to be less than the theoretical ones. The value of the constant, B, is 500 in the present case and in the case of Smith and 411 in that of Badareu and Bratescu. The value of $B = V_i.A$ where V_i is the ionisation potential, as predicted by the theory is about 370. The high values of B compared to the theoretical value is surprising in that all values of this constant determined experimentally are in general lower than the theoretical value.

The equation relating α/p to E/p_o for mercury vapour can

Generalised Secondary Coefficient as a function of E/P_o . Tube 1.

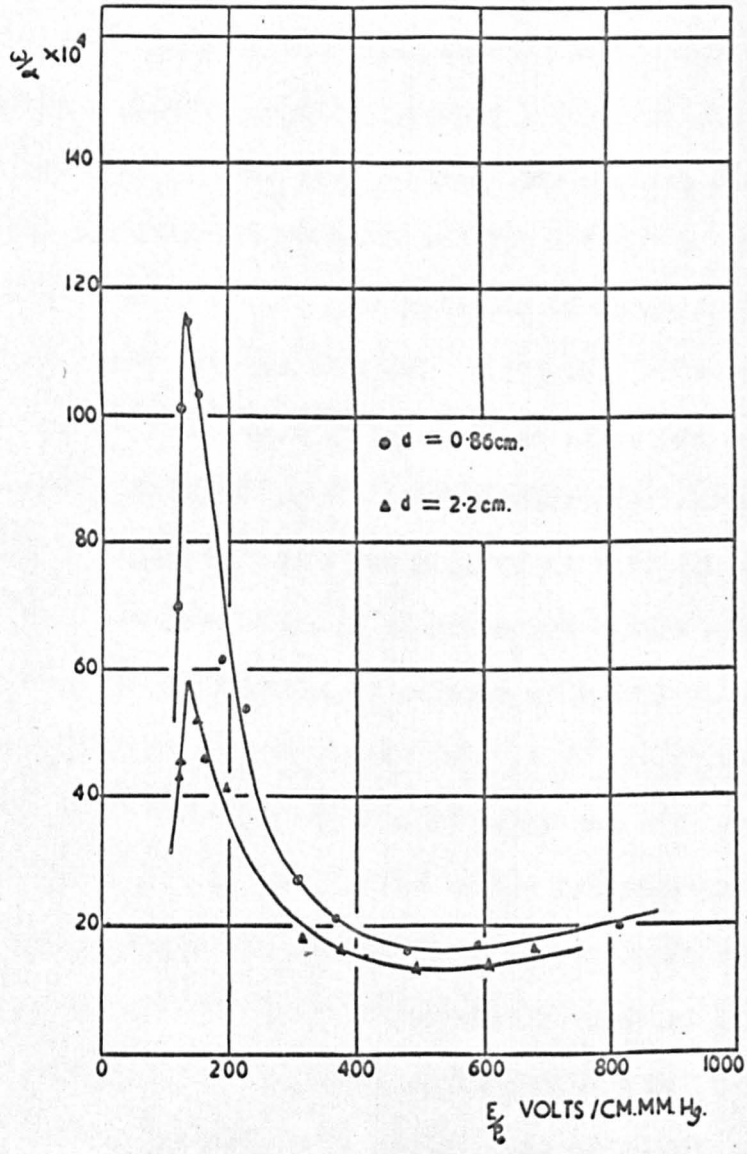

fig. 52.

therefore be written as

$$\alpha/p = 29.1 \quad \exp. - \frac{500}{E/p}$$

for the range 250 to 1800 volts $cm.^{-1}mm.Hg.^{-1}$ As explained in Chapter 2 Badareu and Bratescu attempted to determine the mean electron energy in volts of the electron avalanche for certain values of E/p_o, by comparing α/p_o with the ionisation efficiency. This process was repeated by Smith, who obtained the relation $\bar{\varepsilon} = (E/p_o)^{\frac{1}{2}}$. However, this relation was obtained by a process of curve fitting such that maximum agreement was obtained between the two curves. This occurred when values of α/p at high E/p_o were aligned with the ionisation efficiency at high electron energy. The agreement at low E/p_o was poor (fig. (29)). However, for the reasons given in Chapter 2 and for those given in the discussion above in which the present and Smith's values of α/p_o are compared, the concept of a mean electron energy, or E/p_o, has little meaning at values above that given by the Stoletow point. Comparison of α/p_o with the ionisation efficiencies should therefore be confined to values taken at values of E/p_o below the Stoletow point. If this is done the relations between mean electron energy, $\bar{\varepsilon}$, and E/p_o is found to be linear and is given by

$$\bar{\varepsilon} = \frac{k}{42}(E/p_o) + 6$$

where k is a dimensional constant of the order of unity.

6.4 The second Townsend ionisation coefficient

Using the breakdown criterion $\omega/\alpha(e^{\alpha d}-1) = 1$, values of the generalised secondary coefficient ω/α were obtained from Paschen curves

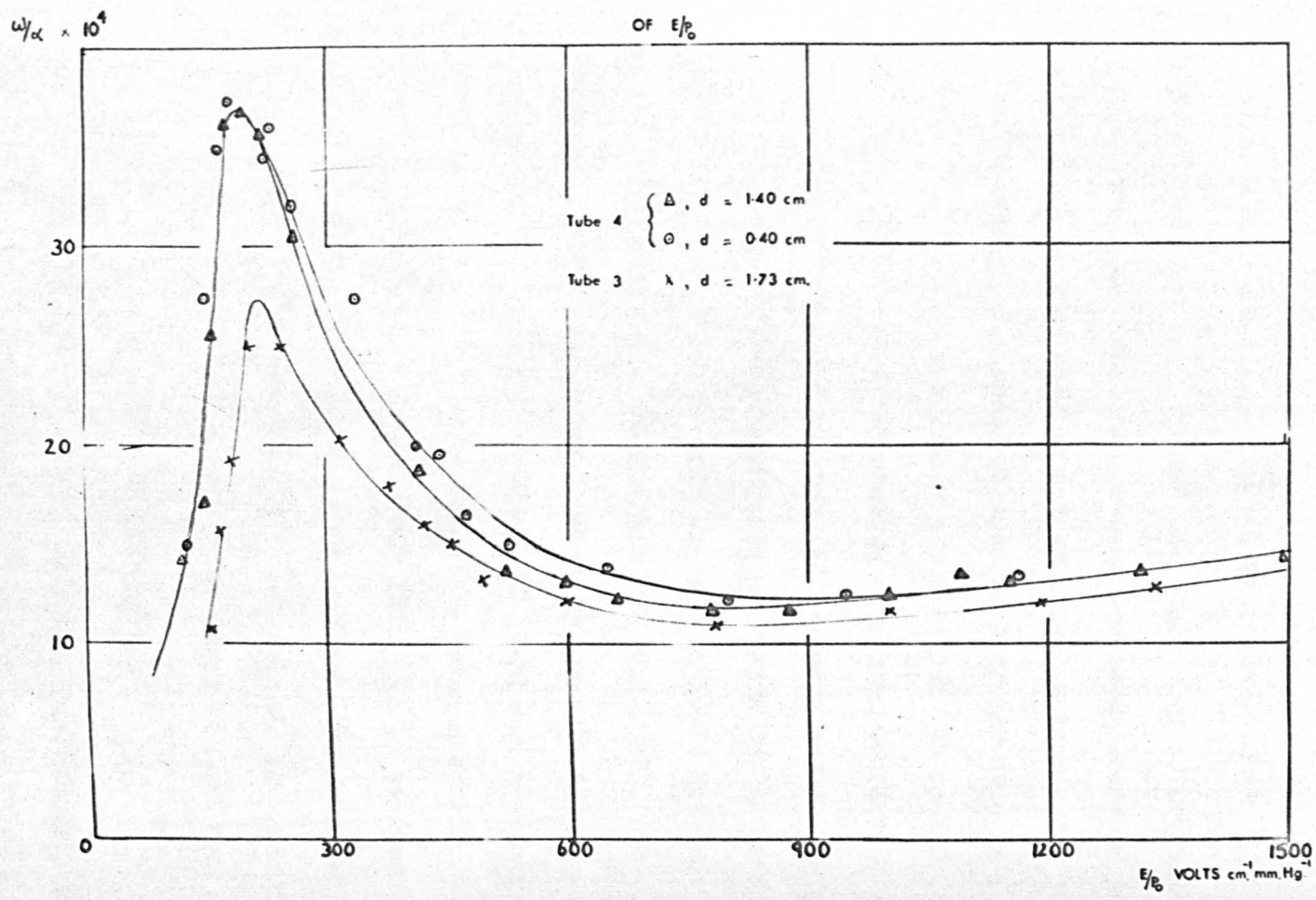
THE GENERALIZED SECONDARY COEFFICIENT AS A FUNCTION OF E/p₀
ω/α × 10⁴
30
20
10
0
300
600
900
1200
1500
E/p₀ VOLTS cm⁻¹ mm. Hg⁻¹
Tube 4
Δ , d = 1·40 cm
⊙ , d = 0·40 cm
Tube 3
× , d = 1·73 cm.

Fig. 53.

and values of the primary ionisation coefficient. The method of calculation is not very accurate, since a small error in αd can produce a large error in the value of ω/α because of the exponential factor. The method nevertheless remains useful for showing the important trends.

The results obtained from tube 1 are shown in fig. (52) and those from tubes 3 and 4 in fig. (53). The curves in fig. (52), showing values of ω/α over a range of E/p_o from 100 to 800 volts $cm.^{-1}mm.Hg.^{-1}$ were obtained from the Paschen curves for the two largest electrode separations taken with tube 1, together with values of α/p obtained with tube 2. Values of ω/α over a range of E/p_o from 100 to 1500 volts $cm.^{-1}mm.Hg.^{-1}$ were obtained with tubes 3 and 4 from the Paschen curves and α/p measurements taken with each tube. The displacement of the curves in fig. (52) along the ω/α axis for different electrodes separations is a reflection of the deviation from Paschen's law obtained with tube 1. A similar displacement of ω/α for different electrode separations was observed by Smith, whose Paschen curves showed the same general features as those obtained with tube 1. The displacement observed with the results calculated from the Paschen curves obtained with the fourth experimental tube is confined to the region of E/p_o around that giving the minimum of the Paschen curve. Reasons for the various displacements of the Paschen curves have been offered in the section dealing with breakdown potentials.

The features of both sets of curves bear a close resemblance to those obtained by Smith, both in order of magnitude and general shape. The most important of these features is the appearance of large peaks

in the region of an E/p_o of 200 volts $cm.^{-1}mm.Hg.^{-1}$. Using an iron cathode with a work function of 4.5 eV, similar to a mercury cathode of work function of about 4.5 eV, Badareu and Bratescu found a general increase in ω/α down to an E/p_o of about 150 volts $cm.^{-1}mm.Hg.^{-1}$, but were unable to draw the curve for values of E/p_o below this value. Since at low E/p_o the ratio of exciting to ionising collisions is large, the increase in ω/α at low E/p_o is most likely to be the result of the contribution of the increased numbers of photons and metastable atoms produced. The states of greatest importance will be the four P states of the mercury atom. Badareu and Bratescu and Smith considered that the two resonance levels, 2^3P_1 and 2^1P_1 stateswere probably the most active.

If it is assumed that the mean electron energy is given by the formula

$$\bar{\varepsilon} = \frac{k}{42} (E/p_o) + 6$$

then the peaks in the secondary coefficient curves occur at an energy of about 11 volts. This is in approximate agreement with the energy found by Penney (1) for which the probability of excitation for the four P states in mercury are a maximum. The excitation potentials are given in the table below:

2^3P_0	Metastable	4.66 volts
2^3P_1	Resonance	4.86 volts
2^3P_2	Metastable	5.43 volts
2^1P_1	Resonance	6.67 volts

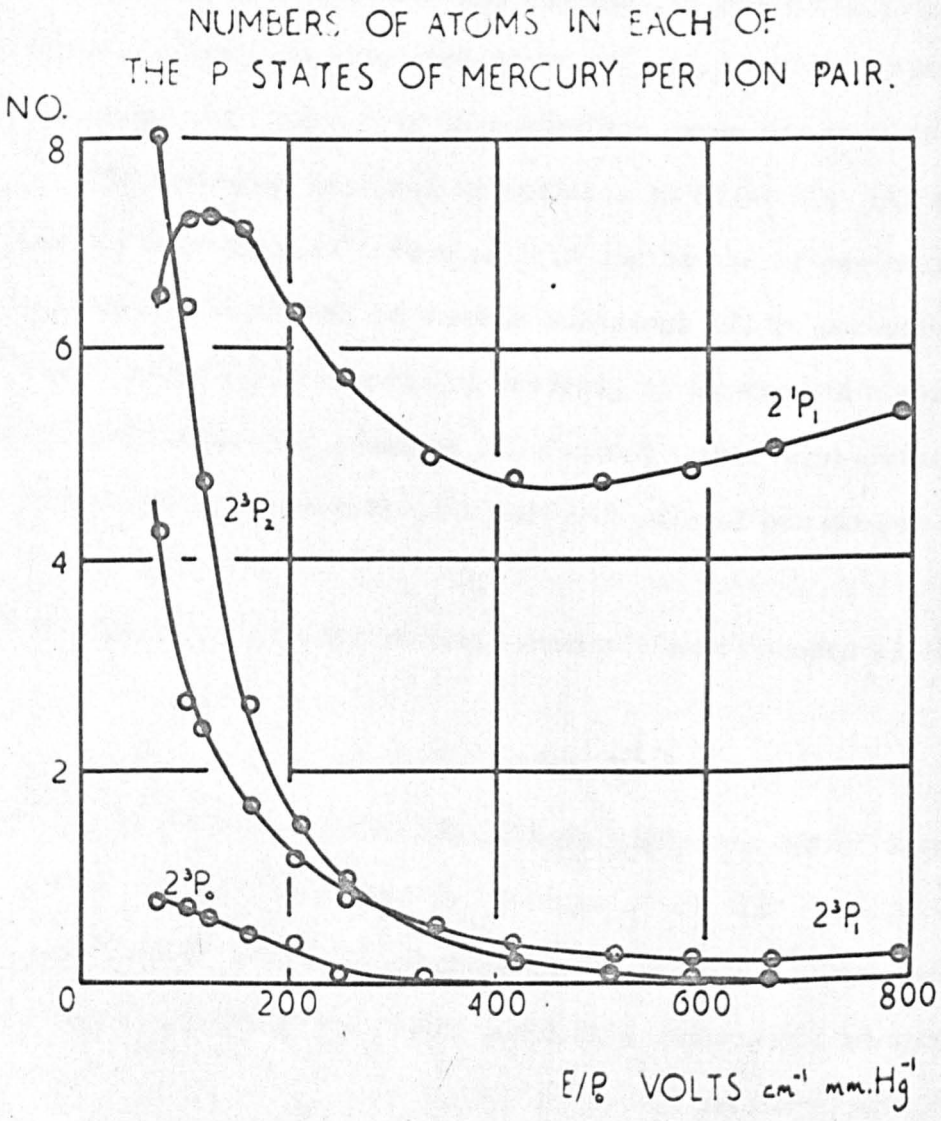
NUMBERS OF ATOMS IN EACH OF
THE P STATES OF MERCURY PER ION PAIR.
NO.
8
6
4
2
0
200
400
600
800
2 ¹P₁
2 ³P₂
2 ³P₀
2 ³P₁
E/p VOLTS cm⁻¹ mm.Hg⁻¹

fig. 54.

Because of its small probab ility of excitation and because of its low energy compared to the work function of the mercury surface, the $^3P_0$ metastable level is not likely to contribute very much to the secondary coefficient. The most efficient state in this respect is likely to be first of all the $^1P_1$ resonance state because of its high energy and high probability of excitation. It should also be of increasing relative importance at high values of E/p_o. The $^3P_2$ metastable state and the $^3P_1$ resonance state are likely to be the next most efficient source of secondary electrons.

As explained in Chapter 2 the numbers of excited atoms produced per ion pair can be calculated from the curve of $\eta = E/\alpha$ as a function of E/p_o providing that E/p_o is known as a function of electron energy and the excitation functions for the various states are available. Using the present values of η as a function of E/p_o and assuming that the mean electron energy in volts is given by

$$\bar{\varepsilon} = \frac{k}{42} (E/p_o) + 6$$

Penney's curves of the probability of excitation to each of the four P states have been used to calculate the relative numbers of atoms in each state per ion pair for values of E/p_o between 75 and 1000 volts $cm.^{-1}mm.Hg.^{-1}$. The curves are shown in fig. (54).

The most striking feature of the curves is the dominance of atoms in the $^1P_1$ resonance level. Atoms in the $^3P_2$ and $^3P_1$ levels become important below an E/p_o of 250 volts $cm.^{-1}mm.Hg.^{-1}$. Atoms in the $^3P_0$ level are few in number and since the energy difference $(eV-2\phi)$ is

is about 0.16 (where ϕ is the work function of the cathode) unless they are extremely efficient in liberating electrons, they are not likely to be important to the secondary process. An interesting feature is the sharp rise in the number of atoms in the $^3P_2$ metastable level, and the $^3P_1$ resonance level and the decline of atoms in the $^3P_2$ resonance level at an E/p_o of about 150 volts cm.$^{-1}$mm.Hg.$^{-1}$. It seems reasonable to correlate this feature of an increase in total nmmber of excited states at low values of E/p_o with the maximum observed in the plots of ω/α as a function of E/p_o. It is important to note that the number of atoms in the metastable $^3P_2$ level increases above that for any other state at low E/p_o. The importance of this state will be discussed further in the section on formative time lags.

The curves in fig. (54) indicate that secondary effects due to metastables should cease at an E/p_o of about 600 volts cm.$^{-1}$mm.Hg.$^{-1}$. A minimum is observed to occur in the curves of ω/α as a function of E/p_o at an E/p_o of about 700 volts cm.$^{-1}$mm.Hg.$^{-1}$ in the curves obtained with the 3rd and 4th tubes. The value of ω/α at this point is about 12×10^{-4}. Thereafter the curve shows a gentle rise until at an E/p_o of 1500 volts cm.$^{-1}$mm.Hg.$^{-1}$, ω/α reaches a value of about 15×10^{-4}. The minimum value of ω/α obtained with the first tube and that obtained by Smith are about 12×10^{-4} but this occurs at an E/p_o of about 500 volts cm.$^{-1}$mm.Hg.$^{-1}$ in the first case, and at about 800 volts cm.$^{-1}$mm. Hg.$^{-1}$ in Smith's Case. Thereafter the curves rise more steeply than is observed with the results from the third and fourth tubes.

The rise in ω/α at values of E/p_o greater than 800 volts

$cm.^{-1}mm.Hg.^{-1}$ was attributed by Smith to the action of the $Hg.^{++}$ ion at the cathode by a virtue of its potential energy. The ionisation potential for this ion is 30 eV and assuming that $\bar{\varepsilon} = (E/p_o)^{\frac{1}{2}}$ this ion would be expected to appear at values of E/p_o above 900 volts $cm.^{-1}mm.Hg.^{-1}$. However, the work of Kovar (41) on the mobilities of mercury ions in a Townsend discharge failed to reveal the presence of the $Hg.^{++}$ ion even up to values of E/p_o of 1500 volts $cm.^{-1}mm.Hg.^{-1}$. The only other ion detected apart from $Hg.^{+}$ was Hg_2^{+} which occurred at low E/p_o. It seems unlikely, therefore, that $Hg.^{++}$ will be important in the range of E/p_o considered.

It should be remembered that the values of ω/α are calculated by inserting the appropriate coefficients in the expression $\omega/\alpha(e^{\alpha d}-1) = 1$. ω/α is therefore sensitive to the value of αd which is given by $\frac{\alpha}{p}.pd$. Low values of α/p_o therefore tend to make ω/α larger. The large increase in ω/α at high E/p_o as found by Smith can be explained when it is remembered that the magnitude of α/p_o at high E/p_o is too low because of the departure from equilibrium conditions. The present values of α/p_o at high E/p_o represent less of a departure from equilibrium conditions and the values of ω/α at high E/p_o probably approximate more closely to the true values of ω/α which should be lower than those obtained. The early rise in ω/α as determined from the Paschen curves from the first tube can also be explained in this manner since the values of α/p_o used were obtained with the second tube. Through the necessary use of low pressures these values of α/p_o have been shown to be too low at high E/p_o.

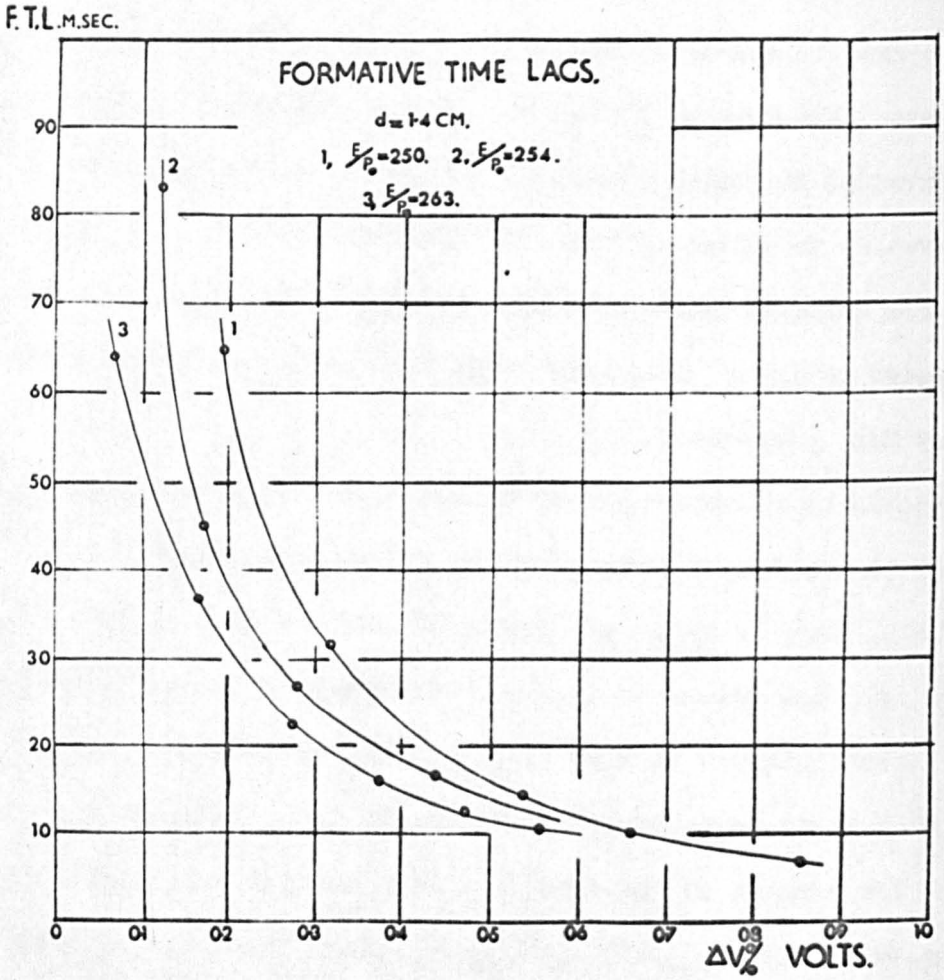
F.T.L. M.SEC.
FORMATIVE TIME LAGS.
d = 1·4 CM.
1, E/p₀ = 250. 2, E/p₀ = 254.
3, E/p₀ = 263.
90
80
70
60
50
40
30
20
10
0
01
02
03
04
05
06
07
08
09
10
ΔV/p₀ VOLTS.
1
2
3

fig. 55a.

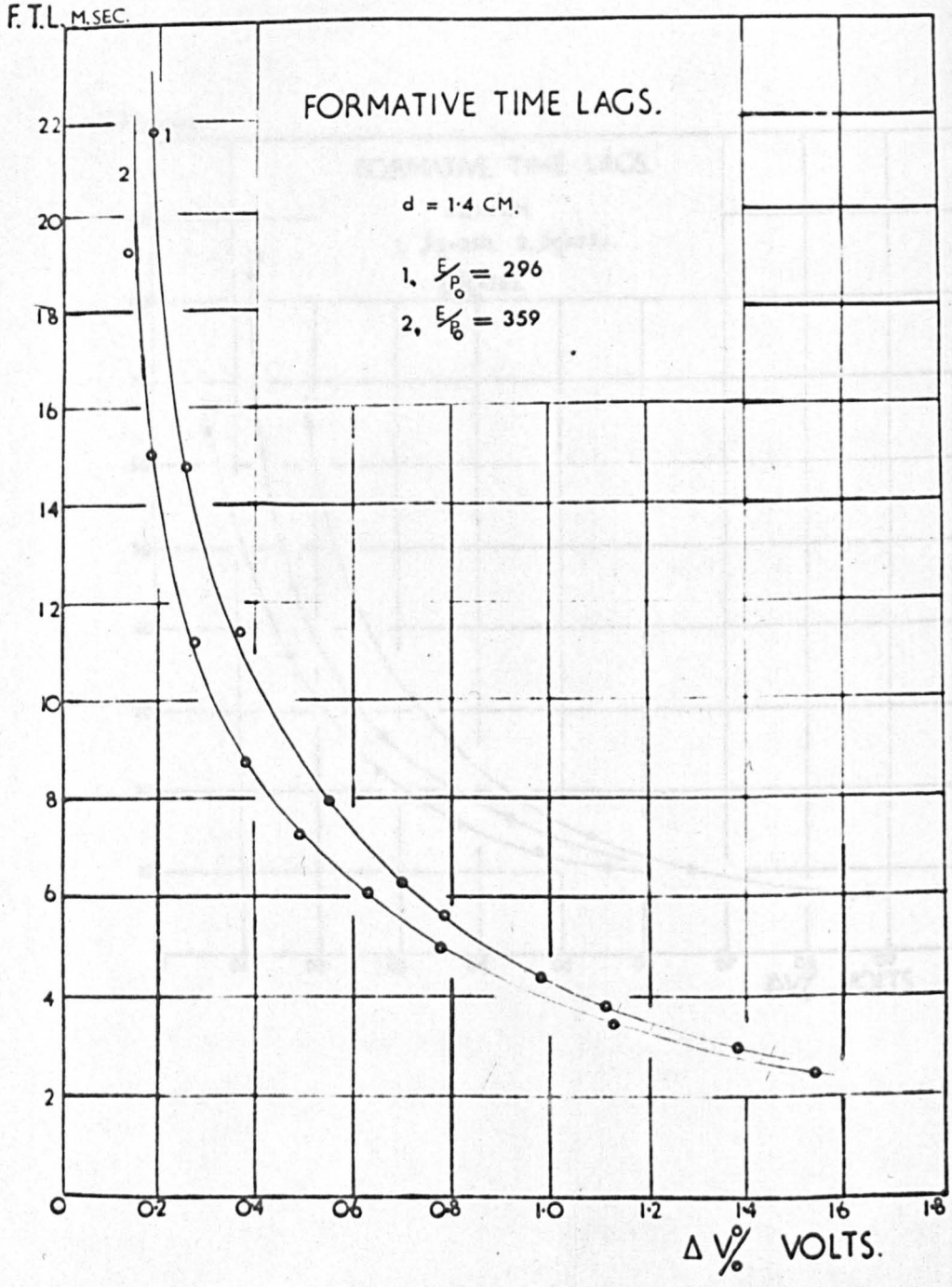
F.T.L. M.SEC.
FORMATIVE TIME LAGS.
d = 1·4 CM.
1. E/P0 = 296
2. E/P0 = 359
22
20
18
16
14
12
10
8
6
4
2
0
0·2
0·4
0·6
0·8
1·0
1·2
1·4
1·6
1·8
Δ V/ VOLTS.

fig. 55b.

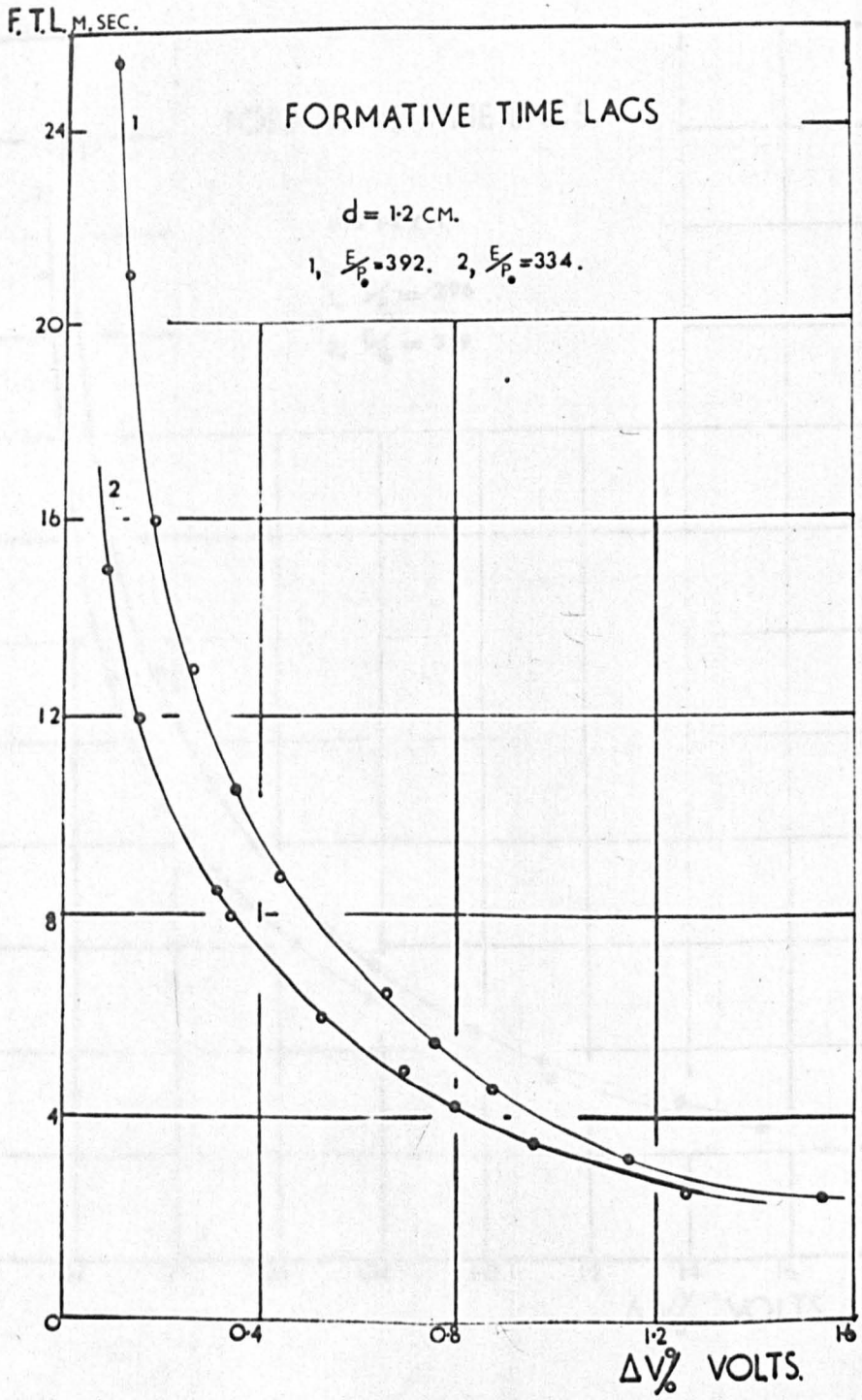
F.T.L. M. SEC.
FORMATIVE TIME LAGS
d = 1·2 CM.
1, E/p = 392. 2, E/p = 334.
1
2
24
20
16
12
8
4
0
0·4
0·8
1·2
1·6
ΔV% VOLTS.

fig. 55a.

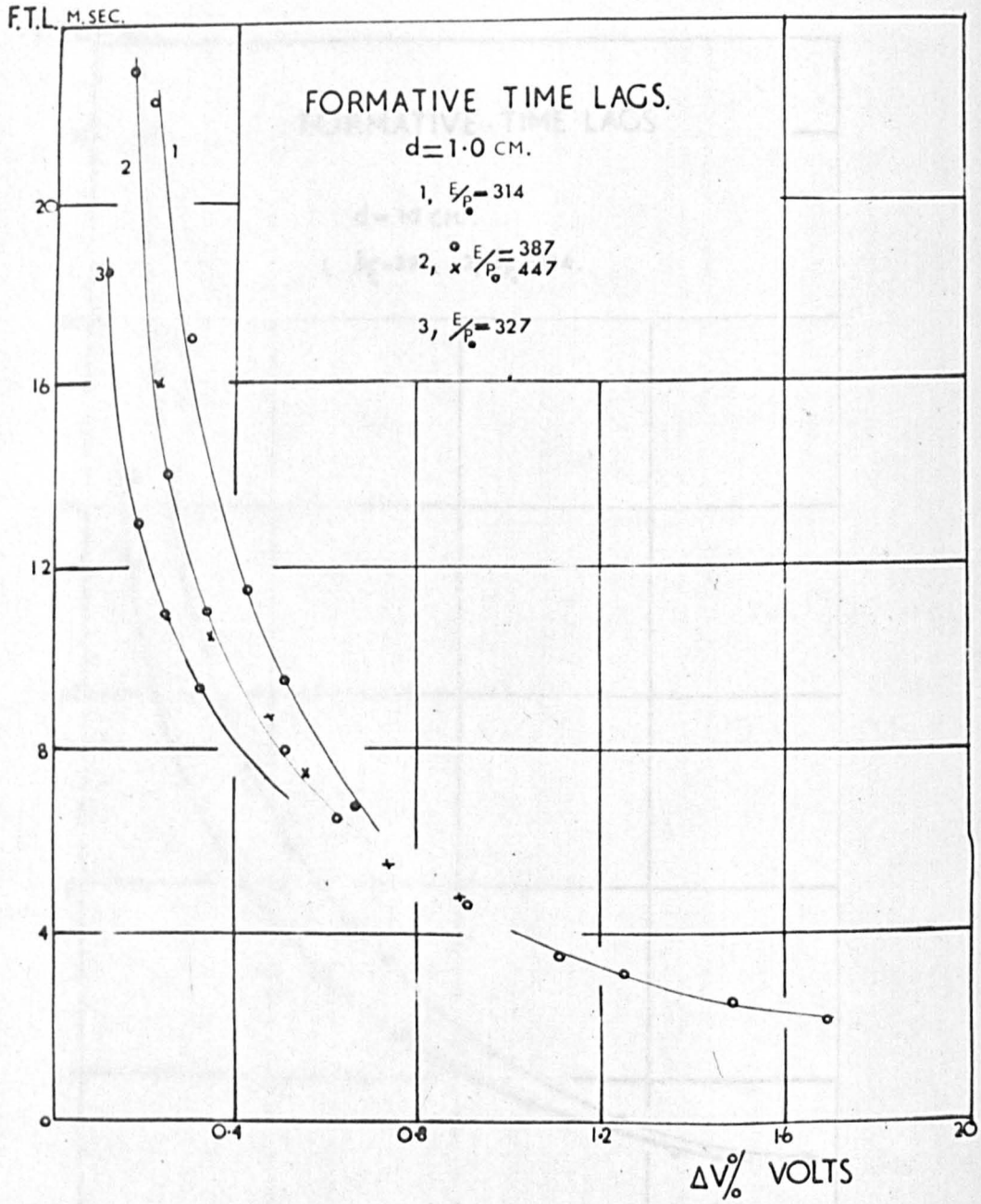
F.T.L. M.SEC.
FORMATIVE TIME LAGS.
d=1·0 CM.
1, E/p = 314
2, ° E/p = 387
× E/p = 447
3, E/p = 327
d
1
2
3
20
16
12
8
4
0
0·4
0·8
1·2
1·6
2·0
ΔV/% VOLTS

fig. 55d.

It therefore seems highly probable that the slope of the curve of ω/α as a function of E/p_o at high E/p_o should be zero. This implies that the $^1P_1$ resonance radiation is of negligible importance and that secondary emission is entirely due to the singly charged ion Hg^+, acting by virtue of its potential energy. Assuming the value of ω/α at an E/p_o of 800 to represent the contribution of Hg^+ to ω/α the relative percent contributions of the four P states and the singly charged ion are presented in the following table

Table 6.1

E/p_o	150	175	200	250	300	350	400	450	500	550	600	650
γ_p %	40	66	67	63	56	48	40	33	25	14	10	0
γ_{ion}%	60	34	33	37	44	52	60	67	75	86	90	100

6.5 Formative Time Lags

Preliminary measurements were attempted with the second experimental tube. These were unsatisfactory because of the difficulty of maintaining the electrode separation at a given value. The results merely indicated breakdown times of the order of milliseconds. A more thorough study was carried out with the aid of tube four over a range of E/p_o from 200 to 500 volts $cm.^{-1}mm.Hg.^{-1}$. The experimental curves are given in figs. 55a to 55d.

A few conclusions can be drawn directly from the experimental curves. In the first place, the times obtained (of the order of milliseconds) suggest that a slow process of a diffusive nature is active. If positive ions were active alone, times of the order of 10^{-4} seconds would be expected. An undelayed photon process would give times of the

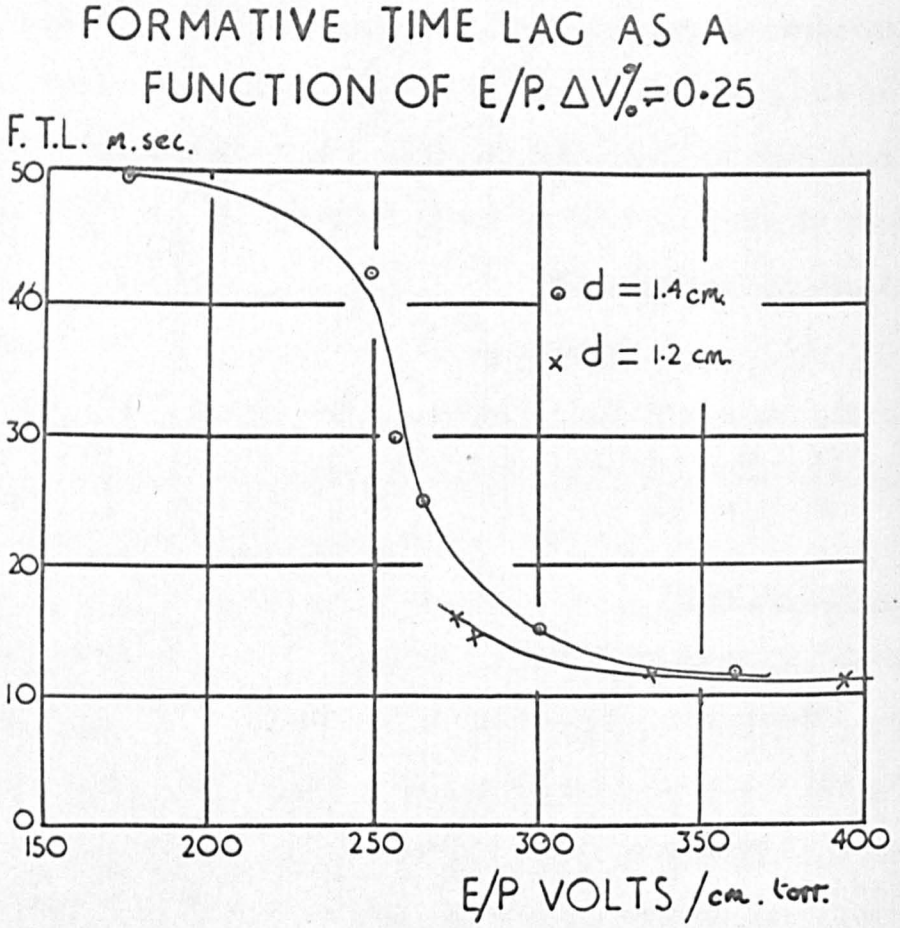
FORMATIVE TIME LAG AS A
FUNCTION OF E/P. ΔV/V = 0·25
F. T.L. m.sec.
50
40
30
20
10
0
o d = 1.4 cm.
x d = 1.2 cm.
150
200
250
300
350
400
E/P VOLTS / cm. torr.

fig. 56.

the order of 10^{-7} to 10^{-6} seconds. Furthermore, a plot of the formative time lag against E/p_o for a given percent overvoltage indicates that at values of E/p_o above 170 volts $cm.^{-1}mm.Hg.^{-1}$ the breakdown process is becoming progressively faster. Fig. (56) shows such a curve for 0.25% overvoltage. The time lags decrease from 50 milliseconds at an E/p_o of 170 volts $cm.^{-1}mm.Hg.^{-1}$ to twelve milliseconds at an E/p_o of 400 volts $cm.^{-1}mm.Hg.^{-1}$. The speeding up of the breakdown process is most likely due to the decrease in population density of slow components, as indicated in fig. (54) with the corresponding increase in the importance of positive ions. The most plausible processes are then (a) the action of delayed resonance radiation, (b) collision induced radiation from metastables, and (c) the destruction of metastables at the cathode, all of which may take place with the additional action of positive ions.

The imprisonment of resonance radiation may result in considerable delay in the arrival of photons at the cathode from their place of production near the anode. The magnitude of the delay is determined by the number of successive emissions and absorptions per unit time and on the life-time of the resonance state. The greater the number of absorptions and the longer the photon is trapped in the atom the greater will be the delay. Reference to fig. (54) will show that the photon of most importance will be that corresponding to the transition $^1P_1$ to $^1S_0$, with a wave-length of 1849^oA, because of its large numbers and high energy. However, Wolfsohn (46) has determined the life-time of this state to be 1.3×10^{-9} sec., so that unless very large absorption takes place, the delay is not likely to be considerable. Unfortunately, absorption

coefficients for this particular state do not appear to be available. Absorption coefficients in general appear to range from 1 $cm.^{-1}$ to about 2000 $cm.^{-1}$ at atmospheric pressure. Assuming an upper limit of 2000 $cm.^{-1}$ for the absorption coefficient, the diffusion coefficient as calculated from the formula given by Davidson is of the order of 5×10^{7} $cm.^{2}sec.^{-1}$, yielding time lags of about 10^{-6} seconds, at an E/p_o of 250 volts $cm.^{-1}mm.Hg.^{-1}$. Thus the times calculated differ little from those expected if an undelayed photon process were acting and are about three orders of magnitude faster than the observed time lags. If the $^3P_1$ to $^1S_0$ transition is considered the calculated time lags are still an order of magnitude too fast.

The next process to be considered is that of collision induced radiation produced by the destruction of metastables. The metastable state involved is most likely to be the $^3P_2$ state because of the relatively large numbers produced per ion pair at low E/p_o. At the pressures used ($\sim$1 torr) the mean free path of a mercury metastable atom is about 5×10^{-3} cm. For an electrode spearation of 1 cm., an atom travelling normally from anode to cathode will on average make 2×10^{4} collisions with normal gas atoms. Couillette (47) has concluded that there is a dissipative process in which one collision in 1300 with normal mercury atoms results in the mercury metastable losing its excitation energy. Under the present experimental conditions it therefore seems that the metastable mercury atom will have ample opportunity of losing its excitation energy in this manner, resulting in complete volume destruction. The possibility of metastable action at the cathode is therefore minimal

at these pressures. This conclusion was tested by comparing the experimental time lags with others computed from Davidson's theory as given in Chapter 2. The evaluation of λ and the calculation of the formative time lag are laborious and a computer was used to facilitate the process. The method of calculation is given in Appendix (3).

The first case assumed was that of the combined action of metastables and positive ions at the cathode. Since a one hundred per cent positive ion action was not expected, the calculations were performed for 0%, 20%, 50% and 80% positive ion contribution to ω/α. All the combinations proved too slow. At an E/p_o of 250 volts cm.$^{-1}$mm.Hg.$^{-1}$, metastable action alone yielded time-lags approximately 200 times too great, whereas an assumption of 80% positive ion action yielded time lags approximately 3 times too great.

Calculations were now performed assuming the combination of the volume destruction of the metastables and positive ion action at the cathode. The calculations were performed for four different overvoltages and for three different assumed life-times of the metastable state, viz. 5×10^{-3} sec., 10^{-3} sec., and 5×10^{-4} sec. Data on the life-time of the mercury metastable state do not appear to be available and it was hoped that the above three values would cover the possible range. Calculations were performed for three values of E/p_o, viz. 250, 358 and 391 volts cm.$^{-1}$mm.Hg.$^{-1}$. At an E/p_o of 250, the time lag was calculated for 0%, 20%, 50% and 80% positive ion action for the three assumed life-times. In all cases where γ_i, the positive ion contribution, was assumed zero, the calculated time lags were too great.

For a life time of 5×10^{-3} sec., the time lags were two orders of magnitude too great. For a life-time of a millisecond the time lags were an order of magnitude too great, and for a life-time of 5×10^{-4} sec., they were approximately twice the experimental values. Fairly close agreement with the experimental values was obtained when it was assumed that the life time was one millisecond and γ equal to 80% of ω/α, and when the life-time was 5×10^{-4} sec. and γ was 50% of ω/α. Both sets of time lags were slightly shorter than the experimental ones. When the life-time was assumed to be 5×10^{-4} sec., and γ equal to 80% of ω/α, the calculated times were approximately half those of the experimental ones. These facts are summarised in the following table.

Table 6.2

$E/p_o = 250$

$\Delta V\%$	.46	.67	.85	1.0	$\gamma\%$	$\tau_{Lec.}$
$t_{exp.}$ m.sec.	15.0	11.0	8.0	7.0		
$t_{calc.}$ m.sec.	12.0	10.0	8.0	6.5	80	10^{-3}
$t_{calc.}$ m.sec.	12.0	9.5	7.5	6.0	50	5×10^{-4}
$t_{calc.}$ m.sec.	6.0	5.0	4.0	3.0	80	5×10^{-4}

At an E/p_o of 250 volts $cm.^{-1}mm.Hg.^{-1}$ a 40% positive ion contribution would be expected from previous considerations, Table 6.1.

At an E/p_o of 358 the calculations were carried out for 20%, 40%, 55% and 80% positive ion contribution. Very good agreement between theory and experiment was obtained for a positive ion contribution of 55% and a life-time of 5×10^{-4} sec. A positive ion contribution of

about 55% would be expected from table 6.1. The results are summarised in the following table:

Table 6.3

$\Delta V\%$	.49	.77	1.13	1.54
α	4.452	4.464	4.488	4.512
$t_{exp.}$ (n.sec)	7.25	4.96	3.40	2.40
$t_{calc.}$ (n.sec)	6.0	4.97	3.84	3.0
λ	614.3	731.6	993.7	1307.9

γ=55% $\omega/\alpha=22\times10^{-4}$ p_o=0.6torr d=1 4cm. E/p_o=358 $\tau=5\times10^{-4}$ sec.

At an E/p_o of 391 volts $cm.^{-1}mm.Hg.^{-1}$ similar calculations were carried out for positive ion contributions of 20%, 40%, 60% and 80%. Again, good agreement between theory and experiment was obtained when the life time of the metastable state was assumed to be 5×10^{-4} sec. for a positive ion contribution of 60% to ω/α. A contribution of 60% is to be expected from table 6.1. The results are presented in table 6.4:

Table 6.4

$\Delta V\%$	.53	.81	1.15	1.54
α	5.279	5.298	5.320	5.345
$t_{exp.}$ (n.sec)	6.0	4.28	3.20	2.40
$t_{calc.}$ (n.sec)	5.0	3.72	3.01	2.38
λ	776.4	986.5	1260.3	1638.0

γ=60% $\omega/\alpha=20\times10^{-4}$ p_o=0.63torr d=1.2cm. E/p_o=391 $\tau=5\times10^{-4}$ sec.

In conclusion, agreement as to the amount of positive ion contribution to ω/α has been obtained between that calculated from consideration of the spatial growth of ionisation in mercury vapour, and that obtained from the application of Davidson's analysis to the temporal growth of ionisation, when the assumption is made that the life time of the metastable state is 5×10^{-4} sec. It is of interest to note that the life time of the metastable state claculated from Couillette's conclusion that the metastable is destroyed on average after 1300 collisions with normal gas atoms at the pressures used in this investigation is of the order of 5×10^{-4} sec. It would appear that the contribution to ω/α attributed to the 'P' states in table 6.1 is entirely due to the volume destruction of the metastable $^3P_2$ state, and that the secondary process in mercury vapour with a mercury pool cathode is a combination of the volume destruction of the $^3P_2$ metastable atom and positive ion action at the cathode, the relative percentages of which are presented in table 6.1.

6.6 Summary of conclusions and suggestions for future work

Deviations from Paschens law in mercury vapour have been observed particularly at the minimum of the curve. Since the rate of change of breakdown potential V with the product p_od is zero at the minimum value of the breakdown potential, any influence of electrode geometry on V due to loss of active particles should be most noticeable at this value. The results obtained of the minimum breakdown potential as a function of electrode separation can be summarised in a linear relationship given by

$$V_m = 285 + 5d$$

This equation is valid to ∓ 0.5 v over the range considered (0.4 to 2.20 cm.).

It would appear that the minimum breakdown potential for a mercury cathode in mercury vapour under uniform field conditions (i.e. as d tends to zero) is (285 ∓ 0.1) volts for all the tubes used in this investigation. In order to compare results for tubes of differing electrode diameter, D, the ratio d:D should be taken into consideration. The equation most likely to apply in this case is

$$V_m = 285 + 29(d/D) \mp 0.5v$$

The close agreement obtained with different tubes for the minimum breakdown potential gives a strong indication that a properly prepared mercury pool cathode will provide a surface of constant work function for low current discharges.

The measurements of first ionisation coefficients agree with those obtained by Smith up to a value of E/p_o of 1000 volts $cm.^{-1}mm.Hg.^{-1}$ where the divergence from equilibrium conditions is not appreciable. It is thought that the present results represent a closer approximation to equilibrium than those of Smith who used very low vapour pressures at high E/p_o. Comparison of α/p_o at low E/p_o with the ionisation efficiency curves of Bleakney yield a relation between the mean electron energy, $\bar{\varepsilon}$, in volts and E/p_o given by

$$\bar{\varepsilon} = k/42(E/p_o) + 6$$

where k is a dimensional constant of the order of unity. This equation has made possible the calculation of the number of atoms in each of the

'P' states for every ion pair created over a range of E/p_o from 175 to 800 volts $cm.^{-1}mm.Hg.^{-1}$.

The curves of the generalised secondary coefficient obtained from first ionization coefficients and breakdown potentials show the same trend as those obtained by Smith. Calculations of the relative populations of atoms in the 'P' states per ion pair and the application of Davidson's analysis suggest that the secondary process operative in this investigation is a combination of the action of collision induced radiation and positive ions, up to an E/p_o of 600 volts $cm.^{-1}mm.Hg.^{-1}$. Above this value, where calculations show no metasaable atoms should be produced, the secondary coefficient is thought to be entirely due to positive ion action at the cathode, the singly charged ion acting by virtue of its potential energy.

In view of the very close agreement obtained for α/p_o as a function of E/p_o below an E/p_o corresponding to the Stoletow point between the four present tubes and that of Smith, no further effort is required to evaluate this coefficient in this range of E/p_o. The technique developed could be profitably extended to the determination of these coefficients in other metallic vapours, notably caesium. However, in order that use can be made of the theory of Emeleus Lunt and Meek relating α/p_o to E/p_o, data on electron drift velocities and electron energy distributions need to be obtained. McCutchen (48) has obtained data on electron drift velocities up to an E/p of three volts $cm.^{-1}mm.Hg.^{-1}$. Such measurements need to be extended over a greater range of E/p. Preliminary investigations into the electron energy

fig. 57.

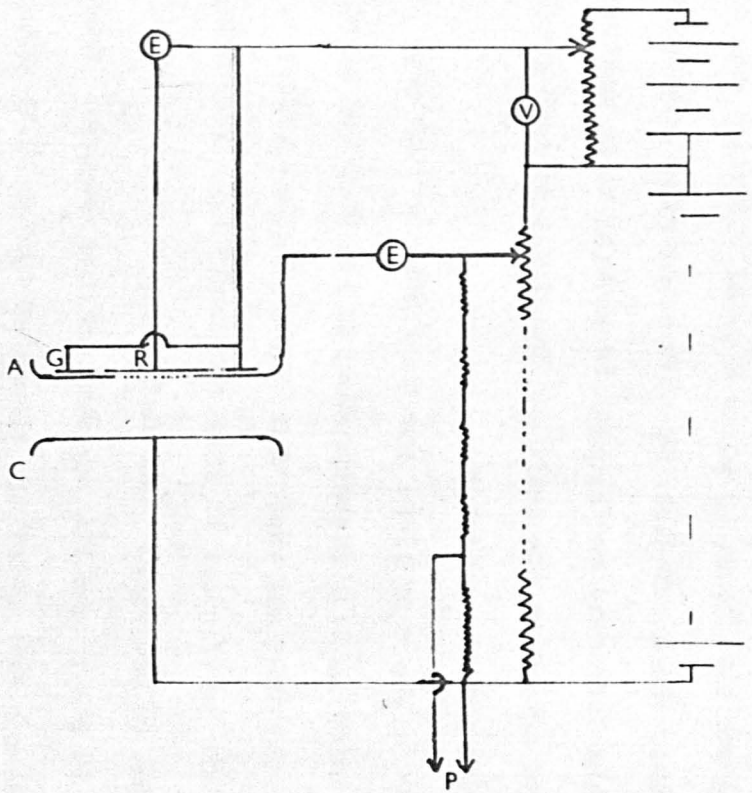

E, ELECTROMETERS

V, VOLTMETER

R, PROBE

G, PROBE GUARD RING

A, ANODE

C, CATHODE

P, POTENTIOMETER

CIRCUIT TO DETERMINE ELECTRON ENERGY DISTRIBUTIONS.

distribution in mercury vapour have been made by the present author using a retarding probe technique. A schematic diagram of the apparatus is shown in fig. (57). The electrodes were of nickel and had bevelled edges to reduce field distortion. A central region of the anode was perforated with 200 holes 0.015" in diameter. A plane probe was situated immediately behind the anode at a distance less than an electron mean free path as calculated from kinetic theory. This distance was chosen so that the energy distribution prevalent in the Townsend gap would not be appreciably modifed by collisions taking place in the region between anode and probe. The probe consisted of graphite painted on a glass substrate. To ensure that no currents flowed between probe and anode along the glass supports the probe was completely surrounded by a graphite guard ring painted on the same substrate and maintained at probe potential. The guard ring was extended to shield the tungsten seal in the tube wall connnecting the probe to the external circuit. A maximum pre-breakdown current was caused to flow in the Townsend gap and the current to the probe measured for different negative biases applied to the probe.

The number of electrons in front of the anode with energies between eV and e(V+dV) normal to the anode can be represented by F(V)dV per unit area. The number passing in unit time through an area A will be $N=F(V)dV.A.c$, where c is the velocity, given by $(2eV/m)^{\frac{1}{2}}$. The current, eN, is therefore given by

$$eN = F(V)dV.e.A.(2eV/m)^{\frac{1}{2}}$$

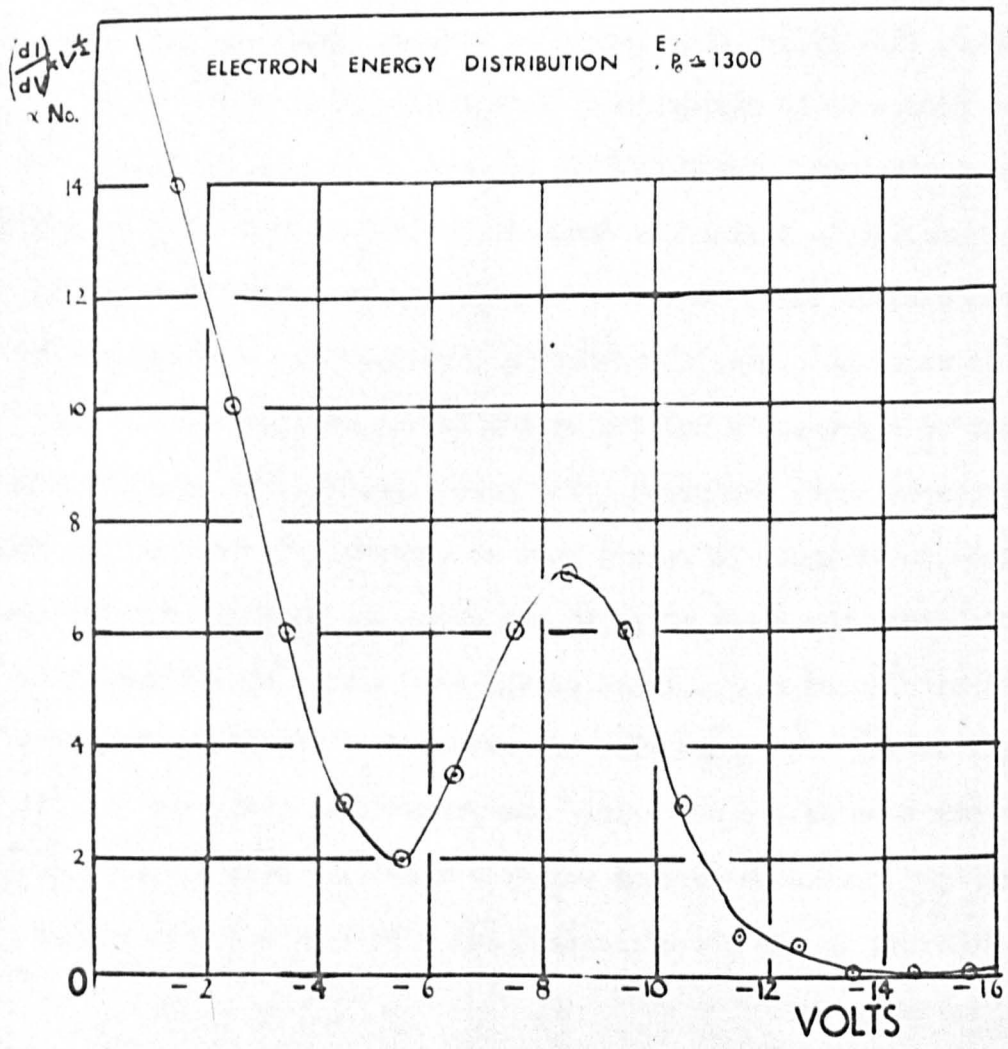
ELECTRON ENERGY DISTRIBUTION
E
P = 1300
(dI/dV) x V^½
x No.
14
12
10
8
6
4
2
0
-2
-4
-6
-8
-10
-12
-14
-16
VOLTS

fig. 58.

This current is due to electrons with energies between eV and e(V+dV) and will be reduced if a negative bias is applied to the probe. If a bias V_b is applied then the current is given by

$$i = \int_{V_b}^{\infty} e.A.(2eV/m)^{\frac{1}{2}}.F(V)dV$$

Therefore

$$di/dV = e.A.(2e/m)^{\frac{1}{2}}.F(V)^{\frac{1}{2}}$$

A graphical differentiation of the current voltage characteristic to the probe should yield the energy distribution multiplied by $V^{\frac{1}{2}}$. Such a curve obtained in mercury vapour is shown in fig. (58). The maximum negative bias applied was -16 volts for fear of field penetration and the consequent collection of positive ions. The distribution shows a large number of electrons with low energies and few with energies between 4 and 7 volts. Most of the important excitation potentials of mercury fall in this range. Depopulation of electrons with energies in this range will occur as a result of inelastic collisions and the low energy population will increase as a consequence. A similar explanation applies to the distribution above 10 volts, the loss in this case going to ionisation.

Unfortunately a short occurred between probe and anode probably due to the distortion of the anode as the temperature of the oven increased, thus preventing the taking of further measurements. In order to prevent this type of difficulty arising it would be better to perform the experiment in the molecular gases which are generally assumed to have a Maxwellian distribution, and the pressure of which can be changed

without altering the temperature. The technique could be improved by using a single hole in the anode and employing a differential pumping method. This would increase the electron mean free path between anode and probe enabling the probe to be further removed from the anode thus reducing the danger of field penetration. The probe has a number of advantages over the more conventional type of probe. Solid objects are not inserted into the discharge region and no current is taken from this region. It is not dependent for its mode of operation on the condition of charge equality and the production of a sheath. It can therefore be used in high field low current discharges.

The present investigation into the temporal growth of ionisation into mercury vapour needs to be extended. To confirm conclusions reached from the application of Davidson's analysis, it is suggested that this approach be supported by that of Molnar. Using this technique the secondary coefficients due to positive ions and metastable atoms can be evaluated experimentally. The method also allows the experimental determination of such useful data as the metastable diffusion coefficient, the time constant of decay of metastables and the amount of volume destruction of metastables. Tube 4 could be used for such an experiment, as it was designed with this possibility in mind. Most of the necessary data for a satisfactory interpretation of the Townsend discharge in mercury vapour using a mercury pool cathode could then be obtained under constant experimental conditions. Finally, the techniques developed to obtain data in mercury vapour can be extended to other metals with a convenient melting point, notably ceasium.

APPENDIX 1

PRIMARY IONIZATION COEFFICIENTS

TUBE 1

α/p_o cm.$^{-1}$mm.Hg.	E/p_o V/cm.mm.Hg.
0.46	100
1.00	125
1.60	150
2.17	175
2.99	200
3.88	225
4.70	250

TUBE 2

α/p_o cm.$^{-1}$mm.Hg.	E/p_o V/cm.mm.Hg.
0.50	100
1.50	150
2.90	200
4.30	250
5.80	300
7.25	350
8.70	400
10.00	450
11.50	500
12.10	550
13.00	600
13.75	650
14.45	700
15.00	750
15.50	800

TUBE 3

(values for E/p_o above 800 are dependent on pressure)

α/p_o cm.$^{-1}$mm.Hg.	E/p_o V/cm.mm.Hg.
0.21	100
0.73	200
3.04	300
5.62	400
8.56	500
10.92	600
13.74	700
14.77	800
16.72	900
17.83	1000
18.50	1100
20.08	1200
20.30	1300
22.77	1400
23.05	1500
23.30	1600
23.60	1700
24.60	1800
25.66	1900
26 10	2000
26.00	2100
26.60	2200
26.40	2300
27.00	2400

TUBE 4

α/p_o cm.$^{-1}$mm.Hg.	E/p_o V/cm.mm.Hg.
3.04	200
10.90	500
18.55	1000
23.70	1500
25.50	2000

APPENDIX 2

DAVIES-MILNE ANALYSIS

Three simultaneous current growth equations of the form

$$i = \frac{i\, e_o^{\alpha(d-d_o)}}{1-\omega/\alpha(e^{\alpha(d-d_o)}-1)}$$

are taken for three values of the electrode separation d and corresponding values of current, i, at a given E/p_o.ω/α, i_o and d_o can then be eliminated, producing

$$f(\alpha) = i_1(i_3-i_2)e^{\alpha(d_3-d_1)} - i_2(i_3-i_1)e^{\alpha(d_3-d_2)} + i_3(i_2-i_1) = 0$$

By using Newton's method of successive approximation a value of α may be obtained to any required accuracy, by estimating a value of α and substituting this in the expression

$$\alpha' = \alpha - \frac{f(\alpha)}{f'(\alpha)}$$

where α' is a closer approximation to the true value of α, and $f'(\alpha)$ is the first derivative of $f(\alpha)$.

APPENDIX 3i

METHOD OF CALCULATING THE FORMATIVE TIME LAG FOR THE CASE OF A COMBINATION OF METASTABLE AND POSITIVE ION EFFECTS AT THE CATHODE

Davidson gives the simplified current growth equation as

$$i_{-}(o,t)/I_o = \frac{1}{1-\omega/\alpha(e^{\alpha d}-1)} + \frac{2(\lambda^2-d^2)(1-\exp(-2\lambda d))\exp D\lambda^2 t}{\lambda(\partial\theta/\partial\lambda)} \qquad (1)$$

where

$$\partial\theta/\partial\lambda = 2\lambda F-X-2X(\lambda d-1)\exp(\alpha-\lambda)d-\exp(-2\lambda d)\{2Fd(d^2-\lambda^2)+2dX(\alpha-\lambda)+2\lambda F+X\} \qquad (2)$$

is given the real value satisfying $\theta(\lambda)=0$, i.e.

$$(\alpha-\lambda)\left[(\alpha+\lambda)F+X\right]\exp(-2\lambda d)+2X\lambda\exp(\alpha-\lambda)d-(\alpha+\lambda)\left[(\alpha-\lambda)F+X\right] = 0 \qquad (3)$$

where $F = 1-(\gamma+\delta/\alpha)(\exp\alpha d-1)$, (unity if γ and δ/α not important)

and X is given by

$$X = (\alpha^2 d.\omega/\alpha.(\exp\alpha d-1))/(\exp\alpha d-\alpha d-1)$$

Values of α are calcualted for small percent overvoltages and $\theta(\lambda)=0$ is solved for each value of α, for each value of γ assumed. This is most conveniently done by plotting $\theta(\lambda)$ against (λ). $\partial\theta/\partial\lambda$ can then be evaluated and substituted in equation (1). t can then be calculated, knowing the diffusion coefficient D. This was calculated from the relation $(2C^2)^{\frac{1}{2}}/3\pi\nu S_{12}^2$, where C is the mean velocity of the atom, ν the number of atoms per c.c. and S_{12} the average diameter of the normal and metastable atom. This was obtained from Couillette's value for the metastable mercury atom, being 4.5×10^{-8} cm. $i_{-}(o,t)$ is given by $i(t)/e^{\alpha d}$, and I_o was measured as 3×10^{-11} amps. When t is calculated, it is plotted as a function of overvoltage.

The equation relating the ratio $\frac{i-(o,t)}{I_o}$ to the formative time lag, t, when the combination of collision induced readiation and positive ion action at the cathode is assumed, is given by Davidson as

$$i_-(o,t)/I_o = A - B\, e^{\lambda t}$$

where

$$A = \frac{1}{\Gamma(0)} \quad , \quad B = -\frac{1}{\lambda\, F'(\lambda)} \quad , \quad \text{and}$$

$$F(\lambda) = 1 - \frac{(e^{\psi d}-1)}{(1+\lambda\tau)} \quad - \frac{\alpha\gamma(e^{\phi d}-1)}{\phi}$$

where $\psi = \alpha - \lambda/w_-$, $\phi = -\lambda/w$, and $\frac{1}{w} = \frac{1}{w_+} + \frac{1}{w_-}$

λ is given the value which makes $F(\lambda)$ zero. If λ is small ($\lambda<1000$) the equation for $F(\lambda)=0$ can be solved explicitly for λ, since ψ and ϕ reduce to α. Alternatively $F(\lambda)$ can be plotted against λ, and the zero value found. This is done for each value of α corresponding to a given overvoltage, and for each combination of δ and α, since δ is given by $\delta/\alpha\times\alpha$. When λ is determined for a given set of coefficients the time lag can be found, after differentiating $F(\lambda)$ to find B.

The values of positive ion drift velocity w_+ were taken from Kovar (41), and the electron drift velocity, w_-, calculated from the relation $\bar{\varepsilon} = (\frac{k}{42})\, E/p_o + 6$. The values of α and ω/α were those determined in the present investigation.

APPENDIX 4.

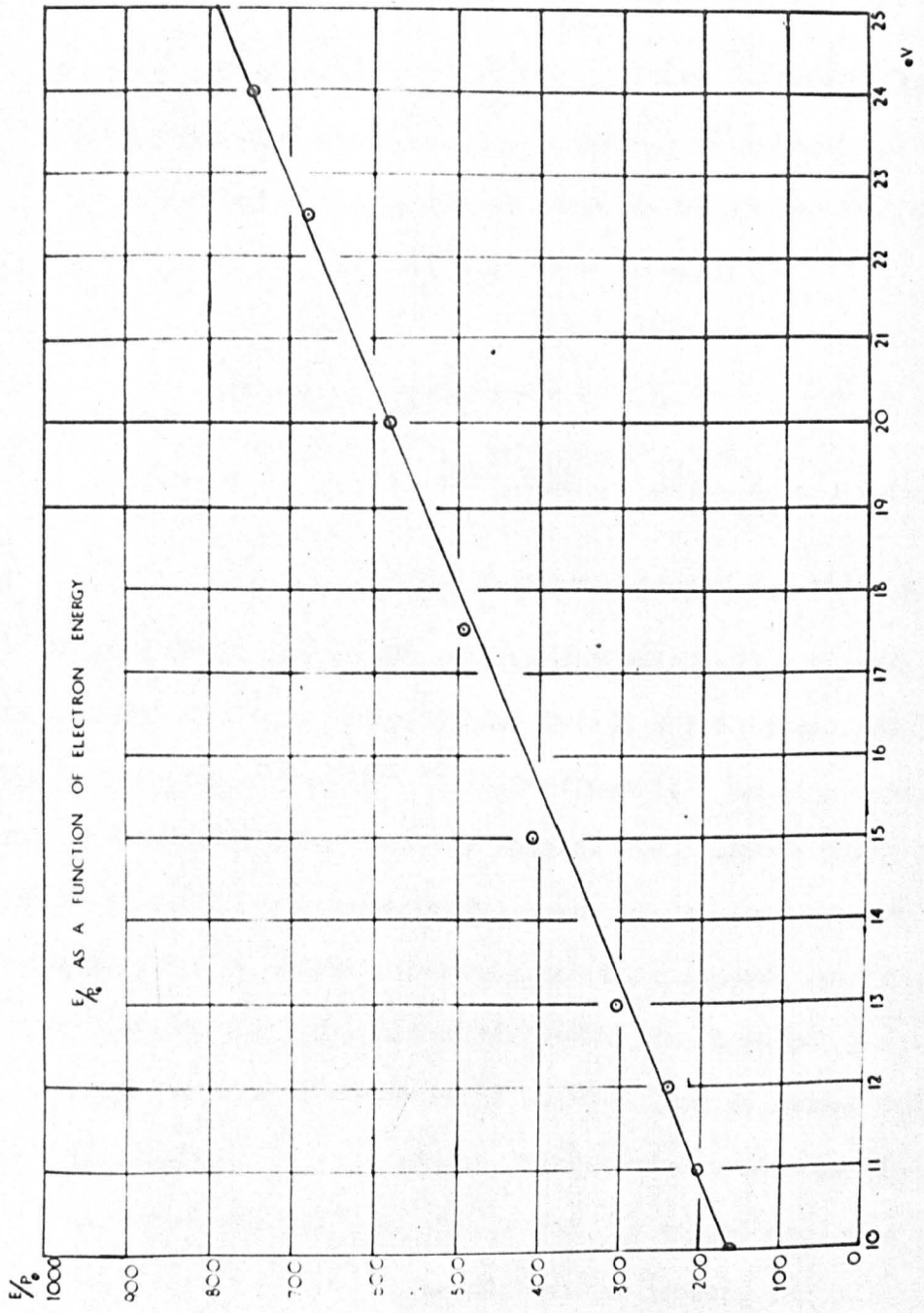
E/P₀ AS A FUNCTION OF ELECTRON ENERGY
E/P₀
1000
900
800
700
600
500
400
300
200
100
0
10
11
12
13
14
15
16
17
18
19
20
21
22
23
24
25
V

LIST OF FIGURES

REFERENCES

(1) Penney, W.G. Phys.Rev. 35, 504 (1930).

(2) Compton, K.T. Phys.Rev. 26, 436 (1925).
van Voorkis, C.C. Phys.Rev. 27, 729 (1926)

(3) Bleakney, W. Phys.Rev. 35, 139 (1930).
Phys.Rev. 36, 1303 (1930).

(4) Townsend, J.S. Electricity in Gases (Oxford: Clarendon Press, 1915).

(5) Crowe, R.W., Bragg, J.K. and Thomas, V.G. Phys.Rev. 96, 10 (1954).

(6) Llewellyn-Jones, F. Encyclopedia of Physics, Volume XXII, p.4 (Springer-Verlag, 1956).

(7) Townsend, J.S. The Theory of Ionization of Gases by Collision (London, Constable, 1910).

(8) Myatt, J. Ph.D. Thesis University of Birmingham (1960).

(9) Posin, D.Q. Phys.Rev. 50, 650 (1936).

(10) Von Engel, A., Steenbeck, . Elektrische Gasentladungen Bd.1 (1932).

(11) Penning, F.M., Druyvesteyn, M.J. Rev.Mod.Phys. 12, 27 (1940).

(12) Emeleus, K.G., Lunt, R.W. and Meek, C.A. Proc.Roy.Soc. A156, 394 (1936).

(13) Penning, F.M. and Addink, C.C.J. Physica 1, 1007 (1934).

(14) Newton, R.R. Phys.Rev. 73, 570 (1948).

(15) Llewellyn-Jones et al Proc.Phys.Soc. 83, (1964).

(16) Rouse, G.F. and Giddings, G.W. Proc.Nat.Acad.Sci. 12, 447 (1926).

(17) Loeb, L.B. and Meek, J.M. The Mechanism of Electric Sparks (California:Standford University Press, 1941).

(18) Reather, H. Z.Angew.Phys. 7, 50 (1955).

(19) Oliphant, M.L.E. Proc.Roy.Soc. A124, 228 (1929).

(20) Oliphant, M.L.E. and Moon, P.B. Proc.Roy.Soc. A127, 388 (1930).

(21) Massey, H.S.W. Rep.Conf.Phys.Ionis.Gases (London Roy.Soc., 1953).

(22) Kapitza, L. Phil.Mag., 45, 989 (1923).

(23) von Engel, A. Ionised Gases (Clarendon Press, 1955).

(24) Llewellyn-Jones, F. Ionisation and Breakdown in Gases (Metheun, 1957).

(25) Hornbeck, J.A. Phys.Rev. 2, 83 (1951).

(26) Varney, R.N. Phys.Rev. 93, 1156 (1954).

(27) Molnar, J.P. Phys.Rev. 83, 933 (1951).

(28) Davidson, P.M. Proc.Roy.Soc. A249, 237 (1959).

(29) Kruithoff, A.A. Physica 7, 519 (1940).

(30) Davidson, P.M. Brit.J.Appl.Phys. 4, 170 (1953).

(31) Llewellyn-Jones, F. and Galloway, W.R. Proc.Phys.Soc. 50, 207 (1938).

(32) Grigorovici, R. Z.Phys. 111, 596 (1939).

(33) Badareu, E. and Bratescu, G.G. Bull.Soc Roum. 42, 82 (1944).

(34) Smith, D. Ph.D. Thesis, University of Birmingham (1962).

(35) Llewellyn-Jones, F. and Davies, D.E. Proc.Phys.Soc. B64, 397,519 (1951).

(36) Langmuir, I. and Jones, H.A. Phys.Rev. 31, 402 (1928).

(37) Smith, P.T. Phys.Rev. 37, 808 (1931).

(38) Arnot, F.L. and Baines, G.O. Proc.Roy.Soc. A151, 256 (1935).

(39) Bratescu, G.G. Bull.Soc.Roum. 42, 82 (1944).

(40) Davies, D.E. and Milne, J.G.C. Brit.Journ.App.Phys. 10, 301 (1959).

(41) Kovar, F.R. Phys.Rev., 3A, 133 (1964).

(42) McCallum, S.P. and Klatzow, L. Phil. Mag. S.7, 17, 111 (1934).

(43) Gozna, C. Ph.D. Thesis University of Birmingham (1960)

(44) Fletcher, J. Ph.D. Thesis University of Keele (1963).

(45) See ref. (6).

(46) Wolfsohn, G. Z.fur.Phys. 83, 634 (1930).

(47) Couillette, J.H. Phys.Rev. 32, 636 (1928).

(48) McCutchen, C.W. Phys.Rev. 112, 1848 (1958).